Effects of Deep Excavations on Circular Tunnels in Fine-grained Soils

A thesis submitted to the
College of Graduate Studies and Research
in partial fulfilment of the requirements for the
Degree of Master of Science
in the Department of Civil and Geological Engineering
University of Saskatchewan, Saskatoon, SK, Canada

by

Rajendra Karki

Permission to Use

In presenting this thesis in partial fulfillment of the requirements for the degree of Master of Science from the University of Saskatchewan, I agree that the Libraries of this University may make it freely available for inspection. I further agree that permission for copying of this thesis in any manner, in whole or in part, for scholarly purposes may be granted by Dr. Jitendrapal Sharma who supervised my thesis work or, in his absence, by the Head of the Department or the Dean of the College in which my thesis work was done. It is understood that any copying or publication or use of this thesis or parts thereof for financial gain shall not be given to me and to the University of Saskatchewan in any scholarly use which may be made of any material in my thesis.

Requests for permission to copy or to make other use of material in this thesis in whole or part should be addressed to:

Head of the Department
Department of Civil and Geological Engineering
57 Campus Drive
University of Saskatchewan
Saskatoon, Saskatchewan, S7N 5A9
Canada

Rajendra Karki
June 30, 2006

Abstract

This thesis presents a study of the effects of deep excavations on adjacent metro or utility tunnel in soft to medium soil. The main objective of the thesis is to develop a method of estimating these effects quantitatively. Extensive review of relevant literature published in the past four decades was conducted in order to understand the trends and the key developments in this area. It was revealed from the literature review that the concurrent use of the Observational Method and the finite element method for monitoring and controlling of ground deformations around the excavation has become a norm for deep excavation projects. Several design charts and guidelines for estimation of effects of deep excavations on adjacent raft foundations or pile foundations were found in the literature; however, no such charts or guidelines were found for estimation of effects of deep excavations on existing circular tunnels. Consequently, the development of these guidelines was established as one of the objectives of this study.

The initial phase of the research was focussed on detailed study and analysis of two well-documented case studies – the Chicago Subway Renovation Project, USA and the Tan Tock Seng Hospital Deep Excavation, Singapore. The back analyses of these two case studies were carried out using the finite element software PLAXIS. Exact site conditions and input parameters for the soil and the structural components were incorporated as much as possible. Appropriate adjustments in some of the input parameters were necessary to achieve good match between the computed and the observed results.

The back analyses were followed by parametric studies to identify important variables controlling the mechanisms of soil-structure interaction. The variables identified from the parametric studies of the two case studies were: soil stiffness, tunnel lining thickness, the depth of the excavation, and the location of tunnel. These variables were used to conduct a series of finite element analyses using simplified geometry and ground conditions for the purpose of formulating preliminary design charts. Results from these analyses were recorded in terms of in-plane and out-of-plane distortion of tunnel lining as well as additional shear forces and bending moments induced in the tunnel lining due to an adjacent deep excavation.

The results were made non-dimensional before presenting them as contour plots. These contour plots constitute preliminary design charts, which can be used for the estimation of tunnel lining deformation caused by adjacent deep excavation.

Based on the results of this study, it can be concluded that a finite element program (such as PLAXIS) that is able to model construction processes associated with tunnelling and deep excavation in urban environment can be an invaluable tool in exploring the mechanism of ground deformation around the deep excavation and in quantifying the effects of ground deformation on existing adjacent structures. The modeller must, however, be aware of the fact that ways of modelling a particular construction process could be different for various finite element programs. It is important to interpret the instructions given in the manual of the program correctly.

Detailed back analyses of well-documented deep excavation case histories are vital from the point-of-view of building confidence in the selected finite element program. Such analyses also have the potential to identify key variables influencing the soil-structure interaction.

Preliminary design charts proposed in this thesis are very convenient for obtaining approximate values of tunnel lining deformation caused by adjacent deep excavation. Non-dimensional nature of these design charts makes it possible to be used for any depth of the deep excavation and for tunnels of any size, depth of cover, and distance from the vertical face of the excavation. These design charts can be used by engineers and contractors for initial estimation, selection and preliminary design of excavation support system, and are particularly useful during the planning phase. Town planners and project managers, who need to decide on the feasibility, damage control and risk management aspects of a deep excavation project, may also find these design charts equally useful. It should, however, be kept in mind that the estimates obtained from these design charts are highly approximate and as such, should be taken as guidelines for decision making processes. These estimates do not replace site specific detailed analysis and monitoring.

Key Words: Deep excavation, circular tunnel, finite element method, soil-structure interaction, parametric study, design charts.

Acknowledgements

Graduate study is a tremendous endeavour of vision, hard work, creativity, persistence and execution of the task, as I discovered during my period of Masters of Science degree here in University of Saskatchewan. It is also a team work where a lot of people are associated in direct or indirect way – contributing to the study in one way or another.

First and foremost, I would like to express my deep sense of gratitude and heartfelt thanks to my supervisor Professor Jitendra Sharma for all of his assistance and valuable suggestions rendered to me for the completion of this research. The *extra mile* he went through to support me to complete this research is ever commendable and highly appreciated. Without his keen vision, this project would not have seen the dawn of the day.

I am thankful to NSERC (Natural Sciences and Research council of Canada) and University of Saskatchewan for the funding provided to me to pursue this research.

I am also very much thankful to my wife, Asmita, for her support and patience. Without her active back up, it would not have been possible for me to pursue this goal. How I wished she and daughter Arya were with me during the research phase of my Master's program! I also owe my gratitude to my parents who had a lot of faith in me and always encouraged me to work hard to complete this project.

I would also like to extend thanks to my friend Manoj Kumar Singh for his valuable suggestions and encouragement during the final period of my thesis writing.

Finally, I would like to thank all of my professors, friends and colleagues who have supported me during my stay at the University of Saskatchewan.

Thank you.

Rajendra Karki

Contents

List of Tables

List of Figures

Notation

Roman

Symbol	Unit	Description
A	m^2	Cross-sectional area of a structural member
BM_{max}	kNm	Maximum bending moment in the retaining wall
$[BM_{max}]_{BC}$	kNm	Maximum bending moment in the retaining wall for the base case
c	kPa	Soil cohesion
C	m	Depth of cover (vertical distance between the crown of the tunnel and the ground surface)
C_b	kPa	Undrained shear strength of the soil beneath the excavation
d	m	Equivalent thickness
D	m	Diameter of tunnel
D_{max}	m	Maximum diameter of tunnel
D_{min}	m	Minimum diameter of tunnel
E	kPa	Young's modulus of soil
E_0	kPa	Young's modulus of soil layer at the top surface
E_{50}	kPa	Primary loading stiffness (secant modulus at 50% strength)
E_{50}^{ref}	kPa	Reference secant stiffness
$[\ E_{50}^{ref}\ ]_{BC}$	kPa	Reference secant stiffness for the base case
EA	kN/m	Normal stiffness of a structural member
E_{BC}	kPa	Young's modulus of soil for the base case in a parametric study
EI	kNm^2/m	Bending stiffness of a structural member
E_{oed}	kPa	Oedometer stiffness
E_{oed}^{ref}	kPa	Reference oedometer stiffness
E_{ur}	kPa	Unloading-reloading stiffness
E_{ur}^{ref}	kPa	Reference unloading-reloading stiffness
H	m	Final depth of excavation
I	m^4	Moment of inertia
K_0	-	Coefficient of earth pressure at rest
K_x	cm/day	Horizontal soil permeability
K_y	cm/day	Vertical soil permeability
L_s	m	Spacing between anchors
m	-	Power for stress law
m_C	kPa/m	Rate of increase of cohesion or undrained shear strength of soil with depth
m_E	kPa/m	Rate of increase of Young's modulus of soil with depth
N	No.	Blow count derived from the Standard Penetration Test (SPT)

Roman (continued)

Symbol	Unit	Description
N_b	-	Stability number using undrained shear strength of the soil beneath the excavation
N_{cb}	-	Critical stability number for basal heave
P	m	Distance between the nearest springing of the tunnel and the retaining wall
p^{ref}	kPa	Reference confining pressure
q	kPa	Deviatoric stress in primary triaxial loading
q_a	kPa	Asymptotic value of shear strength
q_f	kPa	Ultimate deviatoric strength of soil element
R_f	-	Strength reduction factor
R_{int}	-	Interface strength ratio
SF_{max}	kN	Maximum shear force in the retaining wall
$[SF_{max}]_{BC}$	kN	Maximum shear force for the base case
S_U	kPa	Undrained shear strength of soil
S_{U0}	kPa	Undrained shear strength at the ground surface of a soil
$[S_{U0}]_{BC}$	kPa	Undrained shear strength at the ground surface of a soil for the base case
t	m	Thickness
t_{BC}	m	Thickness of retaining wall of the base case
t_L	m	Thickness of tunnel lining
$[t_L]_{BC}$	m	Thickness of tunnel lining for the base case
t_R	m	Thickness of retaining wall under consideration
$[t_R]_{BC}$	m	Thickness of retaining wall for the base case
t_T	m	Thickness of the tunnel
$[t_T]_{BC}$	m	Thickness of the tunnel for the base case
w	kN/m	Weight of a structural element

Greek

Symbol	Unit	Description
ε_1	-	Vertical strain
σ_1	kPa	Major principal stress
σ_2	kPa	Intermediate principal stress
σ_3	kPa	Minor principal stress
σ'_3	kPa	Effective confining pressure (cell pressure)
ψ	^{o}	Dilatancy angle
Γ_{sat}	kN/m^3	Soil unit weight below phreatic level
Γ_{unsat}	kN/m^3	Soil unit weight above phreatic level
ϕ	^{o}	Friction angle
γ	kN/m^3	Unit weight of soil
γ_w	kN/m^3	Unit weight of pore water
μ	-	Poisson's ratio

Mixed

Symbol	Unit	Description
ΔBM_N	-	Normalized change in maximum bending moment in the retaining wall
δC	m	In-plane displacement of tunnel lining due to deep excavation
δC_N	-	Normalized in-plane displacement of tunnel lining due to deep excavation
δD	m	In-plane distortion of tunnel lining due to deep excavation
δD_N	-	Normalized in-plane distortion of tunnel lining due to deep excavation
ΔE_N	-	Normalized change in reference secant stiffness
Δh	m	Maximum horizontal displacement of retaining wall under consideration
δh_{max}	m	Maximum horizontal displacement of retaining wall
$[\delta h_{max}]_{BC}$	m	Maximum horizontal displacement of retaining wall for the base case
Δh_N	-	Normalized change in maximum horizontal displacement of retaining wall or tunnel
δHBM_{max}	kNm	Change in maximum hogging bending moment induced in the tunnel lining
$[\delta HBM_{max}]_N$	-	Normalized change in maximum hogging bending moment induced in the tunnel lining
ΔL_N	-	Normalized change in thickness of tunnel lining
δSBM_{max}	kNm	Change in maximum sagging bending moment induced in the tunnel lining
$[\delta SBM_{max}]_N$	-	Normalized change in maximum sagging bending moment induced in the tunnel lining
δSF_{max}	kNm	Change in maximum shear force induced in the tunnel lining
$[\delta SF_{max}]_N$	-	Normalized change in maximum shear force induced in the tunnel lining
ΔSF_N	-	Normalized change in maximum shear force of the tunnel lining
ΔS_N	-	Normalized change in undrained shear strength at the top of soil layer
Δt_N	-	Normalized change in thickness of retaining wall
δV_{max}	m	Maximum vertical displacement of ground behind the retaining wall
$[\delta V_{max}]_{BC}$	m	Maximum vertical displacement of ground behind retaining wall for the base case
Δv_N	-	Normalized change in ground settlement behind the retaining wall

1 Introduction

Over the past few decades, financial necessity, or perhaps hope of a better quality of life, has fuelled migration of people to big cities. As a result, some of these big cities are experiencing unprecedented population densities. As these urban centres of modern civilization get packed with people, the land required for business and residential purposes becomes scarce. It is, therefore, necessary to build space vertically or in "tiers" – both upwards and downwards – in order to maximize available land use. Deep excavations are almost unavoidable when building structures vertically downwards; for example, a parking lot. There are two main issues associated with deep excavations in an urban environment:

1. The design and construction of adequate temporary support system for the deep excavation.
2. The prevention or minimization of damaging effects of deep excavation on adjacent structures and their foundations.

How can the risk of damage to the adjacent properties be minimized during a deep excavation? Is it safe to carry out excavation with the current state of the site? What are the methodologies that are best suited to monitor and control the effects of a deep excavation? What may be the limiting criteria to stop the work in case of impending failure? Engineers involved with deep excavation construction in an urban environment need to find answers to these pertinent questions.

A deep excavation unloads the surrounding ground because of the large amount of soil removed and, almost invariably, results in ground movement. Even for the stiffest possible support system, some ground movement is inevitable (Peck 1985). Unchecked lateral displacement of the support system (e.g. a retaining wall) can make an excavation unstable. Excessive bending moment developed in the retaining wall may induce cracks in the wall. The effect of this ground movement on an adjacent structure ranges from minor changes in the aesthetics to complete collapse of the structure depending upon the proximity of the structure to the excavated area, the nature of the construction, the type of the support system and the

properties of the soil. Ground movements caused by an open, unsupported excavation or by an excavation supported by a cantilever retaining wall are even greater than those associated with strutted or anchored excavations or deep excavations that are constructed using the top-down method.

1.1 The Need for Research

A deep excavation in the midst of existing structures is a highly complex soil-structure interaction problem. Various components such as support system, surrounding ground, foundations of existing structures, buried structures such as tunnels and underground caverns interact with each other during excavation. The following factors have been identified that influence this interaction (Peck 1969b; Mana and Clough 1981; Peck 1985; Wong and Broms 1989; Clough and O'Rourke 1990; Athanasiu et al. 1991; Hashash and Whittle 1996; Burd et al. 2000):

- stiffness and strength characteristics of the surrounding soil such as anisotropy, rate effects, nonlinearity, and hysteretic behaviour.
- pore-water pressure changes and accompanying consolidation of the surrounding soil
- the type and the stiffness of the support system
- properties of interfaces between the soil and the various structures
- type of the foundation for adjacent structures
- stiffness of the lining system in case of adjacent buried structures
- the location (horizontal distance as well as the depth of cover) of adjacent structures
- the sequence of excavation and the quality of workmanship

Given the wide scope of this soil-structure interaction problem as evident from the above-mentioned factors, it is not surprising that key aspects of this problem are not yet fully understood and there is a plenty of scope to do research in this area.

Typically, the engineer responsible for the design of support system for a deep excavation tries to build a numerical model of the excavation using sophisticated non-linear finite element software and tries to incorporate all aspects of the soil-structure interaction into the numerical model. However, such a numerical model is both highly complex and data deficient, and therefore, its findings cannot be implemented with full confidence. It is therefore, common to use the Observational Method (Peck 1969a) for such projects. In the

Observational Method, the construction is started using initial analysis and design done using the best possible estimates of ground condition and input parameters. Worst case design scenarios are also established using the most unfavourable ground conditions and input parameters, which are used to set trigger values for unacceptable performance and early warning of incipient failure. One of the key components of the Observational Method is the on-site instrumentation to monitor and evaluate the performance during construction. If monitoring data show a below par performance, the design is revised and contingency measures based on revised design are implemented.

It is proposed that preliminary design charts that provide approximate relationships between key parameters would be very useful in the implementation of the Observational Method. Such charts could be used in the planning and the operations of an early warning system, which would help engineers to take timely measures to avoid impending failure of the structure. For example, if preliminary design charts indicate that the maximum bending moment in the retaining wall supporting the deep excavation is closely related to the distribution of undrained shear strength vs. depth of the surrounding ground, and if the assumed and the observed undrained shear strength vs. depth distributions were found to be significantly different, it should be possible to quickly reassess the design of the retaining wall using these charts. In this situation, the retaining wall could be strengthened suitably and its failure could be prevented without having to wait for the results of a sophisticated numerical analysis. Alternatively, the use of design charts could result in efficient execution of numerical analyses as the range of possible outcomes has been established using them.

1.2 Research Objectives

The following objectives have been selected for the research based on the needs identified above:

1. Identify influential components of soil-structure interaction for a deep excavation in an urban environment. This objective is best achieved by creating numerical models of well-documented deep excavation projects that were carried out close to existing surface and subsurface (buried) structures, back analysing the excavation processes, and comparing the results of simulations with observed results. Selection of deep excavation projects for numerical simulation is done on the basis of the availability of

- extensive site investigation and lab data;
- detailed records of construction sequences; and
- instrumentation to monitor and evaluate performance during construction.

2. Quantify the effects of each of the components identified in the numerical simulation of well-documented deep excavation projects. This objective is achieved by conducting parametric studies using numerical analysis software in which the whole plausible range of each component is varied and its effect on the overall behaviour of deep excavation is explored. In order to ensure applicability of results to deep excavations of different dimensions, the results of the parametric study are presented, where possible, in terms of dimensionless parameters.
3. Propose preliminary design charts showing correlations between important parameters. This objective is achieved by observing and identifying patterns of behaviour observed during both the numerical simulation of well-documented deep excavation projects and the parametric studies. Preliminary design charts can be a useful tool for the assessment of feasibility of excavation projects and for the selection of preventive measures if deep excavation must proceed despite unfavourable ground conditions. These design charts can also help in the selection of appropriate bracing and/or anchoring system for the control of lateral movement of retaining wall supporting the deep excavation. As mentioned in the previous section, these design charts could possibly become an integral component of the Observational Method.

1.3 Scope of Research

As mentioned above, the scope of deep excavation-related soil-structure interaction is quite extensive. It is, therefore, not feasible to study all aspects of it during the course of one M.Sc. research project and it is vital to limit the scope of the research. The main limitations of the present research project are listed below:

- Only one class of deep excavations is considered – a vertical deep excavation adjacent to existing circular tunnels.
- Only the effects caused by the deep excavation are studied. Effects caused by the construction of the retaining wall, the installation of bracings (struts) and anchors, and the consolidation and creep of soil are not considered.

- The effect of thickness of the retaining wall supporting the deep excavation is not simulated. The thickness of the retaining wall is kept at 1 m for all the analyses.
- The effects of sequence and timing of installation of struts and anchors are not considered. The same sequence and timing of installation of struts and anchors is adopted for all the analyses.
- The ground surface around the deep excavation is considered horizontal with no surface structures founded on it.
- Only two-dimensional plane strain conditions are considered. For almost all deep excavation projects, there will always be data deficiency, and therefore, it is unlikely that the use of three-dimensional models would result in improved accuracy.
- Only undrained ground response is considered.
- The ground profile is assumed to contain just one deep layer of fine-grained soil with its undrained shear strength increasing linearly with depth. This soil layer is modelled using an isotropic elastic perfectly-plastic model with a Mohr-Coulomb failure criterion.
- Only medium to stiff consistency is considered for the fine-grained soil layer.

1.4 Outline of the Thesis

This thesis is presented in five Chapters.

- Chapter 1 (this chapter) describes the need, the objectives and the scope of the present research project. It also provides a brief overview of the methodology adopted for the present research project.
- Chapter 2 provides a comprehensive review of the literature on soil-structure interaction pertaining to deep excavations in urban environments published during the past four decades. It also provides a historical perspective of the progression of research and technological developments in this area.
- Chapter 3 presents the details and results of numerical analyses of two well-documented deep excavation case studies. It also contains the results of parametric studies conducted to identify important components of deep excavation-related soil-structure interaction.

- Chapter 4 describes the formulation of simple-to-use design charts for the estimation of tunnel deformation due to adjacent deep excavation
- Chapter 5 presents conclusions that can be drawn from the present study. Some applications of the results of the present study as well as some suggestions for future work in this area of research are also given.

2 Literature Review

2.1 Overview

Because of rapid urban growth and increasing space requirements in congested urban environment, problems relating to deep excavation and their effects on surrounding structures are growing. Different methodologies or processes are employed to limit the impact of deep excavation on surrounding structures. The objective of this literature review is to assess the progress made in this area in the recent years in terms of research as well as in the technological developments. The literature review is divided into the following categories:

- Failures involving deep excavations in urban environment
- The use of the Observational Method
- The use of finite element analysis for design as well as performance evaluation
- The development of design charts and guidelines

There may, however, be a considerable overlap in the concepts discussed in the reviewed literature and some of the reviewed papers may belong to more than one of the above categories. It should be noted that only a small number of publications were found that related directly to deep excavations adjacent to existing tunnels. Therefore, in order to establish the trend in numerical analysis of deep excavation-related soil-structure interaction, publications related to other types of deep excavations, such as deep excavations adjacent to existing foundations and tunnel construction adjacent to existing tunnels and foundations, were also reviewed.

2.2 Failures Involving Deep Excavations in Urban Environment

Very few catastrophic failures involving deep excavations in urban environment have been reported in recent years, which could be attributed to the increased use of the Observational Method. Their occurrence, however, presents the engineers with an opportunity to “calibrate” the numerical models and design methods.

Poulos and Chen (1996, 1997) and Poulos (2002) have described a case study where failure of piles under an office building took place due to the adjacent deep excavation. A commercial project located on the island of Java, Indonesia, involved the construction of three buildings – an office block, a hotel, and a shopping centre. After some months of unsupported excavation for an underground water tank in adjacent land, significant settlements started to develop in the 9-storey office block, which had largely been completed. Because of continual increase in settlement that resulted in the tilting of the building, the decision was made to demolish the structure. The analyses of soil-pile interaction for the foundation piles supporting the corner of the office building clearly indicated that excavation-induced ground movements induced additional forces and moments, which, in turn, caused structural failure of the pile.

Gue and Tan (2004) described a case history of failure of the temporary sheet pile wall near Port Klang in Malaysia. The site was a flat marine deposit with the original ground level at grade with access road. The site was on a former residential lot with a detached house and planted with various fruit trees. The project involved the construction of a high rise building with a basement level car park. Reinforced concrete (RC) piles were driven from the original ground level. After the installation of the reinforced concrete piles, excavation was carried out for the construction of the basement and pile caps. A 12 m deep sheet pile wall acting as temporary cofferdam was installed to facilitate the basement and pile caps excavation. The sheet pile wall was stable when the excavation reached the proposed basement level of 2.5 m. However, when the excavation for pile caps in front of the sheet pile, reached 3.5 m to 4 m, the sheet pile moved excessively towards the excavation site and the base of the excavation also heaved up. The excessive movement of the soil pushed and moved the installed RC piles. Some of the piles moved laterally for more than a meter thus damaging the integrity of the piles. The back analysis carried out confirmed that the 12 m penetration depth of the sheet pile was not adequate to support an excavation depth exceeding 3.5 m and that props should have been used near the top of the sheet pile at this site.

In the most recent example involving the failure of a deep excavation, four workers died when a 24 m deep excavation, which was being carried out to house a train station for the Singapore Mass Rapid Transit Circle Line, collapsed on April 20, 2004 (Magnus et al. 2005). The excavation was supported by a combination of concrete diaphragm wall and steel bracings. The collapse of the excavation was triggered by buckling of the bracing system,

which, in turn, resulted in the maximum bending moment in the diaphragm wall exceeding its ultimate limit state value. The Commission of Inquiry appointed by the Government of Singapore to investigate the causes of the collapse identified technical and conceptual errors made in the analysis of the excavation support system using a highly complex numerical model as one of the main causes of the collapse of the deep excavation (Magnus et al. 2005). This collapse is one of the worst case scenarios in the case of deep excavations. It highlighted the lapses in proper control and measures to account for early warning signs of retaining wall failure. Though the Observational Method was implemented from the beginning of the excavation, the performance of the deep excavation was not checked regularly. As a result, the engineers responsible for the deep excavation could not detect impending failure of the retaining wall, and hence, timely remedial measures were not implemented.

2.3 The Use of the Observational Method on Deep Excavation Projects

The term "Observational Method" was first coined by Ralph Peck during his Rankine Lecture (Peck 1969a) to provide a formal definition of the "learn-as-you-go" approach of geotechnical design and construction, which was pioneered by Karl Terzaghi during the early days of the development of soil mechanics as a scientific discipline. Indeed, in 1961, Terzaghi demonstrated that the field of soil mechanics gives the engineer required tools for the implementation of "experimental method" (Terzaghi 1961). According to Peck (1969a), the Observational Method provides a way of ensuring safety while achieving economy in terms of construction costs. Peck (1969a) identified two variations of the Observational Method: *ab initio* – from the start of the project; and *best way out* – during the construction to provide a solution to unexpected problems that might crop up. The Observational Method typically involves the following steps:

1. Site investigation to establish the general nature, distribution and properties of the soil deposits.
2. Assessment of the most probable ground conditions and the most unfavourable (worst case) deviations from these conditions. Peck (1969a) pointed out that geology of the site plays an important role in establishing these two conditions.

3. Design calculations based on the expected behaviour under most probable ground conditions.
4. Identification of key parameters that need to be monitored during construction and calculation of their expected values based on design calculations in Step 3.
5. Estimation of the values of these key parameters for the most unfavourable ground conditions and the use of these "extreme" values as trigger values that will set off alarms when reached.
6. A set of possible contingency measures in case one or more of the trigger values are reached.
7. Continuous evaluation of overall performance and measurement of key parameters.
8. Modification of design using further information gained during construction.

The success (or failure) of the Observational Method depends upon the flexibility in the design. The Observational Method cannot be used on a project whose nature does not permit design alterations during construction (Peck 1969a). Powderham (2002) has described the application of the Observational Method to different construction sites to achieve its main objectives – savings in cost or time or both, and assurance of acceptable safety. He found that the Observational Method promotes innovation through stronger connection between design and construction, increased safety during construction, improved understanding of soil-structure interaction, improvements in the use and performance of instrumentation, higher quality case history data, higher motivation and teamwork.

The application of the Observational Method in deep excavation construction has, in recent times, become the norm rather than the exception because of uncertainty and complexity involved in numerical analysis, and the need to verify the predictions at each stage of the excavation for performance evaluation as well as for prediction of deformations for subsequent excavation stages. A brief outline of some of the recent applications of the Observational Method in deep excavation projects are given below:

Powderham (1994) presented an overview of the Observational Method in the light of the criteria proposed by Peck (1969a) using several case histories from the UK, namely the Channel Tunnel, the Docklands Light Railways and the Limehouse Link. The contractual implications of its use and its role in value engineering (Dell'Isola 1982) were also discussed.

It was recommended that the Observational Method be used much more widely despite its "onerous" requirements.

Young and Ho (1994) described the use of the Observational Method to meet stringent ground movement requirements imposed to ensure minimum disruption to power cables belonging to the British and the French national grids during the construction of the Channel Tunnel. These ground movements were anticipated during a deep excavation supported by an anchored sheet-pile retaining wall. A trial excavation was conducted prior to the construction of the full-scale structure and the observed behaviour was back-analyzed using the finite element method. The results of the field trial and the finite element back-analysis were used to predict ground movements for the full-scale structure. It was concluded that the use of the Observational Method was crucial in meeting the ground movement requirements. Additionally, the Observational Method also resulted in substantial savings in the cost of temporary support system for the excavation.

Ikuta et al. (1994) used an extended form of the Observational Method for the excavation of a deep basement using the top-down construction method. Here, the monitoring data from the first few stages of the excavation were used to obtain improved predictions of ground movements and structural forces and to optimize excavation sequences for the latter stages of the excavation. In fact, on the basis of these improved predictions, the contractor was able to omit inclined struts for the latter stages of the excavation, resulting in substantial cost savings and shorter construction time.

Glass and Powderham (1994) described the application of the Observational Method in the construction of the Limehouse Link, which is a major cut-and-cover highway tunnel connecting the City of London to the London Docklands in the UK. In this case, the Observational Method was successfully used to avoid the use of heavy temporary support structure during the excavation, which resulted in considerable cost and time savings on the project. Potential hazards and risks during the excavation were successfully negotiated by careful implementation of the Observational Method through progressive design modifications and close collaboration between all parties involved in the project.

Koutsoftas et al. (2000) described deep excavation in soft ground conditions along the Embarcadero waterfront in downtown San Francisco, California for the MUNI Metro Turnback project. The design included estimates of deformations caused by the excavations

and other construction activities, evaluation of potential settlements of adjacent buildings, and structural evaluation of the response of the building to the estimated settlements. A comprehensive monitoring program combined with an instrumented test section, appropriate contingency measures, and construction controls were planned to facilitate timely response in the event that the deformations exceeded tolerable limits. Even though significant lateral deformations were developed by pile driving, the mitigation measures taken were quite effective in limiting the settlements caused by pile driving to relatively small values. It was concluded that a well planned and executed instrumentation program must be considered an integral part of the design of the shoring system, especially where the shoring can impact important adjacent structures.

Ou et al. (2000) studied ground movements induced by an excavation using the top-down construction method and the response of adjacent buildings to these ground movements. They concluded that the information regarding a building's location relative to the settlement influence zone is helpful in planning building protection measures during the excavation.

Sharma et al. (2001) described a 200 m long, 140 m wide and 15 m deep excavation for basement construction for the Tan Tock Seng Hospital in Singapore. The excavation was located adjacent to two 6 m diameter existing tunnels of the Singapore Mass Rapid Transit (SMRT) system. The horizontal distance between the diaphragm wall supporting the deep excavation and the nearest tunnel was about 20 m. A sophisticated automatic monitoring system was installed in both the SMRT tunnels to ensure that the stringent requirements for limiting the deformations of the tunnels were not violated during any stage of the excavation. Finite element analyses of the excavation were also carried out and the results were verified during the construction for performance evaluation. The results of the finite element analyses were found to be reasonably close to the monitored results. It was found that the stiffness of the tunnel lining has a crucial role in ensuring its own integrity during excavation. For a given distortion, which was proportional to the magnitude of ground movements induced by the deep excavation, a stiffer tunnel lining induced greater increase in bending moment and shear force. A segmental lining system provides more flexibility to the tunnel lining and ensures its integrity when subjected to distortion.

Chang et al. (2001) used the Observational Method for the performance evaluation of a deep excavation for the basement of a high-rise building adjacent to existing Taipei Rapid

Transit tunnels. The subsoils at the site consisted of a sequence of alternating layers of silty clay and silty sand. Underlying these layers was a thick layer of gravel which was extremely permeable and very rich in water reserves. The silty clay layers were mildly overconsolidated with undrained shear strength generally increasing from 15 to 40 kPa with depth. The SPT N-values in the silty sands generally varied from 10 to 40. Ground movements during the excavation were recorded using inclinometers. Instrumentation was also installed on tunnel linings to measure the strains induced due to the deep excavation. Significant movements of the up-track tunnel, cracks in tunnel lining segments and failure of some structural members were observed. The concrete slab supporting the rail tracks on the tunnel invert was dislocated and detached from the tunnel linings due to distortion of the tunnel cross-section. The down-track tunnel, which was located farther from the deep excavation, was not affected. It was concluded that maximum lateral movement is not a governing factor in evaluating the safety of tunnels. It is the curvature of the lateral movement vs. depth profile that matters. If a tunnel bulges toward the excavation, it is more susceptible to damage because the lining joints will tend to open up. If it bulges away from the excavation, it is less susceptible to damage because the lining joints will tend to close up due to arching.

Finno et al. (2002) reported a deep excavation project in Chicago where the Observational Method was used in combination with stringent monitoring system and inverse analysis to limit the impact of excavation on the raft foundation of a nearby school building. The project was completed successfully with minimal deformations manifested on the structural components of the building, as was envisioned in the planning phase. Inverse analysis proved to be effective in calibrating soil parameters successfully for the prediction of excavation related deformations. It was found that the parametric optimization obtained through regression analysis as well as inverse analysis at the early phases of the excavation was able to give sufficiently good (matching) results for prediction of lateral deformations for the later phases of the excavation.

Hintze (2002) has described the Southern Link Road Construction Project in Stockholm, Sweden where prediction and impact on nearby structures during the excavation for 400 m long cut-and-cover tunnel was studied. Up to 16 m deep excavation required for construction of the concrete tunnel was carried out within anchored steel sheet pile walls, with one to six levels of inclined anchors (tie-back walls), mostly with steel cores at the bottom.

The site included difficult foundation works very close to existing buildings and heavy traffic. To get cost-effective and safe structure, a large number of calculations of expected deformations for different construction stages in the soil had been made. Deformation curves, with upper and lower limits, for retaining wall and forces in anchors and struts were generated. An extensive control program based on these curves, risk analysis and the "Observational Method" was established to monitor the settlements within the working area. Deformations and anchor pressure were measured automatically and trigger limits were set using an alarm system.

Hu et al. (2003) described the design and construction of a deep excavation for the construction of the foundation of a multi-story building in soft, saturated ground conditions adjacent to the twin tunnels of Shanghai Metro system. In this case study, the Observational Method was used to reduce ground movements because the predicted ground movements were deemed unacceptably high from the point-of-view of ensuring integrity of the twin tunnels. The measures included cast-in-place concrete diaphragm walls with bracing structural members, pumping consolidation, deep cement mixing (DCM) columns, and a rational excavation procedure. The rational excavation procedure takes into account the rational planning and sequence of the excavation, including the lifts, plots, symmetry, time, and bracing. The excavation site is divided into alternate long strips for each stage of excavation and bracing is installed in the excavated strip before carrying out the excavation of other long strips. All of the precautionary measures resulted in a reduction of the diaphragm wall horizontal maximum displacement from a predicted 28.5 mm to about 14.2 mm and a reduction of the maximum settlement from a predicted 23.1 mm to about 7 mm. The settlement and horizontal displacement of the tunnels were controlled within 5.0 and 9.0 mm respectively. The curvatures of the longitudinal deformation curves of the twin tunnels were less then 1/15000. The horizontal displacement of the braced diaphragm walls was less than 0.12% of the total excavation depth.

Meier and Winsor (2005) have described deep excavation and bored tunnelling for the Delhi Metro system in India, which is currently being built and scheduled to be completed by 2011. During the first phase construction of the 245-km-long Metro system, the Observational Method was used in combination with one of the most sophisticated instrumentation systems to control ground movements. Two automatic motorized theodolites were installed on the

roofs of two neighbouring buildings and aimed at targets that were fixed on the buildings directly above the tunnels. The theodolites were programmed to take readings of approximately 50 targets at short intervals and transmit the information to a computer that evaluated and graphically displayed the raw data. Trigger values were predefined on the basis of the predictions of ground movements using a series of finite element analyses. In the event that these trigger values were reached, the system automatically raised an alarm and alerted the selected recipients by contacting them on their mobile phones. To eliminate erroneous readings and avoid false alarms, the system waited for two consecutive readings to confirm that a trigger value had been detected. All monitoring data were uploaded to a server, where they could be assessed by authorized personnel via the Internet. In spite of being located underneath one of the most densely populated urban areas in the world, the effects of ground movements on adjacent buildings were successfully minimized and there were no major mishaps.

Out of all the published deep excavation case histories involving the use of the Observational Method, only one example could be found where failure of the deep excavation could not be prevented. This is the case of the Nicoll Highway collapse in Singapore (Magnus et al. 2005). On April 20, 2004, a 24 m deep excavation for the construction of an underground train station for the Singapore Mass Rapid Transit Circle Line collapsed, resulting in the death of four construction workers and widespread structural damage to the adjacent highway and surrounding high-rise buildings. The excavation was supported by a combination of concrete diaphragm wall and steel bracings. The collapse of the excavation was triggered by buckling of the bracing system, which, in turn, resulted in the maximum bending moment in the diaphragm wall exceeding its ultimate limit state value. This collapse is one of the worst case scenarios in the case of deep excavations. It highlighted the lapses in proper control and measures to account for early warning signs of retaining wall failure. Though the Observational Method was implemented from the beginning of the excavation, the performance of the deep excavation was not checked regularly. As a result, the engineers responsible for the deep excavation could not detect impending failure of the retaining wall, and hence, timely remedial measures were not implemented. This case history has highlighted the importance of following all the steps involved in the Observational Method. All the

monitoring data collected using a plethora of sophisticated instruments is useless if it is not used for performance evaluation and risk assessment.

2.4 Finite Element Analysis for Design and Performance Evaluation

The use of the finite element method to analyse geotechnical problems started in 1970s with the advent of digital computing and advances made in terms of analytical and numerical techniques. With the availability of affordable computing power and improved constitutive models of soil behaviour, its use has increased exponentially and its status has changed from luxury to necessity. Nowadays, it is very difficult to imagine geotechnical analysis and design without the use of the finite element method.

Three main applications of the finite element method to deep excavation can be found in the published literature:

1. for design calculations and prediction of ground movements and structural forces;
2. for back-analysis of existing case histories; and
3. for conducting parametric studies.

When used for design calculations and prediction of ground movements and structural forces, it usually forms an important component of the Observational Method. Also, back-analyses of case histories using the finite element method are often accompanied by parametric studies. Some of the notable uses of the finite element method in the analysis and design of deep excavations are given below:

Palmer and Kenney (1972) used the finite element method to evaluate the relative importance of different parameters on the performance of a braced excavation at Oslo Subway in Norway. A rather unique computer modelling technique was used to incorporate both the large number of variables and the problem of interaction and dissimilar behaviour. Parametric studies were carried out for a typical excavation with fully penetrating sheet-pile walls. Of the parameters concerning soil condition, the soil deformation modulus was found to have the greatest influence. Other important parameters for deflection of retaining wall were found to be - stiffness of sheet-pile wall and effective strut stiffness, whereas the rest of the parameters were found to have nominal effect.

Burland and Hancock (1977) described the performance of the multi-propped excavation in sand and gravel overlying stiff, fissured London clay at New Palace Yard and reported that approximately 50% of the total ground movements (both horizontal and vertical) occurred due to the construction of the diaphragm wall and piles.

Eisenstein and Medeiros (1983) reported the performance and analysis of a deep excavation in glacial till (overconsolidated stiff, fissured silty clay) in Edmonton, Canada. In order to analyze the lateral pressures, several stress-strain models - linear elasticity and nonlinear elasticity based on plane strain, stress path dependent triaxial, and conventional triaxial tests – were employed in finite element analyses. While plane strain data and the stress path dependent triaxial test data produced reasonable agreement with the observed lateral displacements, the conventional triaxial test and the assumption of linear elasticity yielded results departing from the field behaviour. Another important finding was that the flexibility of the retaining wall has a significant effect on lateral pressure reduction and on ground movements. The total horizontal load carried by the struts and by the embedded portion of the wall also depends on wall flexibility.

Potts and Fourie (1984) studied the behaviour of a propped retaining wall by the finite element method. The investigation indicated that for an excavated wall in soil with a high initial value of the coefficient of earth pressure at rest (K_0), prop forces and wall bending moments greatly exceed those predicted by limit equilibrium calculations. For backfilled and excavated wall in soils with a low K_0 value, the analyses indicated that the displacements are much smaller in magnitude and that the approximate limit equilibrium calculations produce conservative values of prop force and bending moments.

Finno and Harahap (1991) have used parametric studies to demonstrate the importance of sheet pile installation and other construction factors on finite-element calculations of ground movements for the HDR-4 deep excavation site in Chicago. Simulations of construction of a 12.2-m-deep braced excavation in saturated clays in Chicago have been made using a coupled finite element formulation. Surface and subsurface ground movements, pore water pressures, and sheet-pile deflections were measured throughout construction at the site and were compared to results of the simulations at key stages of the excavation. The finite element simulations closely modelled all phases of construction including sheet-pile installation and the actual duration of construction. While sheet-pile deflections could be

accurately computed throughout construction with a proper finite element simulation, computed ground movement quickly diverged from observed responses when relatively large strains, corresponding to the peak shear stress, were included in the soil mass and resulted in localized strains. Another equally compelling factor to consider for modelling accuracy is anisotropy of soil. The assumption of elastic response inside a yield surface in a conventional elasto-plastic soil model leads to an overly stiff computed response. The empirical approach of bounding surface models that permits inelastic deformation inside the yield surface leads to more realistic computed responses in cases where stress reversal plays an important role. Anisotropy is a factor that must be considered when evaluating potential ground movements associated with a proposed excavation through soft to medium clays.

Powrie and Li (1991) used finite element analyses to study the complex soil-structural interaction between the retaining wall, the soil and a continuous slab propped at a formation level of 9-m-deep excavation in stiff overconsolidated boulder clay. Parametric studies were carried out in which the effects of soil/wall/prop stiffness and pre-excavation earth pressure coefficient were investigated. It was found that computed deformations were governed by assumed stiffness of the soil rather than the flexural rigidity of the wall. Bending moments in the wall were influenced significantly by the assumed pre-excavation lateral earth pressures and, to a lesser extent, by the nature of the structural connection between the wall and the permanent prop slab.

Whittle et al. (1993) described the application of a finite element analysis for modelling the top-down construction of a seven-story, underground parking garage at Post Office Square in Boston. The finite element analysis incorporated coupled flow and real time deformation simulation of construction activities with advanced constitutive modelling of clay behaviour. Predictions for wall deflections, soil deformations, surface settlements, and piezometric elevation were evaluated through comparisons with extensive field data. The difference between predicted and measured wall movements was attributed primarily to post-construction shrinkage of the roof and floor systems. An advanced constitutive soil model MIT-E3 describing the nonlinear and inelastic behaviour of clays was able to refine the predicted results of finite element analyses considerably. The study demonstrated that reliable and consistent prediction of soil deformations and ground water flow can be achieved by this

advanced method of analysis without recourse to parametric iteration when adequate characterization of engineering properties of the soil has been undertaken.

Ng and Lings (2002) evaluated the effectiveness of two relatively simple models: a linear elastic-perfectly plastic Mohr-Coulomb and a nonlinear BRICK model (Simpson 1991) for simulating the top-down construction of a multi-propped excavation in the overconsolidated stiff fissured Gault clay at Lion Yard, Cambridge, with and without wall installation effects modelled. The results of the study shows that the use of the Mohr-Coulomb model with a "wished-in-place" wall can reasonably predict the maximum bending moments and deflections of the wall for design purposes once the input soil parameters are correctly estimated. However, it significantly overestimates strut loads and fails to estimate the general ground deformation pattern.

Bose and Som (1998) carried out parametric studies to find out the effects of some of the parameters in the case of a 13.6-m-deep braced excavation in soft clay in Calcutta Metro Railways, India. The main findings are summarized as follows: (i) Major ground settlement for braced cut is restricted within a distance of 3 times the depth of cut, (ii) Increase in depth of penetration of wall, further beyond that required for excavation stability, generates fixity of the wall toe such that its deflection reduces and tends towards perfect fixity where the deflection is zero for the wall resting on the rigid base, (iii) Increase in wall penetration hardly affects the performance of the braced excavation above final strut level, (iv) Increase of the width of excavation generates a larger zone of plastic deformation. Eventually the wall defection and ground settlement increase without altering the lateral force equilibrium on the diaphragm wall, (v) Strut prestressing considerably affects the deflection of the upper portion of the wall while no change is detected at the bottom portion, and (vi) Ground settlement reduces with the increase in the magnitude of strut prestress.

Yoo (2001) presented the results of analyses on the behaviour of in situ walls, using the monitoring data collected from 62 deep excavation sites with multilayered ground conditions of soils overlaying rock in Korea, covering a wide range of wall types, including H-pile, soil cement, cast-in-place pile, and diaphragm. The measured data were thoroughly analyzed to investigate the effects of wall and support types on lateral wall movements as well as apparent earth pressures. A series of plane strain finite element analyses were also

performed to correlate lateral wall movement and apparent earth pressure to the primary influencing factors affecting the wall behaviour.

Long (2001) used the finite element method to back-analyse a case history of a deep basement excavation in London Clay. Parametric studies of the effect of various parameters indicated that “best estimates” of the wall movements were still well in excess of those measured. It was concluded that these differences were due to three-dimensional effects and deficiencies in the constitutive modelling of soil behaviour.

Seok et al. (2001) carried out model tests in combination with finite element analyses to verify the speculation that in deep excavation situations, building settlement exceeds the amount of associated ground settlement because of additional settlement under the building weight. The building settlement, when at ground level, was found to be up to 500% more than that of ground with no structure on it. The settlement decreased rapidly with the embedment depth of the building’s foundation and became negligible for the depth equal to half of the excavation depth. Soil improvement is required to reduce settlement when a building’s centroid is located within the excavation influence zone, which is supposed be equivalent to the depth of the excavation.

Moormann and Katzenback (2002) studied three-dimensional effects of deep excavations with rectangular shape for a case study with a 13.5-m-deep excavation in soft clay for the Grand Casino next to Lake Geneva. The consequences of spatial effects on the bearing and deformation behaviour of deep excavations with nearly rectangular shape in cohesive soils were investigated by the analysis of several field measurements and a parametric study using a three-dimensional numerical model. The results showed that a plain strain model overestimates the horizontal displacements of the wall and the settlements at the ground surface as well as the internal forces of the side of the wall and of the supporting system. It was suggested that the consideration of the spatial performance of deep excavation leads to a more realistic and more economical design of excavations, and further research is necessary to provide simplified recommendations for application in design practice.

Calvello and Finno (2004) studied the applications and benefits of using inverse analysis techniques to select the appropriate parameters to optimize when calibrating a soil constitutive model. Four layers of Chicago glacial clays were modelled and calibrated by optimizing the elasto-plastic Hardening Soil model. The model was initially calibrated using

results from triaxial compression tests performed on specimens from four clay layers and subsequently re-calibrated using inclinometer data that were used to interpret the displacements of a supported excavation in these clays. Finite element simulations of both the triaxial tests and the supported excavation were performed. The inverse analysis methodology effectively calibrated the soil parameters considered, by minimizing the errors between computed responses and experimental observations and converging to realistic values.

2.5 Design Charts and Guidelines

The formulation of design charts or guidelines to estimate ground movement with respect to the stiffness of the braced support system started with the Peck's design chart (Peck 1969b) for the estimation of settlements around a deep excavation (Figure 2.1). Peck's design chart has been frequently used in geotechnical construction, and has undergone some modification over the years.

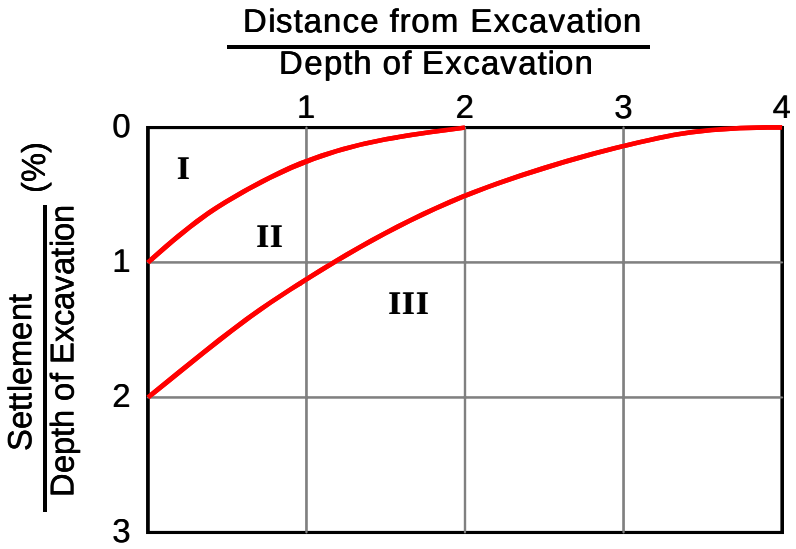

Zone I	Zone II	Zone III
• Sands and Stiff to Hard Clays	• Very soft to soft clay (limited depth of clay below bottom of excavation or significant depth of clay below the bottom of the excavation but $N_b < N_{cb}$) • Settlements affected by construction difficulties	• Very soft to soft clay extending to significant depth below bottom of excavation and with $N_b > N_{cb}$

[N_b – stability number using undrained shear strength of the soil beneath the excavation = $\gamma H / C_b$; γ - unit weight of the soil above the excavation; H – final depth of the excavation; C_b – undrained shear strength of the soil beneath the excavation; N_{cb} – critical stability number for basal heave]

Figure 2.1 Peck's design chart for estimation of settlement around a deep excavation (after Peck 1969b)

Several other researchers have also utilized numerical modelling methods to obtain different simplified design charts or guidelines; some of these design charts are summarized as follows:

Mana and Clough (1981) reported analyses, which showed how the support stiffness and toe fixity of the wall affect maximum lateral deflections. By establishing the link between these numerical experiments and measured field data, they proposed a simplified method for estimating wall movements from the finite-element analyses.

Broms and Pandey (1987) investigated the effects of tunnelling excavation on an adjacent pile foundation supporting various structures on soft clay using the finite element method. Charts were prepared from a series of finite element analysis which could be used to estimate lateral ground movements in the vicinity of a tunnel and its influence on neighbouring piles.

Wong and Broms (1989) proposed a simplified method to estimate the lateral deformation of braced sheet-pile walls in clay with average to good workmanship. The study concluded that the settlements, lateral displacements, and heave are mainly controlled by the factor of safety with respect to base heave, and formed charts to estimate lateral deformations. They suggested that in order to minimize the early deformation of a retaining wall, struts should be installed and preloaded immediately after the excavation has reached the new strut level and the spacing of the struts be small.

Poulos and Chen (1996) used a two-stage analysis involving the finite element method and the boundary element method to study pile response due to lateral soil movements induced by unsupported excavations in clay. Design charts for estimating pile bending moments and deflections were presented for free-head single piles. These charts may be used in practice for assessing the behaviour of existing piles due to the excavation. However, proper account should be taken of the pile head condition, which has been found to have a major effect on the pile bending moment. The key factors influencing the response of a single pile are found to include excavation depth, soil properties, pile properties, and the pile head condition. The design charts are found to provide reasonable estimates of the pile response through the study of a published historical case.

Hashash and Whittle (1996) investigated the effects of wall embedment depth, support conditions, and stress history profile on the undrained deformations around a braced

diaphragm wall in a deep clay deposit, using a series of numerical experiments – nonlinear finite element analyses. The results are combined in prototype "design" charts for estimating ground movements as functions of the excavation depth and the support conditions, and incorporate the effects of wall length on base stability.

Boone et al. (1999) studied the various methods employed to predict the extent of building damage due to excavation-induced ground movements. A modified approach to estimate potential damage categorization was provided. There was good agreement between actual and estimated damage categories.

Chen et al. (1999) used a two-stage approach to analyze the lateral and axial responses of piles caused by tunnelling. Through a parametric study, it was shown that the influence of tunnelling on pile response depends on a number of factors, including tunnel geometry, ground loss ratio, soil strength, pile diameter, and ratio of pile length to tunnel cover depth. Simple design charts were presented for estimating maximum pile responses and may be used in practice to assess the behaviour of existing piles adjacent to tunnelling operations.

Shirlaw et al. (2000) proposed ten 'Limit States' guidelines – five for the tunnel structures and five for trackwork/operations – to establish the actual tolerance of the existing bored tunnel movements due to an adjacent excavation. For each limit state, a tolerable movement for distortion or mode of deformation was suggested, based on the measured movement within each limit state.

Yoo (2001) studied the in-situ behaviour of retaining walls for more than 60 deep excavation sites with multilayered ground conditions of soil in Korea. With the series of 2-D finite element analyses, he provided forms related to lateral movement and apparent earth pressure to the primary influencing factors affecting the wall behaviour, as a tool that can be used for design and analysis.

2.6 Chapter Summary

From the literature review presented in this chapter, it is evident that there is dearth of information on various aspects of soil-structure interaction of a deep excavation adjacent to existing circular tunnels. There is, therefore, a need to undertake further research in this area. It can also be concluded from this literature review that the use of the Observational Method on deep excavation projects has been highly successful with only one major failure so far. Its

use is set to increase with need to achieve cost savings while ensuring safety and serviceability of the surrounding structures. Finite element analyses have been used mainly as a component of the Observational Method or as a tool to back-analyse documented case histories of deep excavations. However, their use for conducting parametric studies for the development of design charts has been rather limited. It can also be concluded that a set of preliminary design charts would make the application of the Observational Method to deep excavation projects less tedious and the routine interpretation of monitoring data easier.

3 Case Studies

3.1 General

On construction projects involving deep excavation, the deformation of retaining wall and its effect on adjacent structures are monitored at different stages of construction using instruments such as inclinometers, settlement gauges and load cells. Such monitoring serves two purposes. First, it minimizes the uncertainty in geotechnical design, which is primarily associated with uncertainty in input parameters for soil, by allowing engineers to "correct" their design in response to soil conditions encountered during construction. Such use of monitoring data is an essential component of the Observational Method (Peck 1969a). Second, it helps to re-calibrate the soil parameters through numerical modelling for use in the design of subsequent deep excavations in similar soil conditions. This process is commonly termed as *back analysis.* Occasionally, it has also been referred to as inverse analysis (e.g. Calvello and Finno 2004). Back analysis done during initial stages of a deep excavation can help to improve prediction and performance of excavation support system during subsequent stages (Calvello 2002; Calvello and Finno 2004). These days, it is a standard practice to use back analysis in deep excavation and other geotechnical constructions. Widespread use of back analysis, however, reflects the difficulty in obtaining reliable predictions from numerical modelling.

One of the advantages of back analysis is its flexibility to allow the numerical modeller to try out different approaches (e.g. the use of different soil models or changes in some of the modelling assumptions or input parameters), and compare numerical modelling results with observed or monitored data. As numerical results are sensitive to input parameters, parameters that affect the results significantly can be identified. Back analysis of published case studies can also be very helpful in understanding the key mechanisms involved. In this research, the following two well-documented case studies were chosen for in-depth study and back analysis:

(1) Chicago Subway Renovation Project, USA (Finno et al. 2002): It represents a typical case of well managed deep excavation project in stiffest bracing excavation

support system. Inverse analysis was used as a tool to control the lateral deformation of retaining wall and to minimize damage to the nearest school foundation.

(2) Deep Excavation next to Existing Mass Rapid Transit (MRT) Tunnels, Singapore (Sharma et al. 2001): In this case study, the effects of a deep excavation on two pre-existing MRT tunnel were quantified using automated instrumentation system, observational methods and numerical analysis.

The objectives of the back analysis of the above-mentioned case studies can briefly be stated as follows:

- Understanding the changes in deformation mechanisms vis-à-vis changes in soil and retaining wall parameters; and,
- Identification of key parameters for use in subsequent parametric studies.

The back analyses of the above case studies were done using geotechnical finite element analysis software PLAXIS V 8.2 (Brinkgreve et al. 2004). The details, results and key findings obtained from the back analyses of these two case studies are presented in this chapter. A brief overview of the salient features of PLAXIS is also presented.

3.2 Finite element software PLAXIS

PLAXIS is a finite element package intended for two-dimensional (2-D) analysis of deformation, stability and groundwater flow problems in geotechnical engineering (Brinkgreve et al. 2004). It is widely used in practice because of its simplicity, user-friendliness and reliability.

PLAXIS is equipped with features to deal with various aspects of complex geotechnical structures. A brief summary of some important features of PLAXIS is given below:

- The input parameters and the boundary conditions of the geometry can be drawn based on computer-aided drawing (CAD) procedures. A 2-D finite element mesh can also be generated easily.
- It allows automatic generation of unstructured triangular 2-D finite element meshes with options for global and local mesh refinements.

- Quadratic 6-node and quadratic 15-node triangular elements are available to model stresses and deformations in the soil.
- Special beam elements (designated as plates) are used to model structural elements such as retaining walls, tunnel linings, shells, and other slender structures.
- Joint elements are used to model relative slip between the soil and the adjacent structural elements.
- Elastoplastic spring elements are used to model anchors and struts.
- The presence of geosynthetic reinforcements (e.g. a geotextile or a geogrid) can be simulated by the use of special tension elements.
- Meshes for circular and non-circular tunnels can be created using arcs and lines.
- Steady-state pore pressure can be generated using either phreatic levels or groundwater flow calculation. Excess pore pressures are computed during plastic calculations when undrained soil layers are subjected to loads.
- Automatic load stepping avoids the need for the user to select suitable load increments for plastic calculations, thus ensuring an efficient and robust calculation process.
- Stage construction feature enables a realistic simulation of construction and excavation processes by activating and deactivating clusters of elements, application of loads, changing of water tables, etc.
- The change in excess pore pressures with time can be computed using a consolidation analysis.
- It incorporates simple linear, isotropic Mohr-Coulomb Soil model as well as more complex and non-linear models such as Hardening Soil model, Jointed Rock model, Soft-Soil-Creep model, Soft Soil model and Modified Cam-Clay model.

For the back analyses of the two case studies, the Mohr-Coulomb (MC) model and the Hardening Soil (HS) model were used to simulate soil behaviour. The details of the Mohr-Coulomb model can be found in any geotechnical engineering text (e.g. Muir-Wood 1990; Budhu 2000). The essential features of the Hardening Soil model are provided in the next section. A comprehensive description of the Hardening Soil model can be found in Schanz et al. (1999).

3.2.1 The Hardening Soil (HS) Model

The Hardening Soil (HS) model is an advanced model that can be used for the simulation of stress-strain behaviour of both soft soils and stiff soils (Schanz 1998). For the case of a drained triaxial test, the HS model approximates the deviatoric stress vs. axial strain curve using a hyperbola. Such hyperbolic deviatoric stress vs. axial strain curve can also be modelled using the well-known Duncan and Chang non-linear elastic model (Duncan and Chang 1970); however, the HS model supersedes the Duncan and Chang model considerably. The HS model uses plasticity theory rather than elasticity theory used in the Duncan and Chang model; therefore, the HS model is capable of modelling irreversible (plastic) stress-strain behaviour. Additionally, the HS model is capable of simulating dilative behaviour as well as volumetric strain hardening behaviour, which are not possible using the Duncan and Chang model.

Similar to the Mohr-Coulomb model, limiting states of stress in the HS model are described in terms of effective stress parameters, i.e. the friction angle, ϕ, the cohesion, c, and the dilatancy angle, ψ, or in terms of undrained shear strength of soil, S_U, by specifying zero values for ϕ and ψ and setting c equal to S_U. The soil stiffness, however, is described much more accurately in the HS model by using three different input stiffness values - the triaxial loading stiffness, E_{50}^{ref}, the triaxial unloading/reloading stiffness, E_{ur}^{ref}, and the oedometer loading stiffness, E_{oed}^{ref}. Unlike the Mohr-Coulomb model, the HS model also accounts for stress-dependency of soil stiffness, i.e. the elastic stiffness values increase with confining stress in the HS model.

The HS model allows for plastic volume change (volumetric hardening) as well as plastic shearing due to deviatoric loading (shear hardening). Compared with the Mohr-Coulomb model, the unloading behaviour of the soil is better taken into account in the HS model. The HS model may be used to calculate realistic pressure distribution below raft foundations and behind soil retaining structures (Brinkgreve et al. 2004).

The formulation of the HS model can be explained using the hyperbolic relationship between the axial strain, ε_1, and deviatoric stress, q, in primary triaxial loading (Figure 3.1).

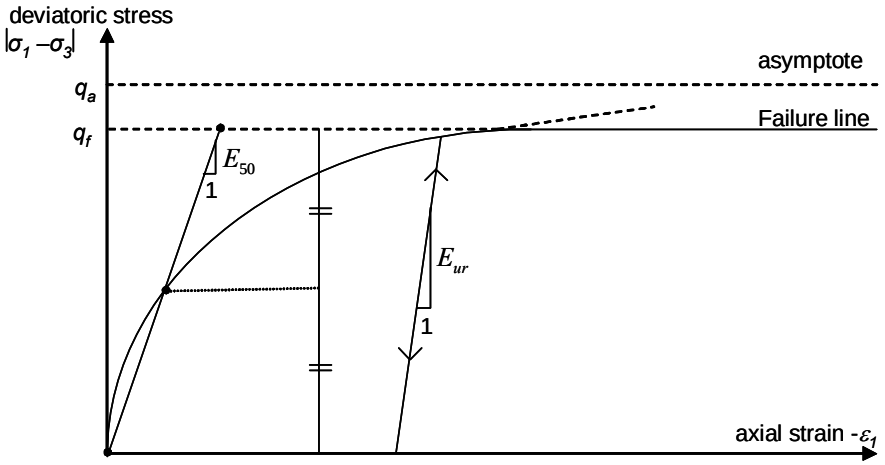

Figure 3.1 Hyperbolic stress-strain relation in primary loading for a standard drained triaxial test

Standard drained triaxial tests tend to yield stress-strain curves that may be described by:

$$-\varepsilon_1 = \frac{1}{2E_{50}} \frac{q}{1 - q/q_a} \qquad [3\text{-}1]$$

where q_a is the asymptotic value of the shear strength, and q_f is the ultimate deviatoric stress. The negative sign in front of axial strain indicates that it is a compressive strain. The parameter E_{50} is the confining stress-dependent stiffness modulus for primary loading and is given by:

$$E_{50} = E_{50}^{ref} \left(\frac{c\cos\phi - \sigma_3' \sin\phi}{c\cos\phi + p^{ref} \sin\phi} \right)^m \qquad [3\text{-}2]$$

where E_{50}^{ref} is a reference stiffness modulus corresponding to the reference confining pressure p^{ref}, c is the cohesion of soil and ϕ is the angle of friction of soil. In PLAXIS, a default setting p^{ref} = 100 stress units is used. The actual stress depends on the minor principal stress, σ_3', which is the effective confining pressure (cell pressure) in a triaxial test. The amount of dependency is given by the power *m.* In order to generate a logarithmic stress dependency, as observed for soft clays, the power should be taken equal to 1.0. Janbu (1963) gives values of *m* around 0.5 for Norwegian sands and silts; for other soils, values of between 0.5 and 1 have been observed by von Soos (1980).

There are several limitations of the HS model. The HS model does not account for softening due to soil dilatancy and de-bonding effects. It is an isotropic hardening model in that it can model neither hysteretic/cyclic loading nor cyclic mobility. In order to model cyclic loading with good accuracy one would need a more complex model. The use of the HS model generally results in longer calculation time than the Mohr-Coulomb model since the material stiffness matrix is formed and decomposed in each calculation step.

3.3 Chicago Subway Renovation Project, USA

3.3.1 Project Overview

Chicago Subway Renovation Project (Finno et al. 2002) involved the installation of a brace-supported stiff excavation support system for the rehabilitation of a metro subway station. The rehabilitation included partial demolition of the existing dual subway tunnel tube and an expansion of the subway station. A 12-m deep excavation was carried out in soft-to-medium glacial clay. The excavation was supported by a 900-mm-thick secant pile wall, one level of cross-lot bracing and two levels of tiebacks (Figure 3.2).

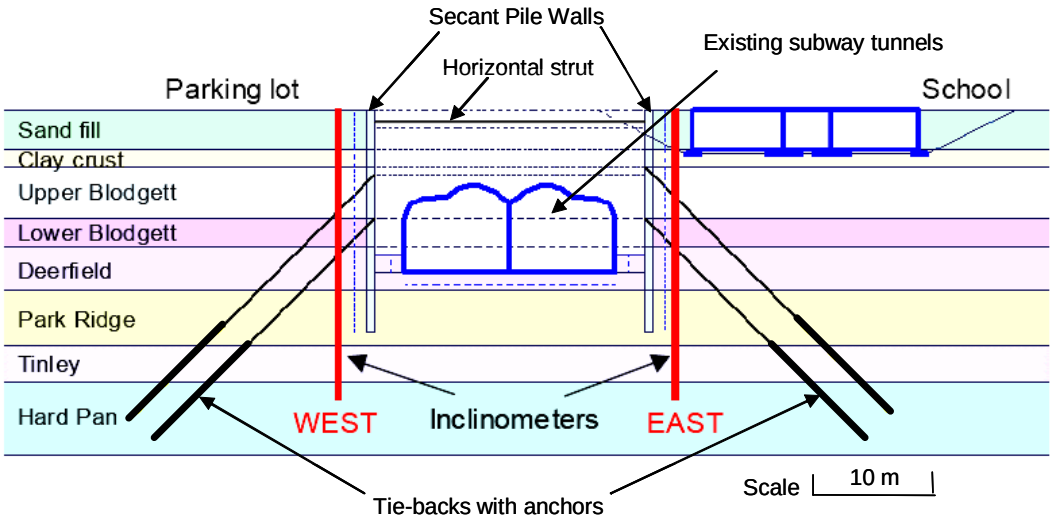

Figure 3.2 Section view of excavation support – Chicago Subway Renovation Project (after Calvello and Finno, 2004)

The project presented a major challenge for excavation due to the presence of a school building in the vicinity. The school was founded on shallow foundations located within 1.3 m

of the wall of the excavation. The bracing and anchoring support system was carefully designed to minimize the damage to the adjacent school. As expected in the planning phase, some minor damage occurred to non-load bearing portions of the building. Out of 28 mm of horizontal movement, 10 mm occurred during wall installation and 18 mm occurred during deep excavation as shown in Figure 3.3 (Finno et al. 2002).

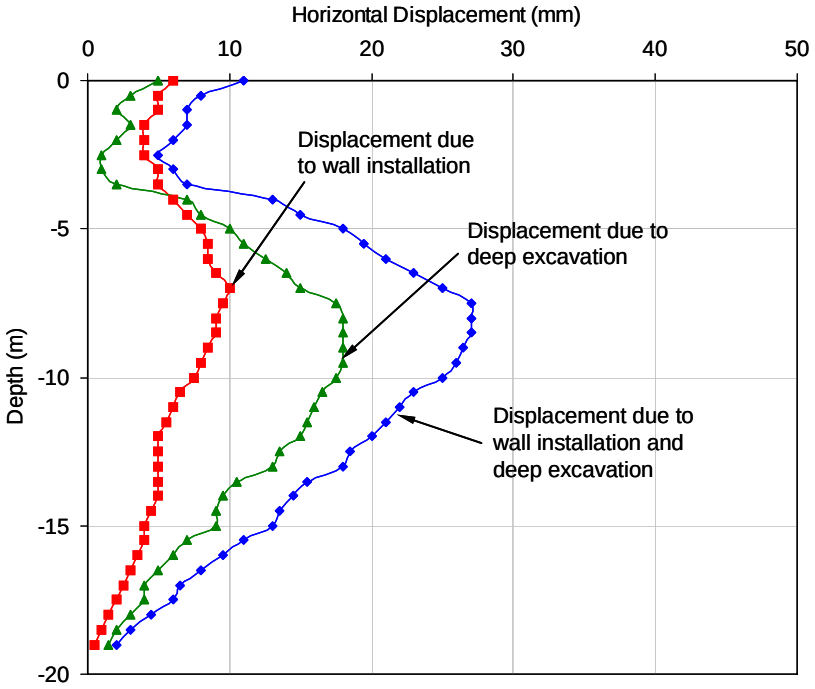

Figure 3.3 Chicago Subway Renovation Project - Observed horizontal displacement of the retaining wall (after Finno et al. 2002)

3.3.2 Geology and Stratigraphy

The site consists of a fill deposit overlying a sequence of glacial clays deposited during the Pleistocene period (Figure 3.2). The fill is mostly medium dense sand with construction debris in some parts. Beneath the fill lie four glacial clays, namely Upper and Lower Blodgett, Deerfield, and Park Ridge. With the exception of a clay crust in the upper portion of the Blodgett stratum, these deposits are lightly overconsolidated as a result of lowering groundwater levels after deposition and/or aging (Calvello 2002).

The Blodgett stratum consists of a desiccated crust and underlying soft clays with undrained shear strengths that increase with depth. This stratum is supraglacial in origin and is characterized by a relatively wide range of water contents and liquid limits. The Deerfield stratum consists of medium stiff clay and is characterized by uniform water contents. The Park Ridge stratum is a stiff to very stiff clay with lower water contents than the Deerfield stratum. Below the four glacial clays is the Tinley stratum, which consists of very stiff to hard clay and silts. The hard soils are encountered at around 18 m depth and are locally known as "Hard Pan" (Roboski 2001; Calvello 2002).

3.3.3 Modelling Assumptions

The following assumptions were made to achieve simplification of the modelling of deep excavation:

- All the deformations are assumed to occur in a plane strain condition even though the length to width ratio of the excavation was only 1.6.
- The geometry of the cross-section shown in Figure 3.2 is assumed to be symmetric about a vertical axis that passes through the web separating the two subway tunnels. In order to save on computational time, only the left half of the cross-section is modelled in PLAXIS. Strictly speaking, the cross-section is not symmetric because of the presence of the raft foundation for the school on the east side of the excavation; however, incorporation the raft foundation for the school in the model would have added unnecessary complexity to the model. It should, therefore, be noted that the results of the back analyses are not applicable to the east side of the cross-section.
- The effect of the construction of the subway tunnel on the surrounding ground is not modelled. The deformations due to tunnel construction are nullified by resetting the displacements to zero.
- The complex cross-section of the tunnel is replaced by a simple box cross-section.
- The retaining wall is modelled as wished-in-place, i.e. the unloading of the ground during the installation of secant pile wall is not modelled.
- Seepage analysis to establish ground water flow condition is not incorporated in the model. It is unlikely that there would be any significant ground water flow from the

surrounding ground into the deep excavation because the soil layers near the base of the excavation have fairly low permeability values and their behaviour is likely to be undrained during excavation. It should be pointed out that when seepage analysis is not incorporated in a PLAXIS model of deep excavation, the pore water pressures on either side of the retaining wall are considered equal as shown in Figure 3.4(a). By default, a submerged excavation is, therefore, simulated. In order to model a deep excavation that is dry, pore water pressure imbalance at the retaining wall must be created manually by using pressure boundary condition at the soil-structure interface of the retaining wall as shown in Figure 3.4(b).

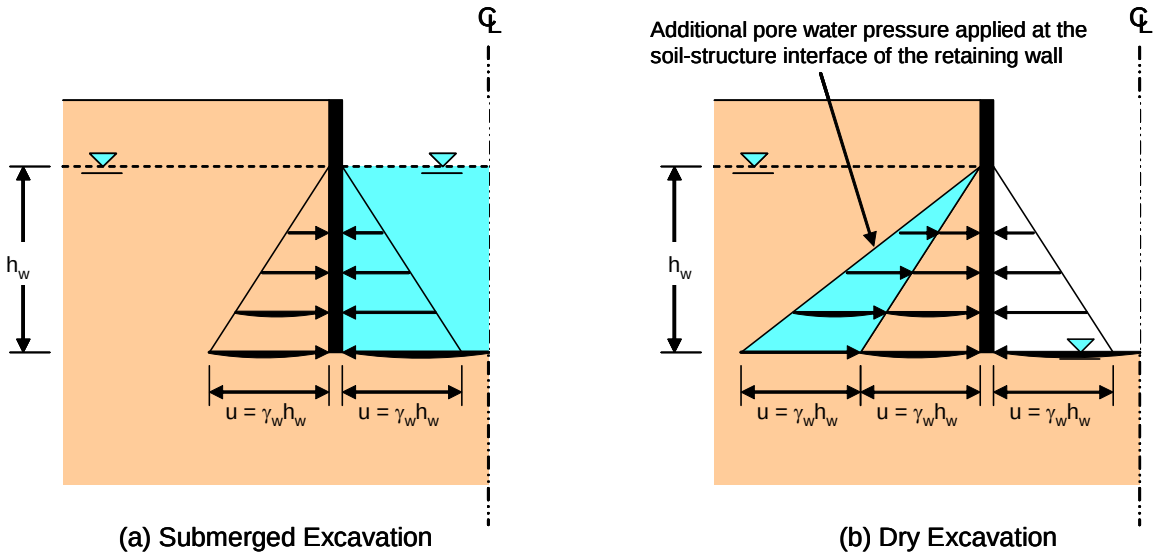

Figure 3.4 Simulation of submerged and dry excavation in PLAXIS

3.3.4 Simulation of Construction Stages

A detailed description of various construction stages for the Chicago Subway Renovation Project can be found in Calvello (2002), Finno et al. (2002) and Calvello and Finno (2004). For the purpose of back analysis, eight construction stages have been identified. Schematic drawings of these eight stages are shown in Figure 3.5. The details of construction activity for each stage are given in Table 3.1.

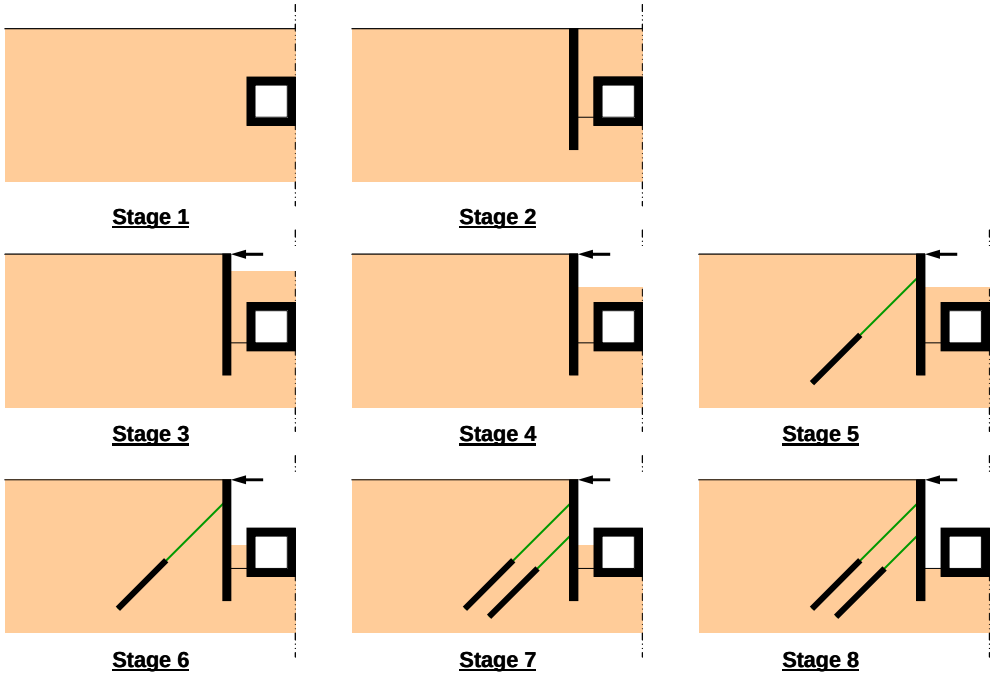

Figure 3.5 Schematic drawings of various stages of construction for Chicago Subway Renovation Project

Table 3.1 Details of various stages of construction for Chicago Subway Renovation Project

Stage	Activity	Description	Type of Calculation
1	Tunnel construction	Simulate tunnel construction.	Undrained plastic
		Allow consolidation. Reset ground deformations resulting from tunnel construction to zero.	Consolidation
2	Wall installation	Simulate installation of secant pile wall as wished-in-place.	Undrained plastic
		Allow consolidation. Reset ground deformation resulting from wall installation to zero.	Consolidation
3	Excavation and installation of props and anchors	Excavate first layer of soil [4.5 m]. Install horizontal prop.	Undrained plastic
4		Excavate second layer of soil [1.0 m].	Undrained plastic
5		Install first anchor rod and pre-stress it to 220 kN/m.	Undrained plastic
6		Excavate third layer of soil [4.0 m].	Undrained plastic
7		Install second anchor rod and pre-stress it to 290 kN/m.	Undrained plastic
8		Excavate the final layer of soil [2.5 m]	Undrained plastic

Simulation of tunnel construction (Stage 1) is achieved by removing the soil elements occupying the tunnel cross-sectional area and adding structural elements that represent the lining of the tunnel. There will inevitably be ground deformations in response to tunnel

construction; however, at the end of Stage 1, such ground deformations are reset to zero but the stress changes are retained. In this way, it is possible to achieve realistic stress distribution within the soil prior to the installation of retaining wall and its support system.

Simulation of installation of the secant pile retaining wall (Stage 2) is achieved in a manner similar to the installation of the tunnel lining, i.e. the structural elements representing the retaining wall are simply added to the finite element mesh, thereby achieving what is known as "wished-in-place" (WIP) modelling of retaining wall installation (De Moor 1994). WIP modelling does not take into account the unloading and subsequent deformation of the ground adjacent to the retaining wall. Such unloading and deformation of the ground during retaining wall installation can be modelled using a "wall-installation-modelled" (WIM) analysis (De Moor 1994); however, it is not a trivial task to conduct a WIM analysis using PLAXIS. It can be argued that the focus of the research is not the simulation of retaining wall installation but the effect of deep excavation on adjacent ground, and for this purpose, a WIP modelling of retaining wall installation is sufficient.

Excavation of soil layers (Stages 3, 4, 6, and 8) is achieved by removing the elements representing these soil layers. The stress change resulting from the removal of soil layers is subdivided into several small increments of stress change using the automatic load stepping option available in PLAXIS.

Installation of anchor (tie back) rods (Stages 5 and 7) is achieved by activating the structural elements representing the anchor rods. The grouted portion of an anchor rod is connected with adjacent finite element nodes using interface elements, and the remaining portion of the anchor rod is connected to the finite element mesh only at the end nodes. The pre-stressing option available in PLAXIS is used to apply a pre-stressing load on an anchor rod.

3.3.5 Back Analyses: Details and Results

3.3.5.1 Overview

Several different types of back analyses of the Chicago Subway Renovation Project deep excavation were conducted using PLAXIS. The details of these back analyses in terms of types of constitutive models used for various soil layers and their input parameters are provided in this Section. Table 3.2 gives a brief description of these back analyses.

Table 3.2 Brief descriptions of the back analyses of Chicago Subway Renovation Project deep excavations

Analysis Identifier	Analysis Description
CAL-D	Repetition of back analysis done by Calvello (2002); simulation of dry deep excavation; no simplification of stratigraphy; input parameters same as those used by Calvello (2002).
CAL-S	Same as CAL-D except for simulation of submerged deep excavation.
SIM-O	Simplification of stratigraphy by combining the clay crust, Upper Blogget, Lower Blogget, Deerfield and Park Ridge layers into one "soft glacial clay" layer with undrained shear strength linearly increasing with depth; simulation of dry deep excavation; stiffness parameters for the soft glacial clay layer obtained by matching the horizontal displacement of the retaining wall and the vertical settlement of the backfill with those computed using CAL-D.
SIM-M	Same as SIM-O except stiffness parameters for the soft clay layer adjusted by matching the horizontal displacement of the retaining wall and the vertical settlement of the backfill with those observed in the field.
SIM-NT	Same as SIM-M except there is no tunnel present inside the deep excavation.
SIM-C	Same as SIM-M except incorporation of waiting period between two successive excavation sequences.

3.3.5.2 Analysis CAL-D

Analysis CAL-D was a repetition of the back analysis conducted by Calvello (2002). Such repetition was necessary from the point-of-view of getting familiar with the operations of PLAXIS and for ensuring the validity of the simulation of construction stages described in Section 3.3.4. Analysis CAL-D simulated a dry deep excavation as explained in Section 3.3.3. Figure 3.6 shows the finite element mesh for analysis CAL-D.

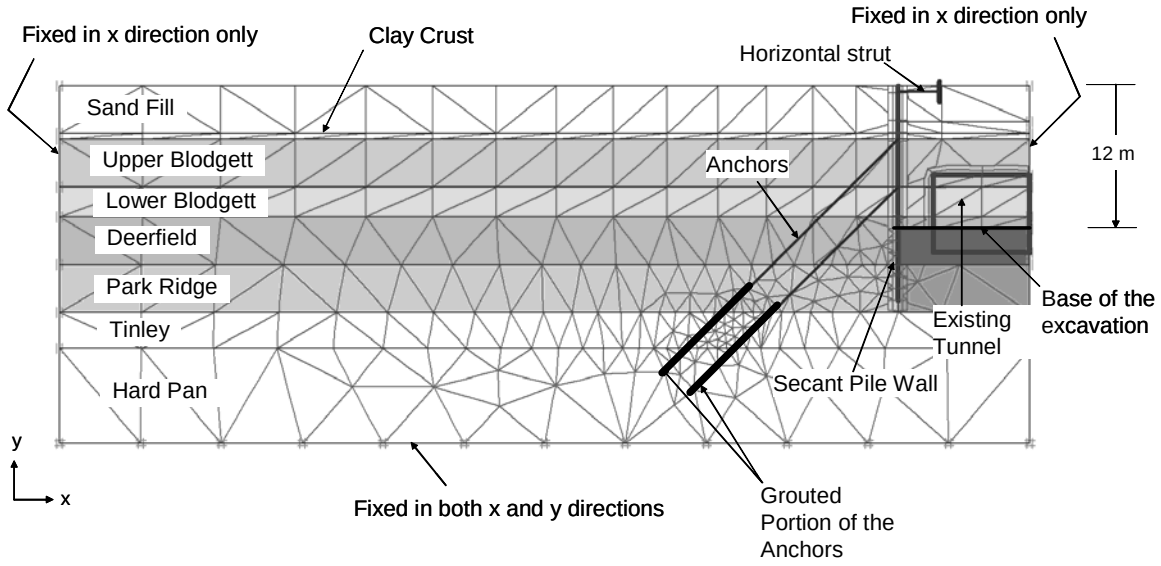

Figure 3.6 Finite element mesh used in analyses CAL-D and CAL-S

Constitutive models used for the various soil layers and their input parameters are given in Table 3.3. Input parameters for structural elements are given in Table 3.4.

Table 3.3 Input parameters for various soil layers for analyses CAL-D and CAL-S

Parameter	Symbol	Units	Sand Fill	Clay Layers						Hard Pan
				Clay Crust	Upper Blodgett	Lower Blodgett	Deerfield	Park Ridge	Tinley	
Model	-	-	MC	HS	HS	HS	HS	HS	HS	MC
Behaviour	-	-	D	U	U	U	U	U	U	U
Unit weight above water table	Γ_{unsat}	kN/m^3	17.0	17.7	16.1	16.1	16.9	17.6	17.6	18.4
Unit weight below water table	Γ_{sat}	kN/m^3	19.0	19.7	18.1	18.1	18.9	19.6	19.6	20.4
Horizontal permeability	K_x	cm/day	150	0.015	0.015	0.015	0.015	0.015	0.015	0.015
Vertical permeability	K_y	cm/day	150	0.0092	0.0092	0.0092	0.0092	0.0092	0.0092	0.0092
Secant stiffness modulus	E_{50}^{ref}	kPa	-	40500	4700	6000	6000	8000	12900	-
Oedometer stiffness modulus	E_{oed}^{ref}	kPa	-	28350	3290	4200	4200	6020	9030	-
Unload-reload modulus	E_{ur}^{ref}	kPa	-	121500	14100	18000	18000	25800	38700	-
Power for stress law	m	-	-	0.8	0.8	0.8	0.85	0.85	0.85	-
Reference mean stress	p^{ref}	kPa	-	100	100	100	100	100	100	-
Poisson's ratio	μ	-	0.33	0.2	0.35	0.35	0.35	0.35	0.2	0.2
Earth pressure coefficient	K_o	-	0.426	0.47	0.603	0.603	0.568	0.458	0.458	0.426
Cohesion intercept	c	kPa	2.0	1.0	1.0	1.0	1.0	1.0	1.0	100.0
Friction angle	ϕ	°	35.0	32.0	23.4	23.4	25.6	25.6	32.8	35.0
Dilatancy angle	ψ	°	5.0	0.0	0.0	0.0	0.0	0.0	0.0	3.0
Young's Modulus at the top of a layer	E_O	kPa	18000	-	-	-	-	-	-	147000
Rate of increase of Young's Modulus with depth	m_E	kPa/m	0.0	-	-	-	-	-	-	0.0
Strength Reduction Factor	R_f	-	-	0.9	0.9	0.9	0.9	0.9	0.9	-
Interface strength ratio	R_{int}	-	0.8	0.5	1.0	1.0	1.0	0.5	0.5	0.5

[Note: MC – Mohr-Coulomb Model; HS – Hardening Soil Model; D – Drained; U – Undrained.]

Table 3.4 Input parameters for structural elements for analyses CAL-D and CAL-S

Parameter	Symbol	Unit	Tunnel Lining	Secant Pile Wall	Grouted Anchor	Horizontal Strut	Top Anchor	Bottom Anchor
Modelled as	-	-	Plate	Plate	Anchor	Fixed Anchor	Anchor	Anchor
Type of behaviour	-	-	Elastic	Elastic	Elastic	Elastic	Elastic	Elastic
Normal stiffness	EA	kN/m	1.40E+07	6.50E+06	2.60E+05	6.75E+05	1.84E+05	2.30E+05
Flexural rigidity	EI	kNm^2/m	1.43E+05	1.00E+05	-	-	-	-
Equivalent thickness	d	m	0.35	0.43	-	-	-	-
Weight	w	kN/m	8.4	10.3	-	-	-	-
Poisson's ratio	μ	-	0.15	0.2	-	-	-	-
Spacing between anchors	L_s	m	-	-	1.5	6	1.5	1.5
Prestress force	-	kN/m	-	-	-	-	220	290

[Note: E – Young's modulus, A – cross-sectional area; I – moment of inertia.]

Figure 3.7 shows a comparison between the observed horizontal displacement of the retaining wall due to deep excavation and the horizontal displacement of the retaining wall computed by analysis CAL-D. Figure 3.8 shows a comparison between the observed ground settlement (east side of the excavation; underneath the raft foundation of the school) behind the retaining wall and the ground settlement computed by analysis CAL-D. It is clear that analysis CAL-D, which simulated a dry deep excavation, overestimated both the horizontal displacement of the retaining wall and the ground settlement behind the retaining wall considerably. This observation is not consistent with that reported by Calvello (2002), whose analysis provided reasonably close predictions of both horizontal displacement of the retaining wall and the ground settlement behind the retaining wall.

Although it is fairly obvious that the deep excavation must have been kept dry during construction for the purpose of installing tie back anchors, it could not be established whether a dry deep excavation was actually modelled. As explained in Section 3.3.3 above, the default option in PLAXIS is to treat a deep excavation as submerged. Perhaps, Calvello (2002) obtained good matching between the observed and computed results because of choosing this default option. It was, therefore, decided to conduct analysis CAL-S in which the same deep

excavation was modelled as submerged. The details and the results of analysis CAL-S are described in the next section.

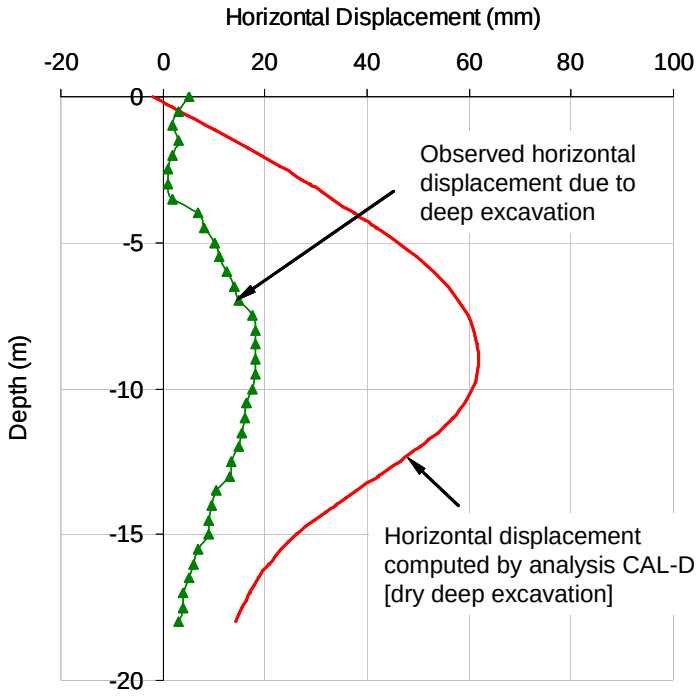

Figure 3.7 Observed and computed horizontal displacement of the retaining wall – Analysis CAL-D

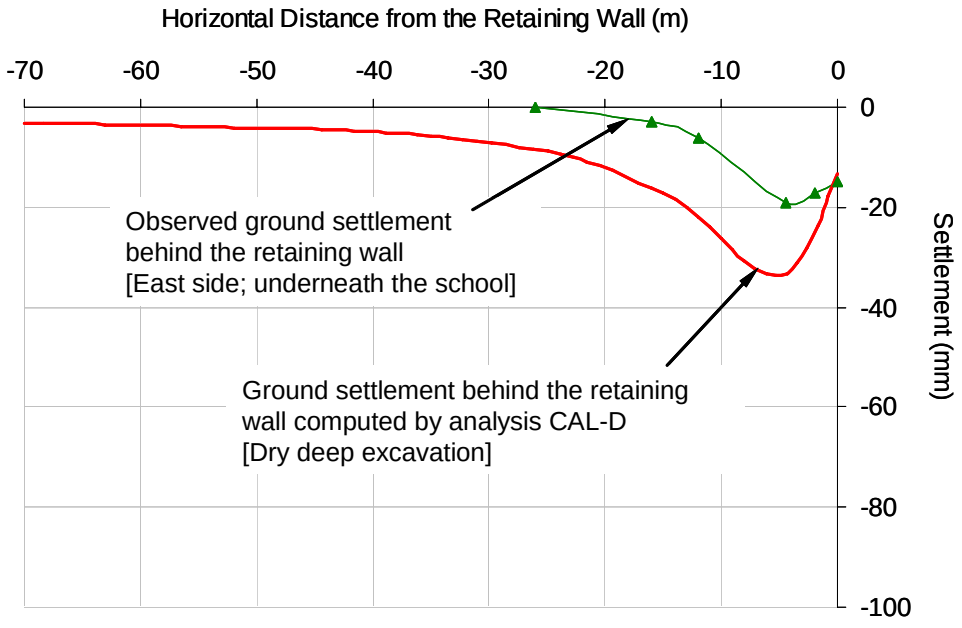

Figure 3.8 Observed and computed ground settlement behind the retaining wall – Analysis CAL-D

3.3.5.3 Analysis CAL-S

Analysis CAL-S was exactly the same as analysis CAL-D except that the deep excavation was modelled as submerged, i.e. there was no imbalance of pore-water pressure between the inside and the outside of the retaining wall. The finite element mesh for analysis CAL-S is shown in Figure 3.6. Constitutive models used for the various soil layers and their input parameters are given in Table 3.3. Input parameters for the structural elements are given in Table 3.4.

Figure 3.9 shows a comparison between the observed horizontal displacement of the retaining wall due to deep excavation and the horizontal displacement of the retaining wall computed by analysis CAL-S. Figure 3.10 shows a comparison between the observed ground settlement (east side of the excavation; underneath the raft foundation of the school) behind the retaining wall and the ground settlement computed by analysis CAL-S. It can be seen that the agreement between the observed and the computed horizontal displacement of the retaining wall is fairly close.

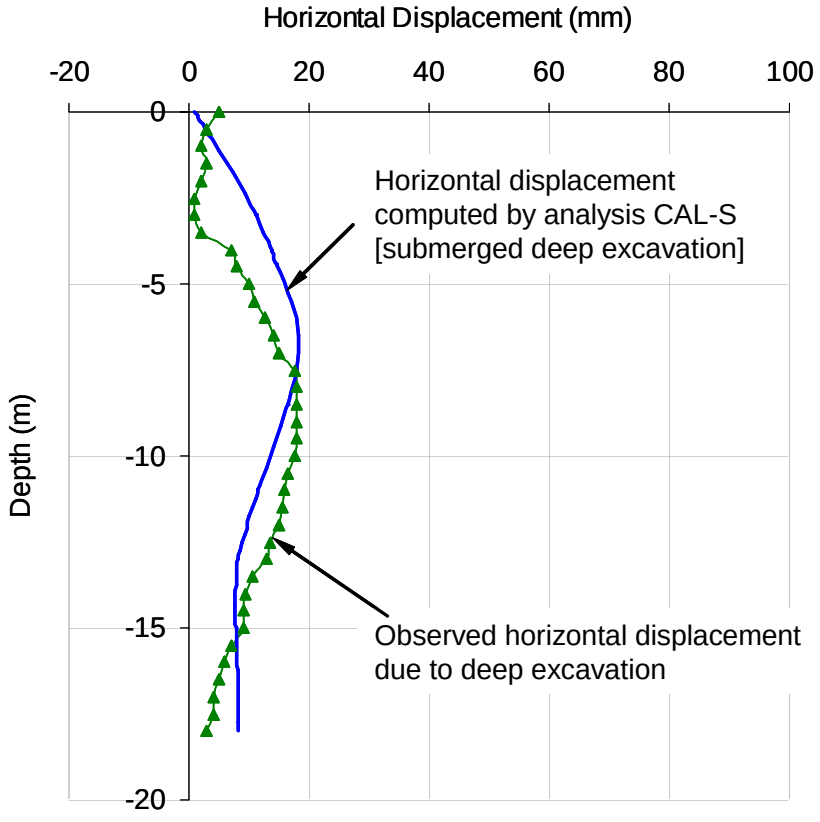

Figure 3.9 Observed and computed horizontal displacement of the retaining wall – Analysis CAL-S

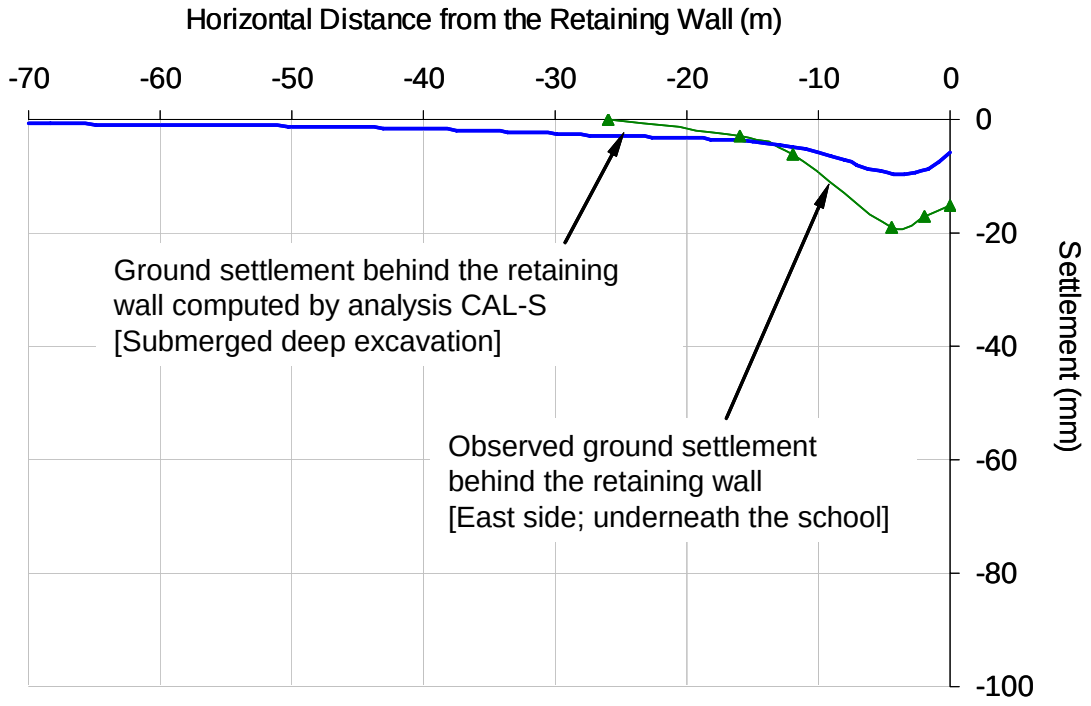

Figure 3.10 Observed and computed ground settlement behind the retaining wall – Analysis CAL-S

The values of computed ground settlement behind the retaining wall, however, are less than the observed ground settlement values. One possible reason for this discrepancy could be the fact that the observed ground settlement values were from the east side of the excavation, underneath the raft foundation for the school, and that the presence of school was not incorporated in any of the back analyses reported herein. The bearing pressure of the raft foundation for the school would have resulted in higher ground settlement behind the retaining wall.

The reasonably close agreement obtained between the observed and computed values of horizontal displacement and ground settlements by modelling the deep excavation as submerged, suggests that Calvello (2002) probably modelled the deep excavation as submerged instead of modelling it as dry. It also highlights potential pitfalls of using a finite element back analysis to calibrate soil parameters and the importance of accurate modelling of construction processes for such calibration.

3.3.5.4 Analysis SIM-O

Incorporation of reasonably accurate soil stratigraphy is important in a finite element back analysis of deep excavation. However, the greater the number of layers, the more difficult it is to quantify the effect of a parameter, e.g. soil stiffness or soil undrained shear strength, on overall behaviour of the structure. It was, therefore, decided to simplify the soil stratigraphy for the Chicago Subway Renovation Project by combining the five glaciated clay layers, i.e. clay crust, Upper Blodgett, Lower Blodgett, Deerfield and Park Ridge, into a single layer termed "soft glacial clay", and combining the Tinley and Hard Pan layers into another single layer termed "hard glacial clay". Analysis SIM-O was done using this simplified soil stratigraphy. The finite element mesh used for analysis SIM-O is shown in Figure 3.11.

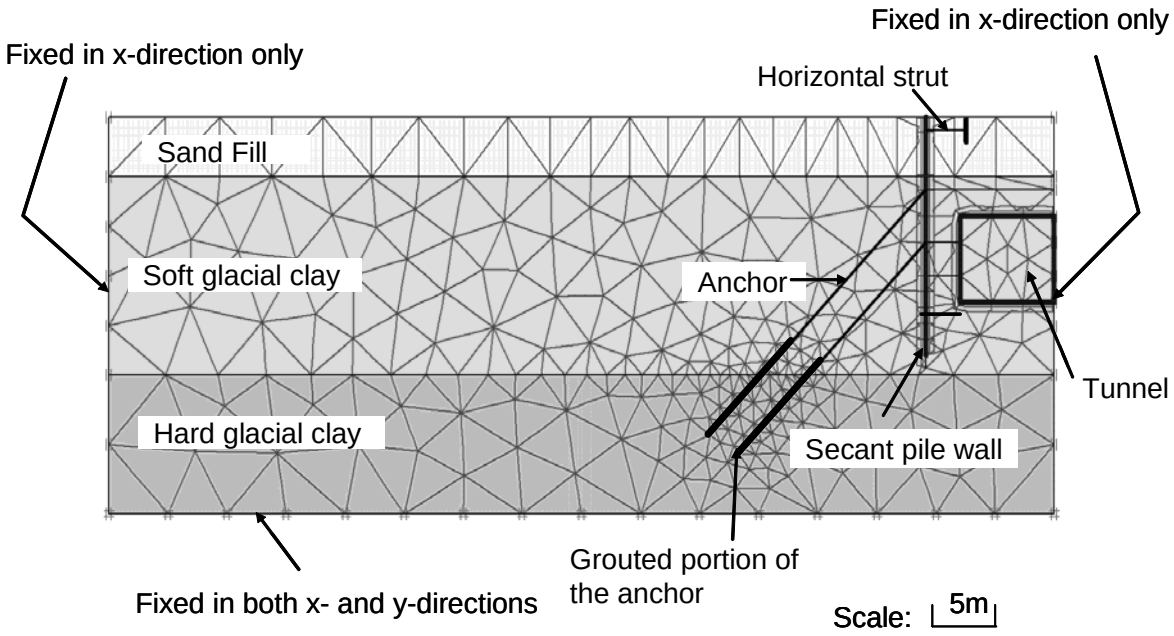

Figure 3.11 Finite element mesh for analyses SIM-O and SIM-M

The soft glacial clay layer and the hard glacial clay layer were modelled using the Hardening Soil model and the Mohr-Coulomb model, respectively. The behaviour of the soft glacial clay layer was modelled as undrained and its undrained shear strength was assumed to increase linearly with depth at a rate of 7.33 kPa/m. Such straight line variation of undrained shear strength with depth was obtained by fitting a straight line through undrained shear strength values of the five component strata obtained by Roboski (2001) using vane shear

testing, pocket penetrometer, unconfined compression tests and triaxial compression/extension tests, as shown in Figure 3.12. The undrained shear strength at the top of the soft glacial clay layer was taken equal to 20 kPa.

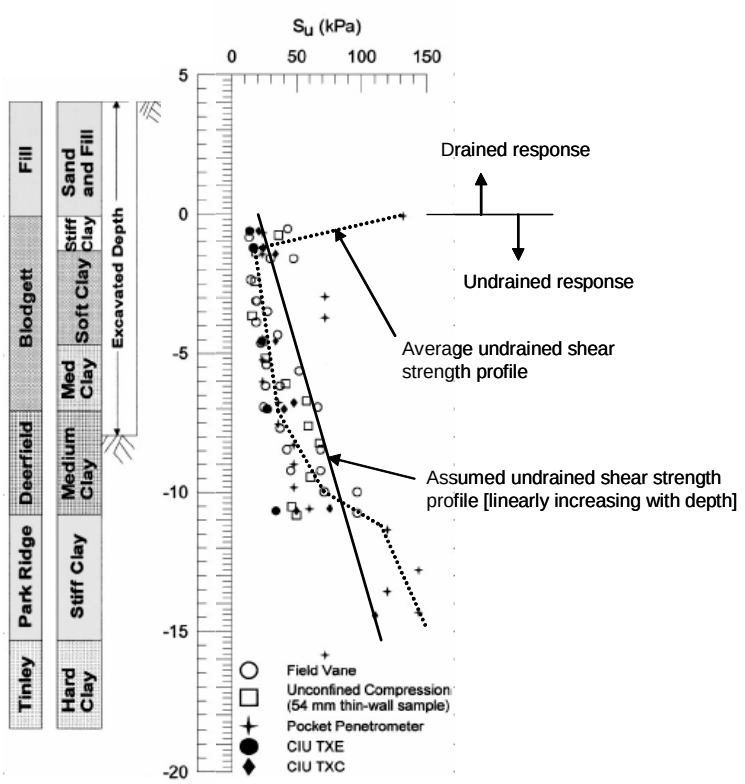

Figure 3.12 Undrained shear strength profile for analysis SIM-O (after Roboski, 2001)

The sequence of construction modelled in analysis SIM-O was exactly the same as that used for analysis CAL-D (see Figure 3.5 and Table 3.1). The input parameters for the three soil layers and the structural elements for analysis SIM-O are given in Table 3.5 and Table 3.6, respectively. For the hard glacial clay layer, the soil parameters were obtained by taking average of soil parameters for the Tinley and Hard Pan strata. For the soft glacial clay, the soil parameters (with the exception of undrained shear strength) were obtained using a calibration procedure in which the horizontal displacement of the retaining wall computed using analysis SIM-O was matched with that computed by analysis CAL-D. The matching was achieved by adjusting only the reference secant stiffness, E_{50}^{ref}, for the soft glacial layer (shown shaded in Table 3.5). The reference oedometer stiffness, E_{oed}^{ref}, was taken equal to the reference secant

stiffness and the reference unload-reload stiffness, E_{ur}^{ref}, was taken equal to three times the reference secant stiffness. Theoretically, soil stiffness parameters for each of the three layers must be calibrated using the matching procedure described above; however, the overall behaviour of the retaining wall and the surrounding ground would be dominated by the soft glacial clay layer because:

- this layer has the least stiffness and strength; and,
- the deep excavation is located almost entirely within this layer.

Table 3.5 Soil input parameters for analysis SIM-O

Parameter	Symbol	Units	Sand Fill	Soft Glacial Clay	Hard Glacial Clay
Model			Mohr-Coulomb	Hardening Soil	Mohr-Coulomb
Behaviour			Drained	Undrained	Undrained
Unit weight above water table	γ_{unsat}	kN/m^3	17.0	16.4	18.0
Unit weight below water table	γ_{sat}	kN/m^3	19.0	18.4	20.0
Horizontal permeability	K_x	cm/day	150	0.01	0.01
Vertical permeability	K_y	cm/day	150	0.01	0.01
Reference secant stiffness	E_{50}^{ref}	kPa	-	2900	-
Reference oedometer stiffness	E_{oed}^{ref}	kPa	-	2900	-
Reference unload-reload stiffness	E_{ur}^{ref}	kPa	-	8700	-
Power for stress law	m	-	-	1.0	-
Reference mean stress	p^{ref}	kPa	-	100	-
Poisson's ratio	μ	-	0.33	0.35*	0.33
Earth pressure coefficient	K_o	-	0.52	0.52	0.52
Cohesion intercept	c	kPa	2.0	-	130.0
Friction angle	ϕ	°	35.0	-	35.0
Dilatancy angle	ψ	°	5.0	-	5.0
Undrained Shear Strength at the top of the layer	S_{UO}	kPa	-	20	-
Young's Modulus at the top of the layer	E_O	kPa	18000	-	65000
Strength reduction factor	R_f	-	-	0.7	-
Interface strength ratio	R_{int}	-	0.8	0.8	0.8
Rate of increase of undrained shear strength with depth	m_C	kPa/m	-	7.33	-
Rate of increase of Young's Modulus with depth	m_E	kPa/m	0	-	500

[Note: *Effective Poisson's ratio; PLAXIS automatically selects a value of 0.495 if undrained option is specified.]

Table 3.6 Input parameters for structural elements – Analyses SIM-O and SIM-M

Parameter	Symbol	Unit	Tunnel Lining	Secant Pile Wall	Grouted Anchor	Horizontal Strut	Top Anchor	Bottom Anchor
Modelled as	-	-	Plate	Plate	Anchor	Fixed Anchor	Anchor	Anchor
Type of behaviour	-	-	Elastic	Elastic	Elastic	Elastic	Elastic	Elastic
Normal stiffness	EA	kN/m	1.40E+07	6.50E+06	2.60E+05	6.75E+05	1.84E+05	2.30E+05
Flexural rigidity	EI	kNm^2/m	1.43E+05	1.00E+05	-	-	-	-
Equivalent thickness	d	m	0.35	0.43	-	-	-	-
Weight	w	kN/m	8.4	10.3	-	-	-	-
Poisson's ratio	μ	-	0.15	0.2	-	-	-	-
Spacing between anchors	L_s	m	-	-	1.5	6	1.5	1.5
Prestress force	-	kN/m	-	-	-	-	220	290

[Note: E – Young's modulus, A – cross-sectional area; I – moment of inertia.]

Figure 3.13 shows the distributions of horizontal displacement of the retaining wall with depth computed by analysis SIM-O (E_{50}^{ref} = 2900 kPa) and analysis CAL-D. The match is quite good up to 9 m depth. Beyond 9 m depth, the horizontal displacements computed by analysis SIM-O are more than those computed by analysis CAL-D. Poor matching beyond 9 m depth can be attributed to the fact that the stiffness of the soft glacial clay layer used in analysis SIM-O is less than the stiffness of Deerfield and Park Ridge strata used in analysis CAL-D. Given that the deep excavation is only 12 m deep, it is encouraging to see good matching of horizontal displacements computed by analyses SIM-O and CAL-D for most of the depth of excavation.

Figure 3.14 shows the distributions of ground settlement behind the retaining wall computed by analyses SIM-O and CAL-D. It can be seen that the matching is reasonably good for a horizontal distance of up to 70 m from the retaining wall even though matching of ground settlement was not sought in the calibration procedure described above. Good matching of both the horizontal displacement of the retaining wall and the ground settlement behind the retaining wall between analyses SIM-O and CAL-D suggests that analysis SIM-O, which was conducted using a simplified stratigraphy, was able to capture the pattern of ground deformation around the deep excavation satisfactorily. It should now be possible to increase

the E_{50}^{ref} value of the soft glacial clay layer to match the observed horizontal displacement of the retaining wall; this is done using analysis SIM-M described in the next section.

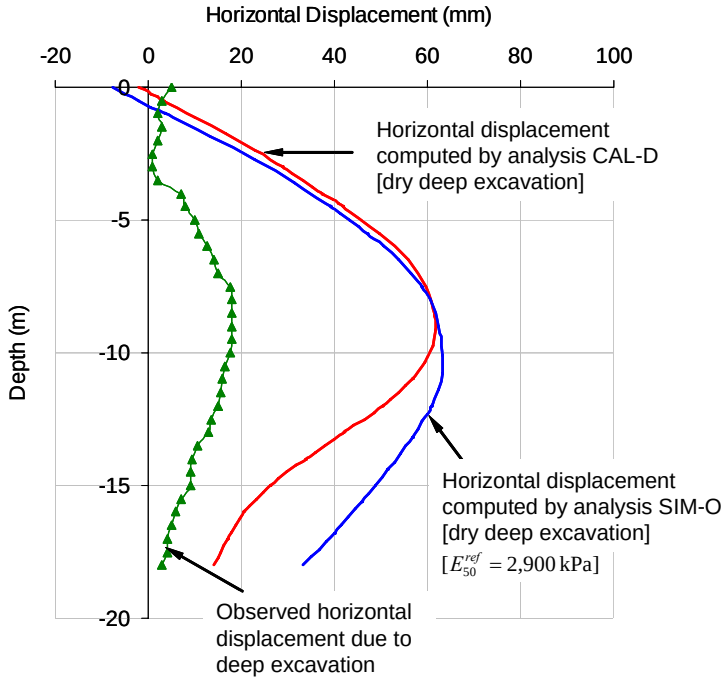

Figure 3.13 Matched horizontal displacement of the retaining wall – analyses SIM-O and CAL-D

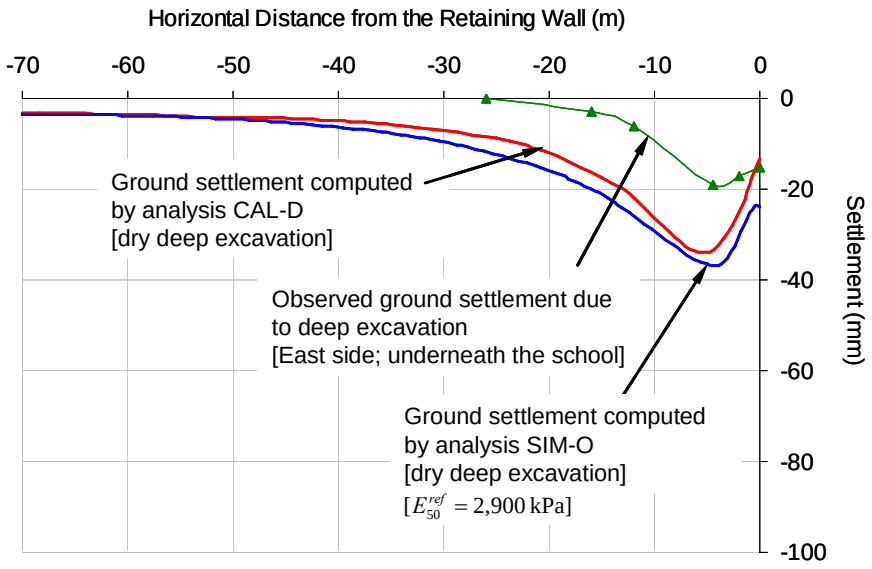

Figure 3.14 Matched ground settlement behind the retaining wall – analyses SIM-O and CAL-D

3.3.5.5 Analysis SIM-M

Analysis SIM-M was exactly the same as analysis SIM-O except for the value of reference secant stiffness, E_{50}^{ref}, for soft glacial clay, which was increased in steps until the computed values of horizontal displacement of the retaining wall matched reasonably well with the observed values. A reasonably good match between computed and observed horizontal displacement values was obtained for E_{50}^{ref} = 17000 kPa as shown in Figure 3.15. The matching of computed and observed ground settlement behind the retaining wall, however, was not as good as the matching of horizontal displacement (Figure 3.16). As explained in Section 3.3.5.3, the observed ground settlement profile was obtained from the east side of the deep excavation underneath the raft foundation of the school, and therefore, it was probably affected by the bearing pressure of the raft foundation. In other words, ground settlements on the west side of the excavation, which were not monitored, would have been considerably less than those observed underneath the raft foundation of the school and would have plotted reasonably close to those computed by analysis SIM-M. It can, therefore, be concluded that both the pattern and the magnitude of ground deformation around the deep excavation can be controlled reasonably accurately using the stiffness of soft glacial clay.

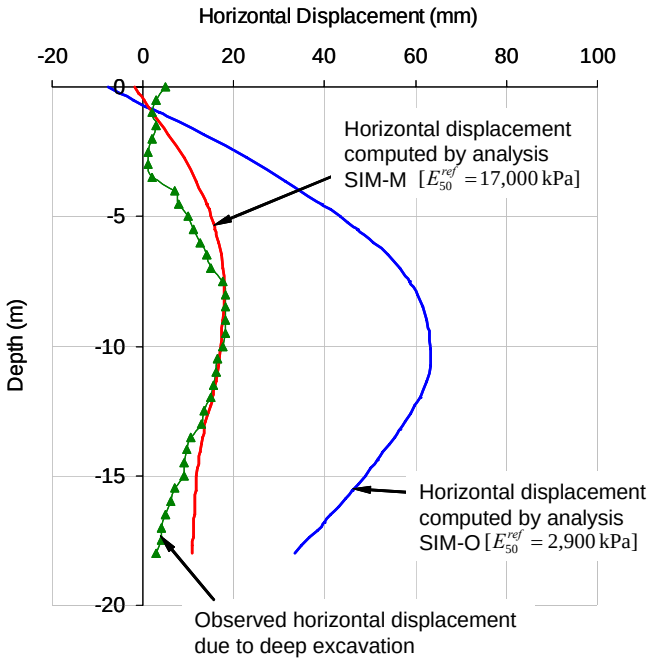

Figure 3.15 Horizontal displacement of the retaining wall computed by analyses SIM-O and SIM-M

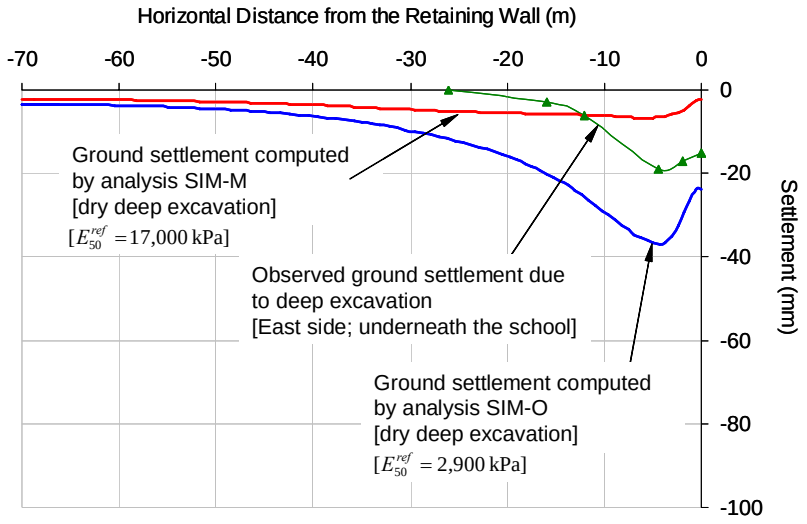

Figure 3.16 Ground settlement behind the retaining wall computed by analyses SIM-O and SIM-M

3.3.5.6 Analysis SIM-NT

The deep excavation for Chicago Subway Renovation Project is unusual because of the presence of a tunnel inside the deep excavation. It is important to quantify the effect of the presence of this tunnel inside the deep excavation; therefore, analysis SIM-NT, which had no tunnel inside the deep excavation, was conducted. The results obtained from analysis SIM-NT were compared with those obtained from analysis SIM-M, which had tunnel inside the deep excavation.

Figure 3.17 shows the distribution of horizontal displacement of the retaining wall with depth computed by analyses SIM-NT and SIM-M. It is evident from Figure 3.17 that the tunnel provides some lateral support to the retaining wall, thereby reducing its horizontal displacement. There could be two ways in which the tunnel provides this lateral support:

- The tunnel applies a vertical overburden pressure (corresponding to its self-weight) on top of the base of the excavation. Consequently, the base of the excavation heaves less compared with a deep excavation with no tunnel present, resulting in less horizontal displacement of the wall. This could be the reason for smaller horizontal displacement of the retaining wall below the base of the excavation for the case of tunnel inside the deep excavation (analysis SIM-M) compared with the no tunnel case (analysis SIM-NT).

- The lining (portal) of the tunnel itself acts like an earth retaining structure and mobilizes passive resistance. This passive resistance provides lateral support to the retaining wall, resulting in a reduction in its horizontal displacement. This could be the reason for smaller horizontal displacement of the retaining wall above the base of the excavation for the case of tunnel inside the deep excavation (analysis SIM-M) compared with the no tunnel case (analysis SIM-NT).

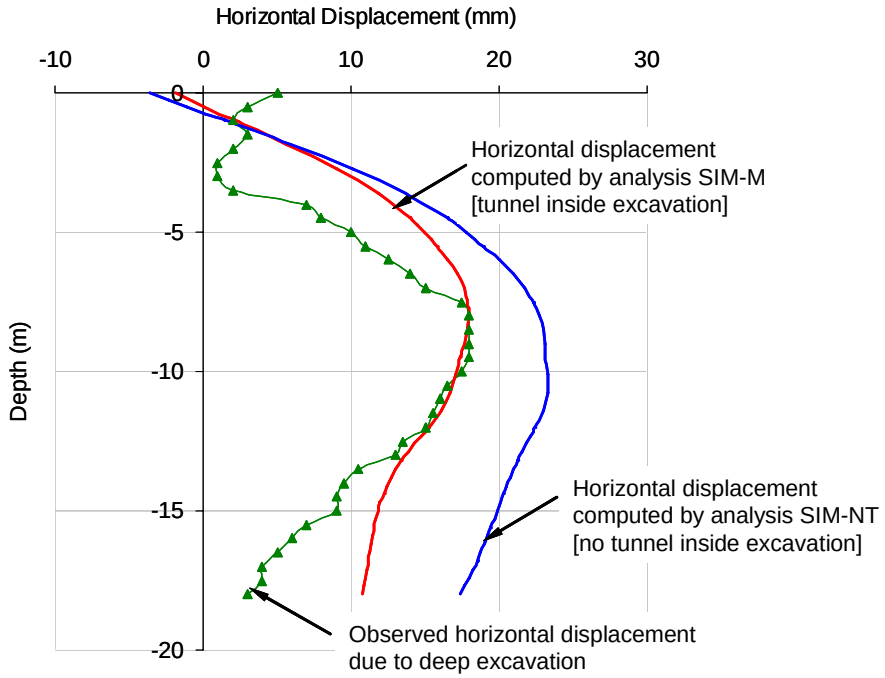

Figure 3.17 Horizontal displacement of the tunnel computed by analyses SIM-NT and SIM-M

3.3.5.7 Analysis SIM-C

For a deep excavation having dimensions comparable to the deep excavation for Chicago Subway Renovation Project, there is usually a waiting period between two successive excavations of soil layers. During this waiting period, several important activities take place, such as dewatering of the excavation, installation of struts, braces and anchors, etc. If the permeability of the ground is sufficiently high, excess pore-water pressures induced by the excavation could potentially dissipate, resulting in consolidation (and deformation) of the surrounding ground. On the other hand, if the ground is fairly impermeable (i.e., having

hydraulic conductivity less than 10^{-7} m/s), there is very little change in pore-water pressure during the waiting period and the behaviour of the ground can be modelled as undrained.

There were several waiting periods for the Chicago Subway Renovation Project deep excavation (Finno et al. 2002). It was, therefore, decided to conduct analysis SIM-C, which modelled consolidation of the surrounding ground during waiting periods between successive excavation sequences. The results of analysis SIM-C were then compared with the results of analysis SIM-M in which there was no waiting period between successive excavation sequences. Figure 3.18 shows the distribution of horizontal displacement of the retaining wall computed by analyses SIM-C and SIM-M.

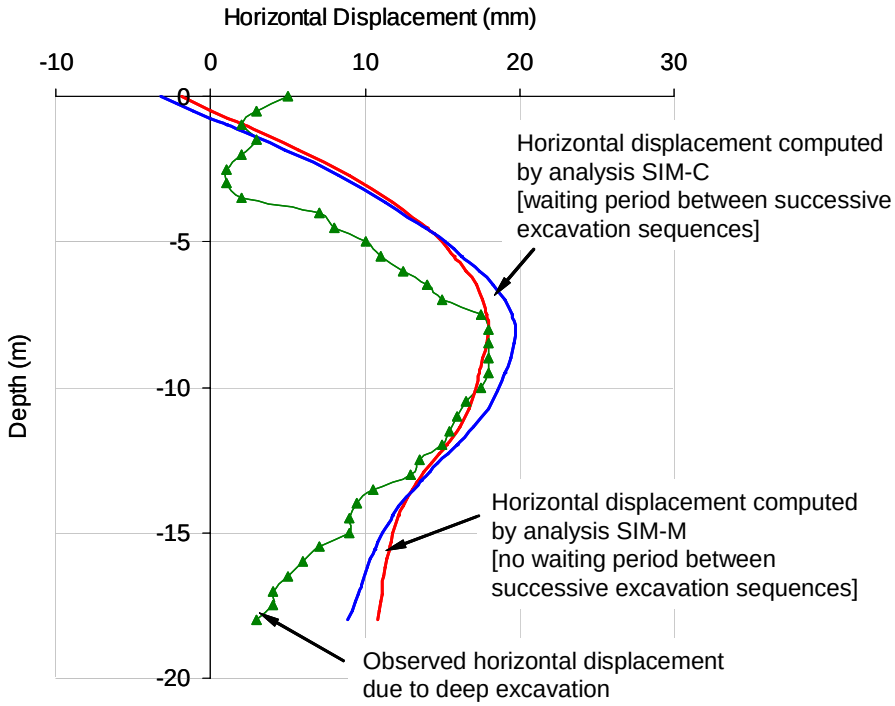

Figure 3.18 Horizontal displacement of the retaining wall computed by analyses SIM-C and SIM-M

It can be seen from Figure 3.18 that there is a slight increase in the maximum horizontal displacement of the retaining wall above the base of the excavation and a slight decrease in the horizontal displacement of the retaining wall below the base of the excavation when consolidation during waiting periods is modelled. The increase in the maximum horizontal displacement of the wall above the base of the excavation is likely due to

consolidation settlement of the ground behind the retaining wall. The decrease in the horizontal displacement of the retaining wall below the base of the excavation could be possible because of the stiffening of the ground underneath the tunnel caused by dissipation of excess pore-water pressures during the waiting periods. For all practical purposes, however, the effect of modelling consolidation of the surrounding ground during waiting periods is not significant, and therefore, analysis SIM-M, which does not incorporate waiting periods between successive excavation sequences, can be considered to model the overall behaviour of the deep excavation adequately.

3.3.5.8 Summary

Several different back analyses were conducted of the deep excavation for Chicago Subway Renovation Project. Actual stratigraphy of the ground was incorporated in first two of these analyses. The remaining analyses were done using a simplified stratigraphy. The following key observations can be made based on the results of these back analyses:

- It is important to model construction processes accurately when using back analyses of instrumented case histories to calibrate soil parameters. The modeller must be aware of specific procedures prescribed by the modelling software to model these construction sequences.
- It is possible to capture both the pattern and the magnitude of ground deformation around a deep excavation using a simplified stratigraphy obtained by grouping several successive soil layers into one layer provided there is some physical basis for such grouping and the combined layer dominates the overall behaviour of the ground. The physical basis could be the common origin of these soil layers or common type of soil behaviour. In case of Chicago Subway Renovation Project, the grouping was done on the basis of the observation that all the grouped layers were clays of glacial origin which exhibited undrained shear strength of linearly increasing with depth.
- Deep excavation is a relatively fast construction activity that can be modelled by assuming undrained behaviour of the surrounding ground, provided the average permeability of the surrounding ground is sufficiently low.

3.3.6 Parametric Study

3.3.6.1 Overview

In this Section, the details and the results of a parametric study based on the Chicago Subway Renovation Project deep excavation are presented. The following parameters were varied:

- Reference secant stiffness of the soft glacial clay layer [E_{50}^{ref}]
- Undrained shear strength at the top of the soft glacial clay layer [S_{UO}]
- Stiffness of the secant pile wall represented by its thickness [t_R]

When one of the above three parameters was varied, the other two parameters were kept constant. The effect of varying a parameter was quantified by obtaining the variation in the following three quantities:

- Maximum horizontal displacement of the retaining wall [$\delta h_{\max}$]
- Maximum ground settlement behind the retaining wall [$\delta v_{\max}$]
- Maximum bending moment in the retaining wall [$BM_{\max}$]

For all the analyses conducted for the purpose of this parametric study, the following quantities or features were kept the same:

- Rate of increase of undrained shear strength with depth (m_C = 7.33 kPa/m)
- All the parameters for the other two soil layers, i.e. sand fill and hard glacial clay
- Parameters and locations of all the structural components such as tunnel lining, horizontal strut, anchors, etc.
- Depth of excavation (H = 12 m)
- Construction sequences (as described in Section 3.3.4)
- Finite element mesh (as shown in Figure 3.11)

Since analysis SIM-M (Section 3.3.5.5) which incorporated a simplified stratigraphy, was able to reproduce both the pattern and the magnitude of ground deformation for the deep excavation, it was used as the base case for the parametric study. The values of the three parameters for the base case were:

- $[E_{50}^{ref}]_{BC}$ = 16000 kPa
- $[S_{UO}]_{BC}$ = 40 kPa
- $[t_R]_{BC}$ = 1.0 m

The results of the parametric study are presented in terms of normalized changes in parameters and the affected quantities as shown in Table 3.7. When the value of a parameter is smaller than its value for the base case, the normalized change in that parameter is negative. Similarly, when the value of a parameter is greater than its value for the base case, the normalized change in that parameter is positive. The results for the base case always plot at the origin. For example, if the undrained shear strength of the soil for the base case analysis is 40 kPa and it is reduced to 30 kPa, the normalized change in undrained shear strength will be (30-40)/40 = - 0.25 or 25 per cent decrease in strength. If, on the other hand, the undrained shear strength is increased to 50 kPa, the normalized change in undrained shear strength will be (50-40)/40 = +0.25 or 25 per cent increase in strength.

Table 3.7 Normalized changes in parameters and quantities for the Chicago Subway Renovation Project parametric study

Parameter or quantity	Symbol	Formula
Normalized change in reference secant stiffness	ΔE_N	$\Delta E_N = \frac{E_{50}^{ref} - \left[E_{50}^{ref}\right]_{BC}}{\left[E_{50}^{ref}\right]_{BC}}$
Normalized change in undrained shear strength at the top of soft glacial clay layer	ΔS_N	$\Delta S_N = \frac{S_{UO} - \left[S_{UO}\right]_{BC}}{\left[S_{UO}\right]_{BC}}$
Normalized change in thickness of the secant pile retaining wall	Δt_N	$\Delta t_N = \frac{t_R - \left[t_R\right]_{BC}}{\left[t_R\right]_{BC}}$
Normalized change in maximum horizontal displacement of the retaining wall	Δh_N	$\Delta h_N = \frac{\delta h_{max} - \left[\delta h_{max}\right]_{BC}}{\left[\delta h_{max}\right]_{BC}}$
Normalized change in maximum ground settlement behind the retaining wall	Δv_N	$\Delta v_N = \frac{\delta v_{max} - \left[\delta v_{max}\right]_{BC}}{\left[\delta v_{max}\right]_{BC}}$
Normalized change in maximum bending moment in the retaining wall	ΔBM_N	$\Delta BM_N = \frac{BM_{max} - \left[BM_{max}\right]_{BC}}{\left[BM_{max}\right]_{BC}}$

3.3.6.2 Effect of Change in Soil Stiffness

Table 3.8 gives the range of values for the reference secant stiffness (referred to as "soil stiffness" from this point onwards) used in the parametric study.

Table 3.8 Range of values for reference secant soil stiffness used in the parametric study

Parameter	Units	Range of Values used in the Parametric Study								
E_{50}^{ref}	kPa	4000	8000	12000	16000	20000	24000	28000	32000	48000
ΔE_N	-	-0.75	-0.5	-0.25	0.00	0.25	0.50	0.75	1.00	2.00

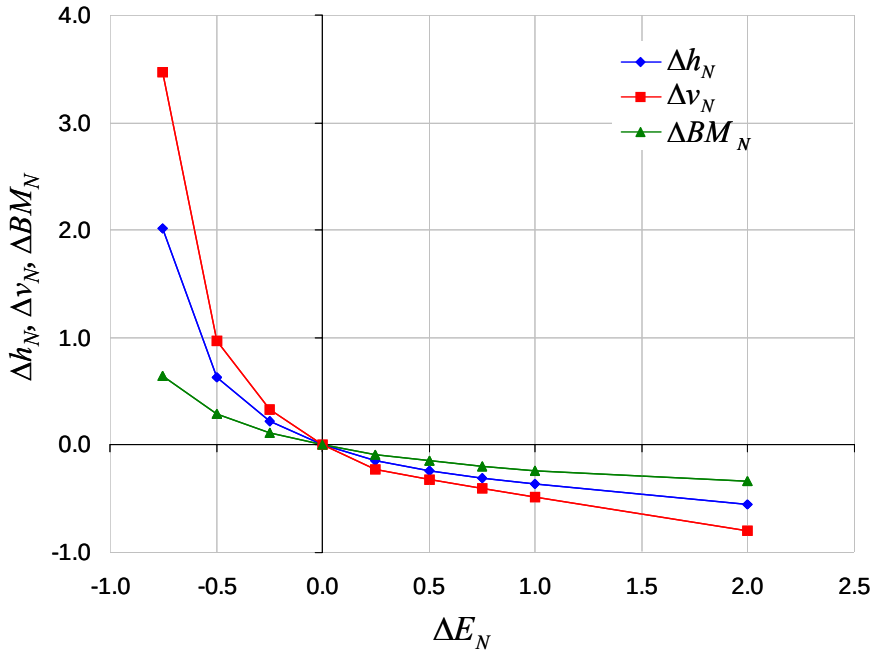

Figure 3.19 Effect of change in soil stiffness on horizontal displacement of the retaining wall, ground settlement behind the retaining wall and bending moment in the retaining wall

Figure 3.19 shows the effect of change in soil stiffness on the maximum horizontal displacement of the retaining wall, maximum ground settlement behind the retaining wall and the maximum bending moment induced in the retaining wall due to deep excavation. A significant increase in the ground deformation around the deep excavation is observed when the soil stiffness is decreased from its value for the base case. The maximum bending moment in the retaining wall also increases in response to decrease in soil stiffness; however, the

increase in maximum bending moment is less than the increase in horizontal displacement or ground settlement. Similarly, a decrease in ground deformation and a decrease in bending moment in the retaining wall are observed when the soil stiffness is increased from its value for the base case; however, the effect of increasing the soil stiffness is much less compared with the effect of decreasing the soil stiffness.

3.3.6.3 Effect of Change in Soil Undrained Shear Strength

Table 3.9 gives the range of values of undrained shear strength at the top of the soft glacial clay layer used in the parametric study. As mentioned before, the rate of increase of undrained shear strength with depth was kept constant at 7.33 kPa/m for the entire parametric study.

Figure 3.20 shows the effect of change in soil undrained shear strength on the maximum horizontal displacement of the retaining wall, maximum ground settlement behind the retaining wall and the maximum bending moment induced in the retaining wall due to deep excavation.

Table 3.9 Range of values for soil undrained shear strength used in the parametric study

Parameter	Units	Range of Values used in the Parametric Study						
S_{UO}	kPa	20	30	40	50	60	70	80
ΔS_N	-	-0.50	-0.25	0.00	0.25	0.50	0.75	1.00

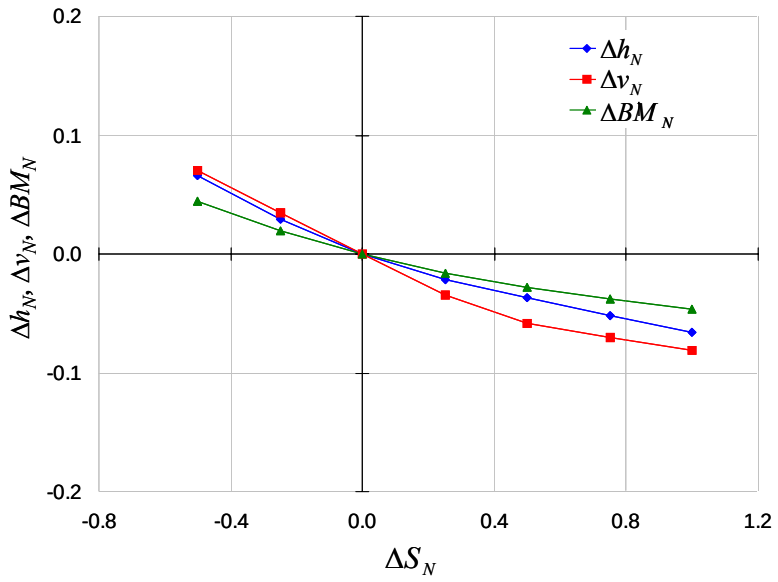

Figure 3.20 Effect of change in soil undrained shear strength on horizontal displacement of the retaining wall, ground settlement behind the retaining wall and bending moment in the retaining wall

It is evident from Figure 3.20 that change in soil undrained shear strength only marginally affects the magnitude of ground deformation and the bending moment in the retaining wall. A change in undrained shear strength from -50% to +100% has resulted in less than ±10% change in horizontal displacement, ground settlement and bending moment. This result is not surprising because the ground surrounding the deep excavation is not close to failure, and therefore, its response to deep excavation is influenced much more by change in soil stiffness compared with change in soil undrained shear strength.

3.3.6.4 Effect of Change in Thickness of the Retaining Wall

Table 3.10 gives the range of values for the thickness of the retaining wall used in the parametric study. Since the Young's modulus of the retaining wall was kept unchanged for all the analyses, a change in thickness of the retaining wall represents a change in both the bending stiffness and the axial stiffness of the retaining wall.

Table 3.10 Range of values for the thickness of the retaining wall used in the parametric study

Parameter	Units	Range of Values used in the Parametric Study						
t_R	m	0.4	0.6	0.8	1.0	1.2	1.4	1.6
Δt_N	-	-0.6	-0.4	-0.2	0.0	0.2	0.4	0.6

Figure 3.21 shows the effect of change in thickness of the retaining wall on the maximum horizontal displacement of the retaining wall, maximum ground settlement behind the retaining wall and the maximum bending moment induced in the retaining wall due to deep excavation. It can be seen from Figure 3.21 that the effect of change in thickness of the retaining wall is not as prominent as the change in soil stiffness; however, it is more significant than the effect of change in soil undrained shear strength. It is interesting to note that the maximum bending moment in the retaining wall increases but the horizontal displacement of the retaining wall decreases when the thickness of the retaining wall is increased. Clearly, a thicker retaining wall is able to resist horizontal deformation better but at the expense of inducing greater bending moment. In other words, a stiffer retaining wall also needs greater bending strength. It is also worth noting that the horizontal displacement of the retaining wall does not reduce appreciably but the maximum bending moment continues to increase when the thickness of the retaining wall is increased by more than 40%. This implies

that it is not useful to increase the stiffness of the retaining wall beyond a certain maximum value.

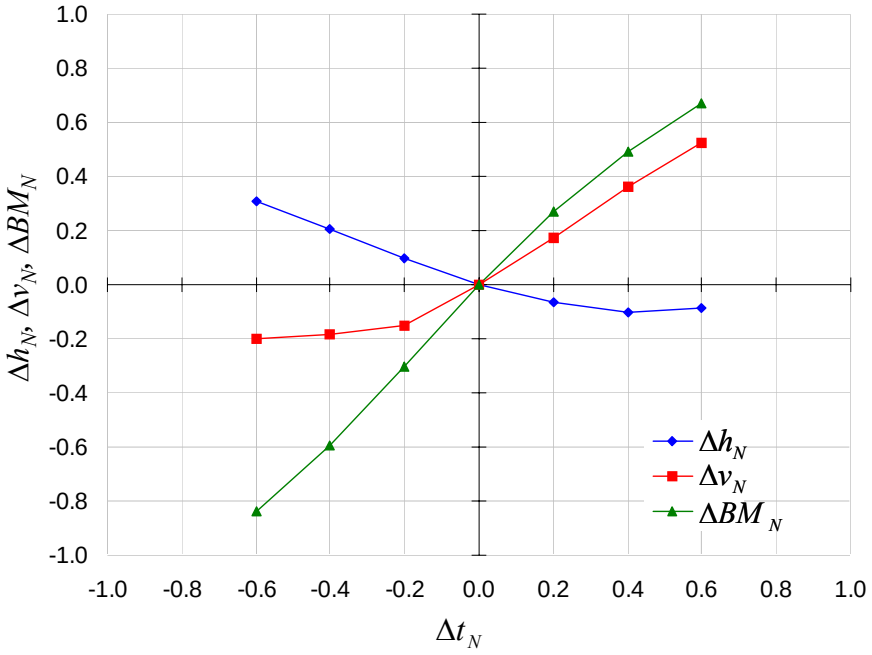

Figure 3.21 Effect of change in thickness of the retaining wall on horizontal displacement of the retaining wall, ground settlement behind the retaining wall and bending moment in the retaining wall

The horizontal displacement of the retaining wall and the ground settlement behind the retaining wall show contrasting trends with the change in thickness of the retaining wall. The horizontal displacement of the retaining wall decreases but the ground settlement behind the retaining wall increases as the thickness of the retaining wall is increased. In case of a stiffer retaining wall, the ground is prevented from spreading horizontally. The deformation of the ground, therefore, occurs mainly in the vertical direction, resulting in increase in ground settlement behind the retaining wall. In other words, the consolidation of the ground behind a stiff retaining wall is mainly one-dimensional. For a relatively flexible retaining wall (smaller thickness), there is a reduction in horizontal stresses in the ground behind the retaining wall, which results in increase in horizontal displacement and decrease in ground settlement.

3.3.6.5 Summary

From the results of the parametric study described above, it can be concluded that the stiffness of the soil and the stiffness of the retaining wall influence the deformation of the ground surrounding the deep excavation significantly. It is important to obtain accurate estimates of soil stiffness in order to obtain accurate estimates of ground deformation. It is also important to appreciate that even the stiffest of retaining walls will result in some horizontal displacement of the ground. If the major concern is to limit the ground settlement behind the retaining wall, it might be better to use a slightly flexible retaining wall system.

3.4 Deep Excavation next to Existing MRT Tunnels, Singapore

3.4.1 Project Overview

A large 15 m deep basement excavation approximately 140 m wide and 200 m long was carried out for the Tan Tock Seng Hospital (TTSH) in Singapore during 1995 (Sharma et al. 2001). The excavation was close to two existing Mass Rapid Transit tunnels (MRT) of 6 m diameter each. The side of the excavation was approximately 20 m from the edge of the nearest MRT tunnel. The layout of the site and the location of MRT tunnels along with idealised soil profile of the site are as shown in Figure 3.22(a). Further details of this project can be found in Chan (1995) and Sharma et al. (2001).

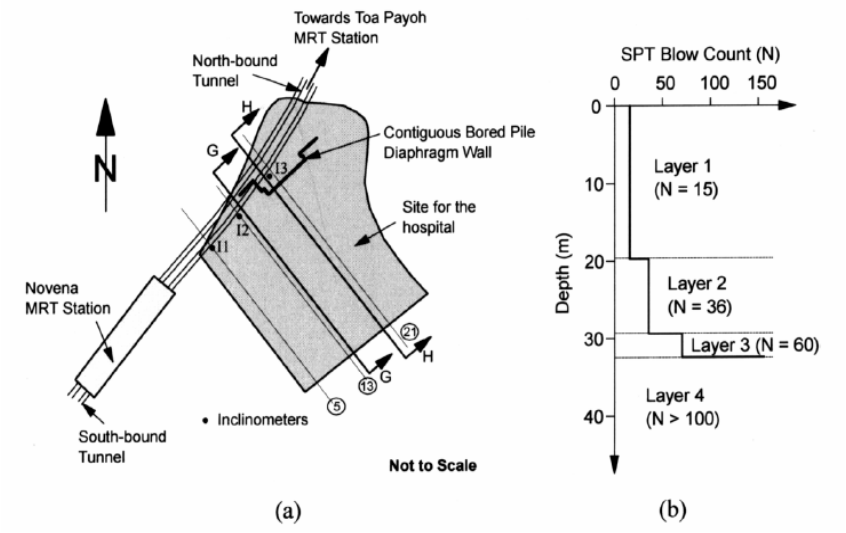

Figure 3.22 TTSH Deep Excavation Project, Singapore: (a) Layout of the site and the location of MRT tunnels, (b) idealised soil profile based on SPT N values (Sharma et al. 2001)

3.4.2 Ground Conditions

The site was located on the side of a hillock dipping towards NNW-SSE direction (Figure 3.22 (a)). The northern part of the site was located in weathered sedimentary rocks of the Jurong Formation and the southern part was located in completely decomposed granite rocks of the Bukit Timah Formation (Sharma et al. 1999). The depth to ground water was generally less than 10 m; therefore, dewatering was necessary to keep the excavated area dry during the excavation.

The idealised soil profile is shown in Figure 3.22 (b). The four overconsolidated stiff soil layers have been distinguished by blow count (N) derived from the Standard Penetration Test (SPT). Undrained shear strength (S_U) for each layer was estimated from the empirical correlation $S_U = 5 \times N$, which is generally found to be satisfactory for the residual soils of the Jurong and the Bukit Timah formation (Sharma et al. 1999). The ratio of Young's modulus to undrained shear strength (E/S_U) varied from 400 to 1000 for these soil layers.

3.4.3 Major Issues and Key Observations

One of the major issues concerning the deep excavation was the likely impact it could have on the existing MRT tunnels. The Code of Practice for Railway Protection of Singapore has set a limit of 15 mm maximum allowable tunnel displacement caused by nearby construction activities such as deep excavation or installation of a pile foundation. It prescribes severe penalties for those found responsible if this limit is exceeded. It was, therefore, of vital importance to stay within the allowable limit of tunnel displacement during the deep excavation. For this purpose, a state-of-the-art computerized automatic monitoring system was installed in the MRT tunnels to continuously monitor the displacements (Chan 1995, Sharma et al. 2001). A schematic diagram of this monitoring system is shown in Figure 3.23. Inclinometers were also set up at several locations to record the lateral deformations of the retaining wall. Numerical modelling of the deep excavation using the finite difference software FLAC was also conducted prior to the deep excavation as well as during the construction of the deep excavation as a part of the Observational Method (Chan 1995).

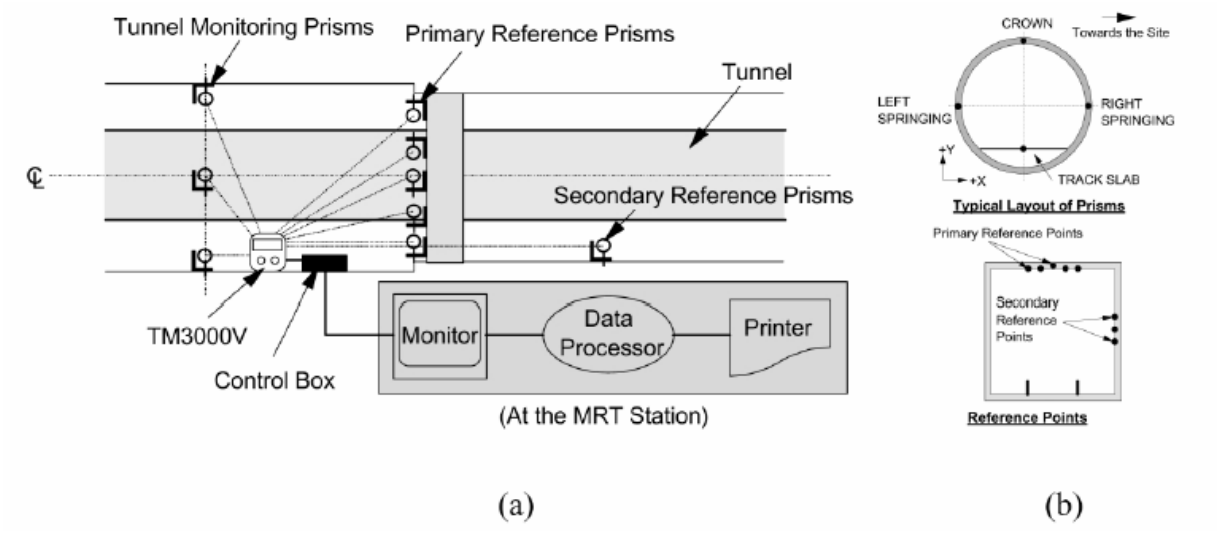

Figure 3.23 TTSH Deep Excavation Project, Singapore: (a) Schematic diagram of the automatic tunnel monitoring system; (b) Location of monitoring prisms inside the tunnel (Sharma et al. 2001)

Tunnel displacements caused by adjacent excavation were successfully kept within the acceptable limit of 15 mm (Chan 1995, Sharma et al. 2001). Numerical modelling gave fairly good prediction of ground deformation. The verification of modelling results using the Observational Method ensured its success.

3.4.4 Modelling Assumptions

The following modelling assumptions were made during back analysis:

- The effect of the construction of the MRT tunnels on the surrounding ground was not modelled. The deformations due to tunnel construction were nullified by resetting the displacements to zero.
- The contiguous bored pile retaining wall was modelled as wished-in-place, i.e. the unloading of the ground during the installation of the retaining wall was not modelled.
- The exact depth of the retaining wall could not be verified from Chan (1995) or Sharma et al. (2001). It is likely that the base of the retaining wall was founded in Soil Layer 4 from the point-of-view of minimizing disturbance to the existing tunnels; therefore a depth of 30 m was assumed for the retaining wall.

- At the section H-H of which back analysis was carried out, the ground water table lies 7 m below the original ground surface. As in the case of Chicago case study, dewatering of excavated area was effected by using pressure boundary condition.
- Since the four soil layers have fairly high undrained shear strength, plastic deformations were not likely to occur in these layers. It was, therefore, decided to use the Mohr-Coulomb model for these four layers.

3.4.5 Simulation of Construction Stages

Table 3.11 gives the details of the construction stages simulated in the back analysis of TTSH Deep Excavation Project, Singapore. The sequence of excavation is shown in Figure 3.24.

Table 3.11 Details of construction stages for TTSH Deep Excavation Project, Singapore

Stages	Activity	Description	Type of Calculation
1	Tunnel Construction	Simulate tunnel construction.	Undrained plastic
		Allow consolidation. Reset ground deformations resulting from tunnel construction to zero.	Consolidation
2	Wall Installation	Simulate installation of contagious bored pile wall as wished-in-place.	Undrained plastic
		Allow consolidation. Reset ground deformations resulting from installation of pile wall to zero.	Consolidation
3	Excavation Stages [Figure 3.24]	Excavate Layer #1 [3m].	Undrained plastic
4		Excavate Layer #2 [4m].	Undrained plastic
5		Excavate Layer #3 [4m].	Undrained plastic
6		Excavate Layer #4 [4m].	Undrained plastic

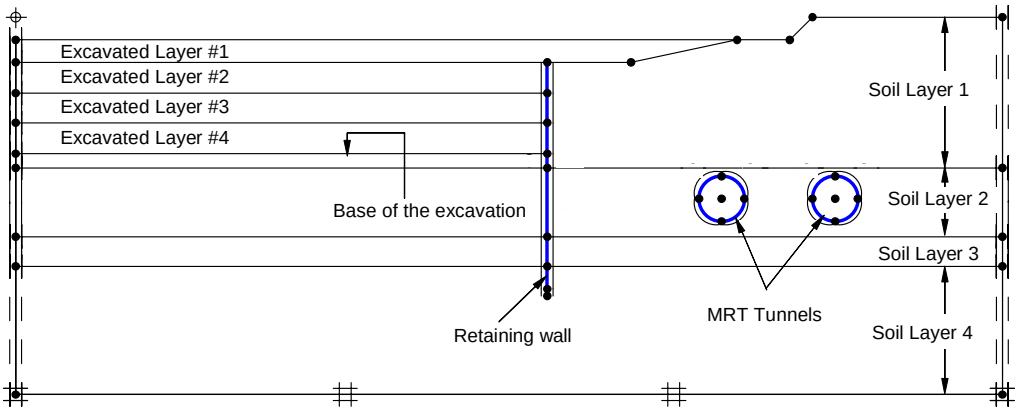

Figure 3.24 Excavation stages for TTHS Deep Excavation Project, Singapore

3.4.6 Back Analysis: Details and Results

Figure 3.25 shows the finite element mesh used in the back analysis of TTSH Deep Excavation Project, Singapore. It represents the soil conditions and the position of tunnels and the retaining wall at the vertical cross-section H-H shown in Figure 3.22(a). The MRT tunnel nearest to the wall is the Southbound MRT tunnel. The horizontal distance between this tunnel and the retaining wall is 20 m. The excavation is 15 m deep. As mentioned before, the four soil layers were modelled using the Mohr-Coulomb model. Undrained behaviour was assumed for these layers. Input parameters for the four soil layers are given in Table 3.12 and the input parameters for the structural components, i.e. retaining wall and tunnel linings, are given in Table 3.13.

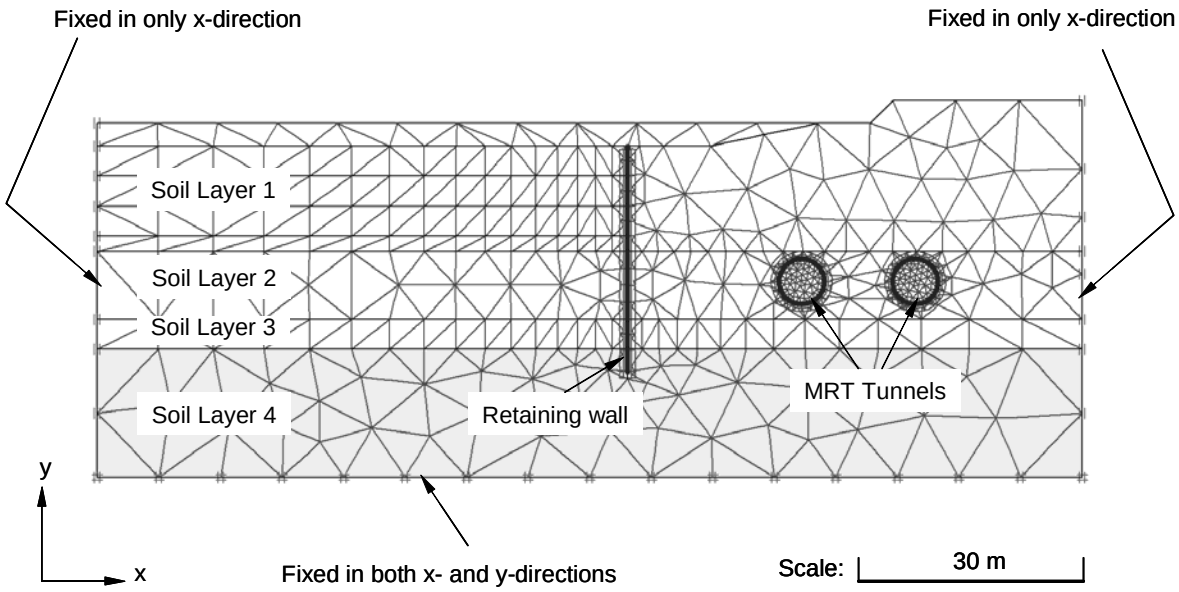

Figure 3.25 Finite element mesh for the back analysis of TTSH Deep Excavation Project, Singapore

In their back analysis of TTSH Deep Excavation Project using the finite difference program FLAC, Sharma et al. (2001) used a ratio of Young's modulus to undrained shear strength of soil (E/S_U) equal to 400 based on the experience of Wong and Broms (1989), and obtained a reasonably close agreement between the observed and the computed movements at the invert, crown and springings (Figure 3.26) of the two MRT tunnels. It was, therefore, decided to use E/S_U = 400 for the initial back analysis using PLAXIS. The movements at the

invert, crown and springings of both the Southbound (nearest) and the Northbound (farthest) tunnels were overpredicted by about 50% by this initial analysis. A reasonably close agreement between the observed and the computed movements could only be obtained when E/S_U = 1500 was used. It is well-known that soil stiffness can be very high at very small strain levels and that the stiffness of the soil decreases as the strain levels are increased (Simpson 1992, Viggiani and Atkinson 1995, Atkinson 2000). An estimate of the strain level for the TTSH Deep Excavation Project can be obtained by dividing the observed maximum horizontal movement of the tunnel lining (around 6 mm; Sharma et al. (2001)) by the depth of the excavation (15 m), i.e. 0.006/15 = 0.0004 or 0.04%. At this strain level, the Young's modulus value mobilized by the soil is likely to be significantly higher than that obtained, for example, from conventional triaxial compression tests in which the minimum recordable strain level is of the order of 0.1%. It is, therefore, not surprising to see that a higher than normal value of E/S_U is required to obtain good matching between the observed and the computed movements of the tunnel lining.

Table 3.12 Input parameters for the four soil layers for TTSH Deep Excavation Project, Singapore

Parameter	Symbol	Units	Soil Layer 1	Soil Layer 2	Soil Layer 3	Soil Layer 4
Model	-	-	Mohr-Coulomb	Mohr-Coulomb	Mohr-Coulomb	Mohr-Coulomb
Behaviour	-	-	Undrained	Undrained	Undrained	Undrained
Unit weight above water table	γ_{unsat}	kN/m^3	18.0	18.0	18.0	18.0
Unit weight below water table	γ_{sat}	kN/m^3	20.0	20.0	20.0	20.0
Horizontal permeability	K_x	cm/day	0.1	0.1	0.1	0.1
Vertical permeability	K_y	cm/day	0.1	0.1	0.1	0.1
Effective Poisson's ratio[1]	μ	-	0.2	0.2	0.2	0.2
Earth pressure coefficient	K_o	-	0.5	0.5	0.5	0.5
Undrained shear strength at the top of a clay layer	S_{U0}	kPa	75	150	250	500
Rate of increase of undrained shear strength with depth	m_C	kPa/m	0.0	0.0	0.0	0.0
Young's Modulus at the top of a layer	E_O	kPa	112500	225000	375000	750000
Rate of increase of Young's Modulus with depth	m_E	kPa/m	0.0	0.0	0.0	0.0
Interface strength ratio	R_{int}	-	1.0	1.0	1.0	1.0

[Note: [1] PLAXIS automatically sets Poisson's ratio equal to 0.495 for undrained loading.]

Table 3.13 Input parameters for structural components for TTSH Deep Excavation Project, Singapore

Parameter	Symbol	Unit	Tunnel Lining	Retaining Wall
Modelled as	-	-	Plate	Plate
Type of behaviour	-	-	Elastic	Elastic
Normal stiffness	EA	kN/m	1.92E+07	2.88E+07
Flexural rigidity	EI	kNm^2/m	4.00E+05	2.40E+06
Equivalent thickness	d	m	0.50	1.00
Weight	w	kN/m	11.52	23.00
Poisson's ratio	μ	-	0.15	0.15

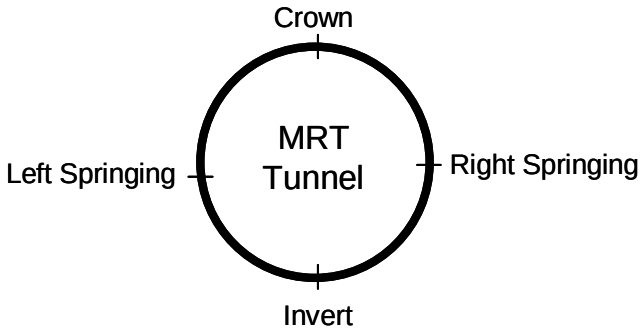

Figure 3.26 Cross-section of tunnel lining showing crown, invert and springings

Comparisons between the observed and the computed horizontal and vertical displacement of the tunnel linings at the crown, the invert and the two springings of the MRT tunnels are shown in Table 3.14.

Table 3.14 Comparison of observed and computed displacement of the two MRT tunnels – TTSH Deep Excavation Project, Singapore

Tunnel Position →	Southbound (Nearest to the retaining wall)						Northbound (Farthest away from the retaining wall)					
Parameter →	Horizontal Displacement (mm)			Vertical Displacement (mm)			Horizontal Displacement (mm)			Vertical Displacement (mm)		
At ↓	TM	FLAC	BA	TM	FLAC	BA	TM	FLAC	BA	TM	FLAC	BA
Invert	3.6	5.2	**4.7**	3.3	1.9	**1.4**	2.7	4.3	**2.6**	2.1	1.4	**1.2**
Crown	5.6	4.8	**6.0**	3.6	2.9	**2.6**	4.0	4.2	**3.2**	2.0	3.0	**2.4**
Left Springing	5.5	4.6	**6.0**	3.8	3.0	**2.0**	3.2	3.9	**3.5**	2.0	2.5	**1.9**
Right Springing	4.5	5.2	**4.7**	3.0	2.0	**1.8**	2.9	4.6	**2.3**	2.0	2.4	**1.7**

[Note: TM – Observed displacement; FLAC – Computed by Sharma et al. (2001); BA – Computed using PLAXIS.]

Overall, the agreement between the observed and computed horizontal displacements can be considered satisfactory, but the observed and computed vertical displacements differ significantly. Whereas the observed vertical displacements at the crown and at the invert are roughly the same, which indicates that the tunnels have not undergone significant distortion or ovalization, the computed vertical displacements at the crown and at the invert differ significantly, indicating ovalization of the tunnel cross-section along its horizontal axis. This discrepancy could be attributed to the fact that soil stiffness is generally anisotropic in the field whereas isotropic soil stiffness was specified in the back analysis. It is interesting to note Sharma et al. (2001) report similar discrepancy in the observed and computed vertical displacements at the crown and at the invert in their back analysis results obtained using FLAC.

3.4.7 Parametric Study

3.4.7.1 Overview

In this Section, the details and the results of a parametric study based on TTSH Deep Excavation Project are presented. The stratigraphy was simplified for the purpose of parameteric study by combining the four soil layers (Figure 3.24) into one layer as shown in Figure 3.27. The Mohr-Coulomb model was used to model the behaviour of this layer. Undrained behaviour was assumed. The following parameters were varied:

- Reference Young's Modulus of the soil layer [E]
- Undrained shear strength of the soil layer [S_{UO}]
- Stiffness of the retaining wall represented by its thickness [t_R]
- Stiffness of the tunnel lining represented by its thickness [t_T]

When one of the above four parameters was varied, the other three parameters were kept constant. The following parameters were specified for the base case for the parametric study:

- $[E]_{BC}$ = 80000 kPa
- $[S_{UO}]_{BC}$ = 120 kPa
- $[t_R]_{BC}$ = 1.1 m
- $[t_T]_{BC}$ = 0.4 m

The effect of varying a parameter was quantified by obtaining the variation in the following three quantities:

- Maximum horizontal displacement of the Southbound (nearest) tunnel [δh_{max}]
- Maximum bending moment in the tunnel lining of the Southbound tunnel [BM_{max}]
- Maximum shear force in the tunnel lining of the Southbound tunnel [SF_{max}]

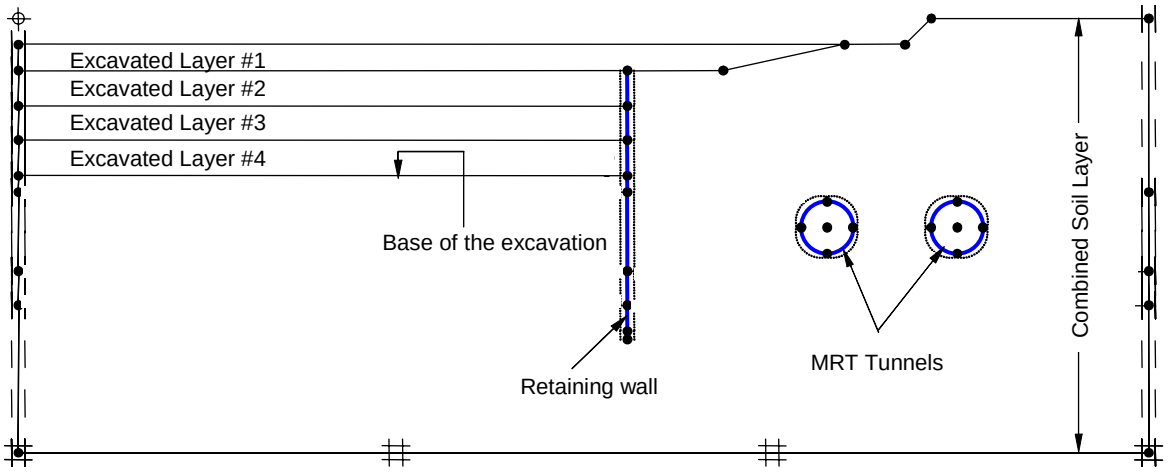

Figure 3.27 Simplification of stratigraphy for TTSH Deep Excavation Project, Singapore by combining four soil layers into one layer

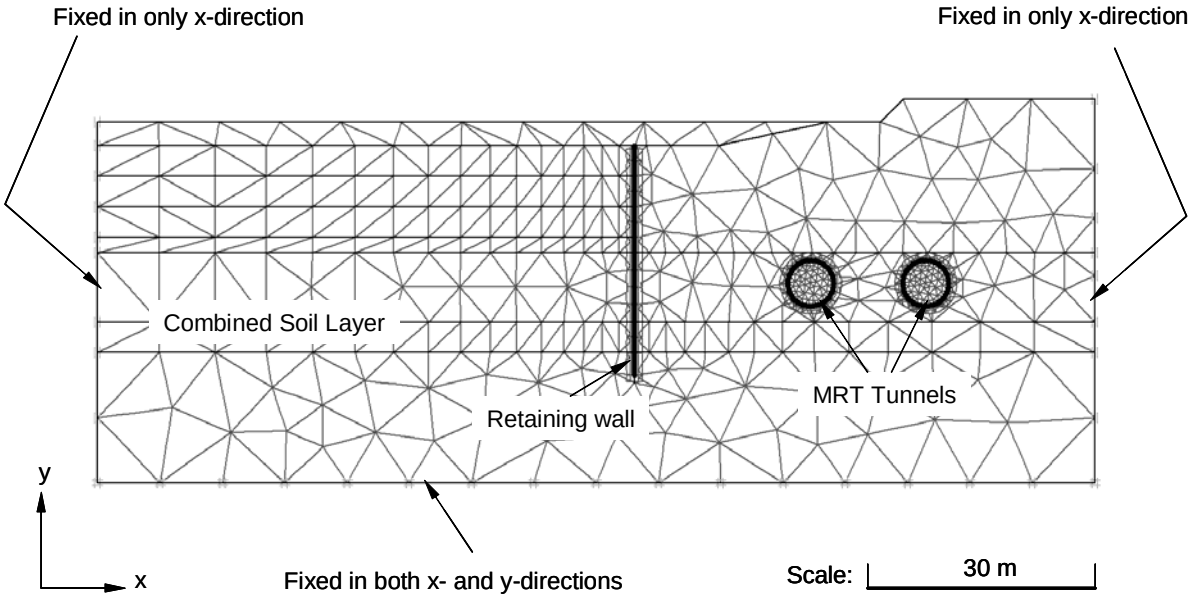

Figure 3.28 Finite element mesh for the parametric study based on TTSH Deep Excavation Project

For all the analyses conducted for the purpose of this parametric study, the following quantities or features were kept the same:

- Rate of increase of undrained shear strength with depth (m_C = 0.0 kPa/m)
- Rate of increase of Young's modulus with depth (m_E = 0.0 kPa/m)
- Depth of the retaining wall (30 m)
- Depth of excavation (15 m)
- Construction sequences (as described in Section 3.4.5)
- The diameter of the two MRT tunnels and their positions with respect to the retaining wall as well as with respect to each other
- Finite element mesh (as shown in Figure 3.28)

Similar to the presentation of results for Chicago Subway Renovation Project parametric study, the results of the TTSH Deep Excavation Project parametric study are presented in terms of normalized changes in parameters and the affected quantities as shown in Table 3.15.

Table 3.15 Normalized changes in parameters and quantities for the TTSH Deep Excavation Project parametric study

Parameter or quantity	Symbol	Formula
Normalized change in Young's modulus of the combined soil layer	ΔE_N	$\Delta E_N = \frac{E - [E]_{BC}}{[E]_{BC}}$
Normalized change in undrained shear strength of the combined soil layer	ΔS_N	$\Delta S_N = \frac{S_{UO} - [S_{UO}]_{BC}}{[S_{UO}]_{BC}}$
Normalized change in thickness of the retaining wall	Δt_N	$\Delta t_N = \frac{t_R - [t_R]_{BC}}{[t_R]_{BC}}$
Normalized change in thickness of the tunnel lining	ΔL_N	$\Delta L_N = \frac{t_L - [t_L]_{BC}}{[t_L]_{BC}}$
Normalized change in maximum horizontal displacement of the Southbound (nearest) tunnel	Δh_N	$\Delta h_N = \frac{\delta h_{max} - [\delta h_{max}]_{BC}}{[\delta h_{max}]_{BC}}$
Normalized change in the maximum shear force in the lining of the Southbound (nearest) tunnel	ΔSF_N	$\Delta SF_N = \frac{SF_{max} - [SF_{max}]_{BC}}{[SF_{max}]_{BC}}$
Normalized change in maximum bending moment in the lining of the Southbound (nearest) tunnel	ΔBM_N	$\Delta BM_N = \frac{BM_{max} - [BM_{max}]_{BC}}{[BM_{max}]_{BC}}$

3.4.7.2 Effect of Change in Young's modulus of Soil

Table 3.16 shows the range of values of Young's modulus of the combined soil layer used in the parametric study of the TTSH Deep Excavation Project, Singapore. Figure 3.29 shows the effect of change in Young's modulus of the combined soil layer on the maximum horizontal displacement, the maximum shear force and the maximum bending moment in the lining for the tunnel nearest to the retaining wall. The effect on maximum horizontal displacement is significantly greater than that on maximum shear force or maximum bending moment, which indicates that the stiffness of the soil affects the in-plane translation of the tunnel lining much more than its in-plane distortion. It is worth noting that this result has been obtained using a two-dimensional plane strain approximation of a three-dimensional problem. In reality, in-plane translation would result in out-of-plane distortion of the tunnel along its longitudinal axis, resulting in increase in a bending moment and shear force in that direction.

Table 3.16 Range of values for Young's modulus of soil used in the parametric study

Parameter	Unit	Ranges of Values used in the Parametric Study						
E	kPa	20000	40000	60000	80000	100000	120000	140000
ΔE_N	-	-0.75	-0.50	-0.25	0.00	0.25	0.50	0.75

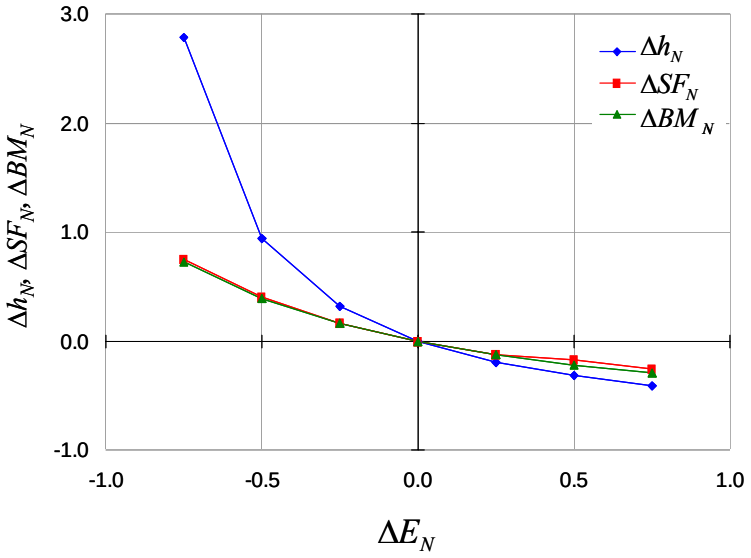

Figure 3.29 Effect of change in Young's modulus of soil on the maximum horizontal displacement, the maximum shear force and the maximum bending moment in the tunnel lining

3.4.7.3 Effect of Change in Soil Undrained Shear Strength

Table 3.17 shows the range of soil undrained shear strength used in the parametric study. The undrained shear strength value could not be reduced below 70 kPa without avoiding the collapse of the deep excavation. Figure 3.30 shows the effect of change in undrained shear strength of the combined soil layer on the maximum horizontal displacement, the maximum shear force and the maximum bending moment in the lining for the tunnel nearest to the retaining wall.

Table 3.17 Range of values for soil undrained shear strength used in the parametric study

Parameter	Unit	Ranges of Values used in the Parametric Study						
S_U	kPa	70	80	100	120	140	160	180
ΔS_N	-	-0.42	-0.33	-0.17	0.00	0.17	0.33	0.50

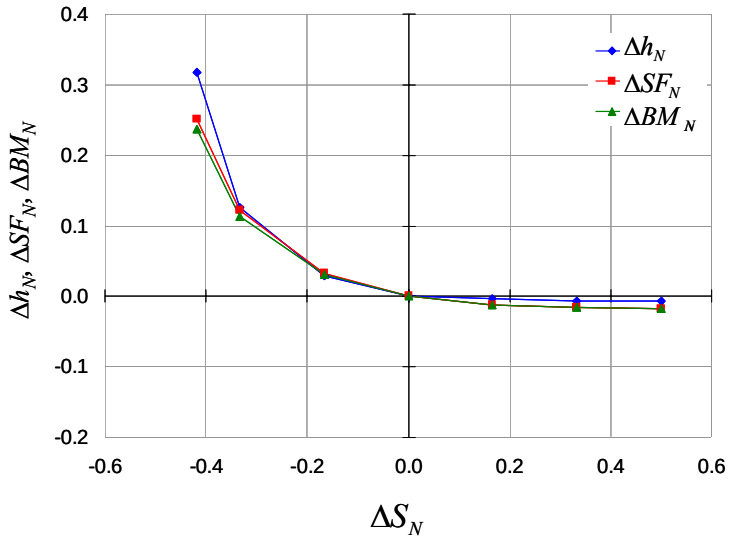

Figure 3.30 Effect of change in soil undrained shear strength on the maximum horizontal displacement, the maximum shear force and the maximum bending moment in the tunnel lining

A comparison of Figure 3.30 with Figure 3.29 indicates that the effect of change in undrained shear strength is not as significant as change in soil stiffness. This result is consistent with that obtained from the Chicago Subway Renovation Project parametric study. Increasing the value of undrained shear strength has virtually no effect because as the factor of safety against overall failure of the deep excavation increases, the ground deformation is

controlled by soil stiffness instead of soil strength. It is only when the value of the undrained shear strength is decreased that one begins to see a significant effect on the tunnel lining. Clearly, as the undrained shear strength is reduced, the ground adjacent to the deep excavation undergoes plastic deformation, resulting in significant in-plane translation and in-plane distortion of the tunnel lining.

3.4.7.4 Effect of Change in Thickness of the Retaining Wall

Table 3.18 gives the range of values for the thickness of the retaining wall used in the parametric study. Since the Young's modulus of the retaining wall was kept unchanged for all the analyses, a change in thickness of the retaining wall represents a change in both the bending stiffness and the axial stiffness of the retaining wall.

Table 3.18 Range of values for the thickness of the retaining wall used in the parametric study

Parameter	Unit	Ranges of Values used in the Parametric Study						
t_R	m	0.5	0.7	0.9	1.1	1.3	1.5	1.7
Δt_N	-	-0.55	-0.36	-0.18	0.00	0.18	0.36	0.55

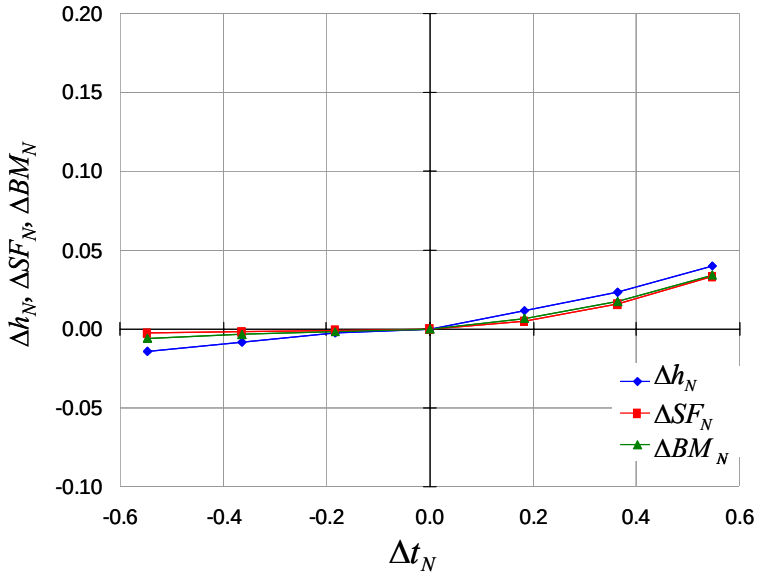

Figure 3.31 Effect of change in thickness of the retaining wall on the maximum horizontal displacement, the maximum shear force and the maximum bending moment in the tunnel lining [E = 80000 kPa and S_U = 120 kPa for the combined soil layer]

Figure 3.31 shows the effect of change in thickness of the retaining wall on the maximum horizontal displacement, the maximum shear force and the maximum bending moment in the lining for the tunnel nearest to the retaining wall. It can be seen from Figure 3.31 that changing the stiffness of the retaining wall has virtually no effect on the tunnel lining. At first glance, this result may seem a little surprising because engineers usually go for a stiff retaining wall when there are existing structures located close to the deep excavation for the purpose of minimizing ground deformation. It should be kept in mind that for the seven analyses shown in Table 3.18, the Young's modulus and the undrained shear strength of the combined soil layer were 80000 kPa and 120 kPa, respectively. Since the soil surrounding the deep excavation is both stiff and strong, the retaining wall has a fairly minor role to play. For a softer and weaker soil layer, the stiffness of the retaining wall would likely have a greater effect on the tunnel lining. In order to confirm this hypothesis, the seven analyses shown in Table 3.18 were repeated with lower value of Young's modulus (40000 kPa instead of 80000 kPa) and lower value of undrained shear strength (80 kPa instead of 120 kPa) for the combined soil layer. The results of these repeated analyses are shown in Figure 3.32. A comparison between Figure 3.32 and Figure 3.31 suggests that the stiffness of the retaining wall has a greater effect on the tunnel lining for a soil having lower stiffness and strength.

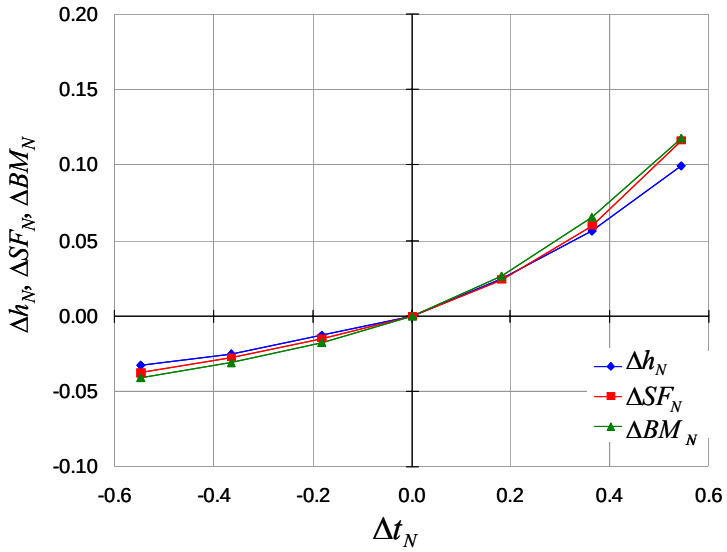

Figure 3.32 Effect of change in thickness of the retaining wall on the maximum horizontal displacement, the maximum shear force and the maximum bending moment in the tunnel lining [E = 40000 kPa; S_U = 80 kPa for the combined soil layer]

3.4.7.5 Effect of Change in Thickness of the Tunnel Lining

Table 3.19 shows the range of values for the thickness of the tunnel lining used in the present study. Figure 3.33 shows the effect of change in thickness of the tunnel lining on the maximum horizontal displacement, the maximum shear force and the maximum bending moment in the lining for the tunnel nearest to the retaining wall. It can be seen from Figure 3.33 that a change in the thickness of the tunnel lining has virtually no effect on its maximum horizontal displacement; however, as the thickness is increased, there is a substantial increase in the maximum shear force and maximum bending moment induced in the tunnel lining. This result, which is consistent with the findings of Sharma et al. (2001), indicates that a relatively flexible tunnel lining is probably better at tolerating ground movements associated with adjacent deep excavation compared with a relatively stiff tunnel lining.

Table 3.19 Range of values for the thickness of the tunnel lining used in the parametric study

Parameter	Unit	Ranges of Values used in the Parametric Study						
t_L	m	0.25	0.30	0.35	0.40	0.45	0.50	0.55
ΔL_N	-	-0.38	-0.25	-0.13	0.00	0.13	0.25	0.38

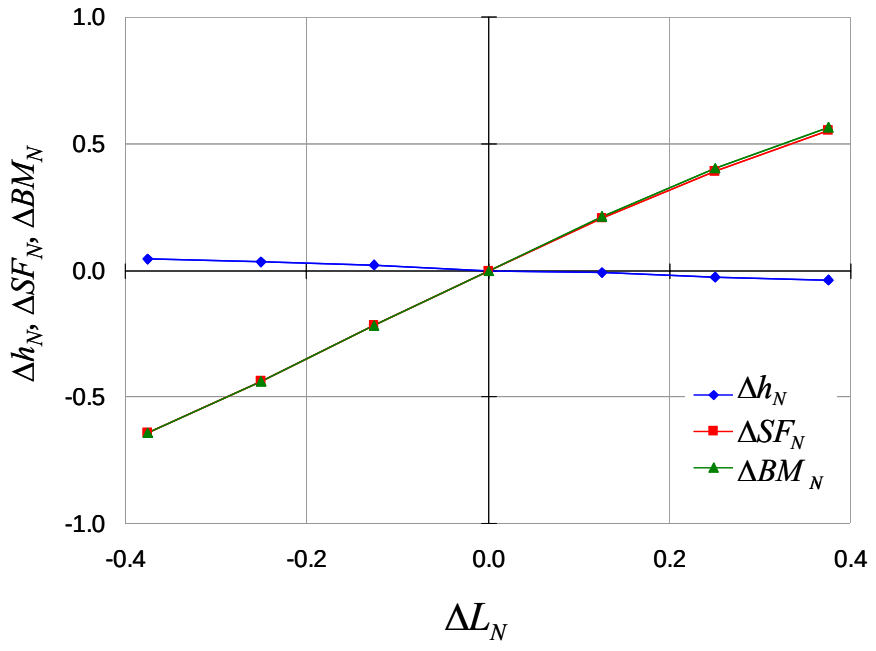

Figure 3.33 Effect of change in thickness of the tunnel lining on the maximum horizontal displacement, the maximum shear force and the maximum bending moment in the tunnel lining

3.4.7.6 Summary

The results of the parametric study conducted on TTSH Deep Excavation Project have revealed the following important information:

- Ground movements associated with deep excavation are strongly influenced by the stiffness of the soil surrounding the deep excavation.
- Undrained shear strength of the soil surrounding the deep excavation has a relatively insignificant effect on ground movements except in cases where lowering of undrained shear strength brings the factor of safety against shear failure close to 1.
- Selecting a stiff retaining wall is beneficial from the point-of-view of limiting ground movements when deep excavation is being carried out in soft ground conditions.
- A flexible tunnel lining is able to resist ground movements associated with adjacent deep excavation better than a stiff tunnel lining.

3.5 Chapter Summary

In this Chapter, two well-documented case studies of deep excavations in urban environment – Chicago Subway Renovation Project, USA and Tan Tock Seng Hospital (TTSH) Deep Excavation Project, Singapore – were back analyzed using the finite element software PLAXIS. While the damage control to the school foundation in the near vicinity (within 2 m) of the deep excavation was major concern for Chicago Subway Renovation Project, to monitor and control the effect of deep excavation for Tan Tock Seng Hospital on two MRT tunnel located 20 m away from the face of the excavation was the major issue in TTSH Deep Excavation Project. The results from the back analyses of these case studies were supplemented with results from parametric studies in which key parameters such as soil stiffness, soil undrained shear strength, stiffness of the retaining wall and the stiffness of the tunnel lining were varied. The following key observations can be made on the basis of the results obtained from these back analyses and parametric studies:

- It is extremely important to model construction processes and ground conditions accurately when using back analyses of instrumented case histories to calibrate soil parameters. The modeller must be aware of specific procedures prescribed by the modelling software to model these construction sequences.

- It is possible to capture both the pattern and the magnitude of ground deformation around a deep excavation using a simplified stratigraphy obtained by grouping several successive soil layers into one layer provided there is some physical basis for such grouping and the combined layer dominates the overall behaviour of the ground. The physical basis could be the common origin of these soil layers or common type of soil behaviour.
- Deep excavation is a relatively fast construction activity that can be modelled by assuming undrained behaviour of the surrounding ground, provided the average permeability of the surrounding ground is sufficiently low.
- The stiffness of the soil and the stiffness of the retaining wall influence the deformation of the ground surrounding the deep excavation significantly. It is important to obtain accurate estimates of soil stiffness in order to obtain accurate estimates of ground deformation.
- A stiff retaining wall should be used for controlling horizontal ground movements resulting from deep excavation; however, it is also important to appreciate that even the stiffest of retaining wall will result in some horizontal displacement of the ground.
- If the major concern is to limit the ground settlement behind the retaining wall, it might be better to use a slightly flexible retaining wall system.
- A flexible tunnel lining is able to resist ground movements associated with adjacent deep excavation better than a stiff tunnel lining.

Lessons learned from the back analysis of these two case histories and their parametric studies are used in Chapter 4 for the development of design charts for preliminary assessment of soil-structure interaction effects in case of deep excavation in soft ground conditions next to existing circular tunnel.

4 Design Charts

4.1 Overview

Deep excavation adjacent to existing structures such as tunnels, raft foundations or pile foundations, is a highly complex soil-structure-interaction problem because of the many different construction processes involved and highly variable ground conditions. It is often difficult to visualize the mechanism of ground deformation around the deep excavation as well as around the existing structures and to obtain ball park estimates of deformation prior to embarking on a full-fledged finite element analysis of the problem. For these purposes, design charts that are obtained from finite element analyses conducted using simplified geometry and idealized material behaviour. These charts can be used to obtain quantitative estimates of the deformation of an existing structure in response to an adjacent deep excavation. This chapter describes the details and the results of the finite element analyses conducted for the formulation of such design charts for the case of a deep excavation conducted next to an existing circular tunnel.

4.2 Characterization of Deformation of the Tunnel Lining

It is important to identify key parameters that characterize the deformation of the tunnel lining so that the design charts can be formulated in terms of those parameters. A conceptual diagram of the deformation of tunnel lining in response to ground deformation around a deep excavation is shown in Figure 4.1(a). As the retaining wall undergoes lateral displacement towards the excavated area, the ground behind the retaining wall follows its movement and causes the tunnel lining to move towards the excavation. Deep excavation is also accompanied by unloading of ground in the horizontal direction. In response to this unloading in horizontal direction, the vertical overburden stress at the crown of the tunnel becomes greater than the horizontal stress at the nearest springing of the tunnel, resulting in distortion of the tunnel lining. The deformation of the tunnel lining can, therefore, be considered to have two

components: (i) in-plane displacement of the tunnel lining towards the deep excavation; and, (ii) in-plane distortion of the tunnel lining, mainly along the horizontal axis of the tunnel.

The in-plane displacement of the tunnel lining can be represented by the shortest distance, δC, by which the centre of the tunnel cross-section moves towards the deep excavation as shown in Figure 4.1(b). In the estimation of δC, it is assumed that the distorted cross-section of the tunnel is elliptical. In other words, the distorted cross-section of the tunnel is assumed to be symmetric about two mutually perpendicular axes, and the centre of the distorted cross-section is located at the intersection of these two axes, as shown in Figure 4.1(b).

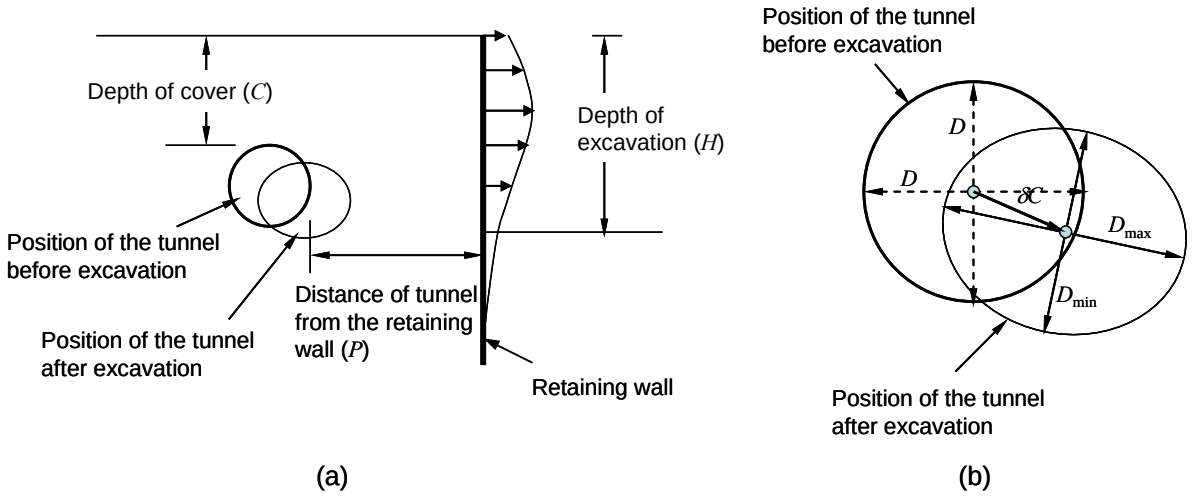

Figure 4.1 (a) Movement of the tunnel lining in response to ground deformation around a deep excavation; (b) in-plane distortion and in-plane displacement of the tunnel lining

The in-plane distortion of the tunnel cross-section can be represented by the difference δD between the length of the major axis (D_{max}) and the length of the minor axis (D_{min}), i.e. $\delta D = D_{max} - D_{min}$ as shown in Figure 4.1(b). The larger the value of δD, the larger will be the extent of in-plane distortion of the tunnel cross-section.

In the case of a 2-D plane strain analysis of deep excavation adjacent to an existing circular tunnel, the in-plane displacement may give the impression of being harmless from the point-of-view of causing structural distress in tunnel lining. In reality, such a displacement of the tunnel lining can be equally, if not more, detrimental as the in-plane distortion. The

problem of deep excavation adjacent to existing circular tunnel is actually three-dimensional because the deep excavation generally has a limited area in the plan view, as shown in Figure 4.2. The in-plane displacement calculated using a 2-D plane strain analysis, e.g. along a section A-A in Figure 4.2, would not be experienced uniformly by the tunnel along its length. Segments of tunnel lining on either side of section A-A would experience less displacement towards the deep excavation. As a result, the tunnel would experience flexural deformation in the horizontal plane and increase in bending moment and shear force at the zones of inflexion, as shown in Figure 4.2. It is, therefore, important to obtain estimates of in-plane displacement of the tunnel lining due to adjacent deep excavation.

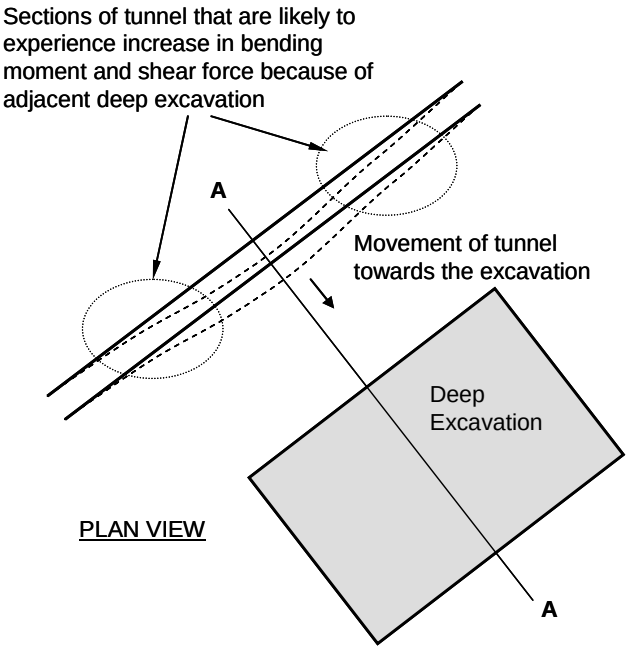

Figure 4.2 In-plane displacement of tunnel lining resulting in flexural deformation of the tunnel in the horizontal plane

4.3 Dimensional Analysis

Design charts formulated in terms of dimensional parameters are not very useful because it is difficult to ensure their proper scaling as the geometry of the problem is scaled by a given factor. It is better to use non-dimensional or normalized parameters in the design charts. A dimensional analysis of the problem must be conducted prior to the formulation of design charts in terms of normalized parameters. Such a dimensional analysis can be carried out by

conducting two numerical analyses of the problem using similar geometric configurations that are related to each other by a scaling factor for the linear dimension. Scaling factors for key parameters obtained from the two analyses should be reasonably close to the geometric scaling factor.

4.3.1 Geometric Configuration and Input Parameters

Finite element analyses were conducted for two geometrically similar cases – Case#1 and Case#2. Case #1 simulated a 6 m deep excavation supported by a 12 m deep retaining wall whereas Case #2 simulated a 9 m deep excavation supported by an 18 m deep retaining wall. Two analyses were conducted for each case – one without the tunnel and the other with the tunnel. For Case #1, the diameter of the tunnel was 6 m and it was located at a horizontal distance of 6 m from the retaining wall. For Case #2, the diameter of the tunnel was 9 m and it was located at a horizontal distance of 9 m from the retaining wall. The geometric configurations for Case #1 and Case #2 are shown in Figure 4.3. It can be seen from Figure 4.3 that the two cases are geometrically similar with a scaling factor of 1.5 for the linear dimension. Input parameters for the structural components and the soil layers for Case #1 and Case #2 are given in Table 4.1 and Table 4.2, respectively.

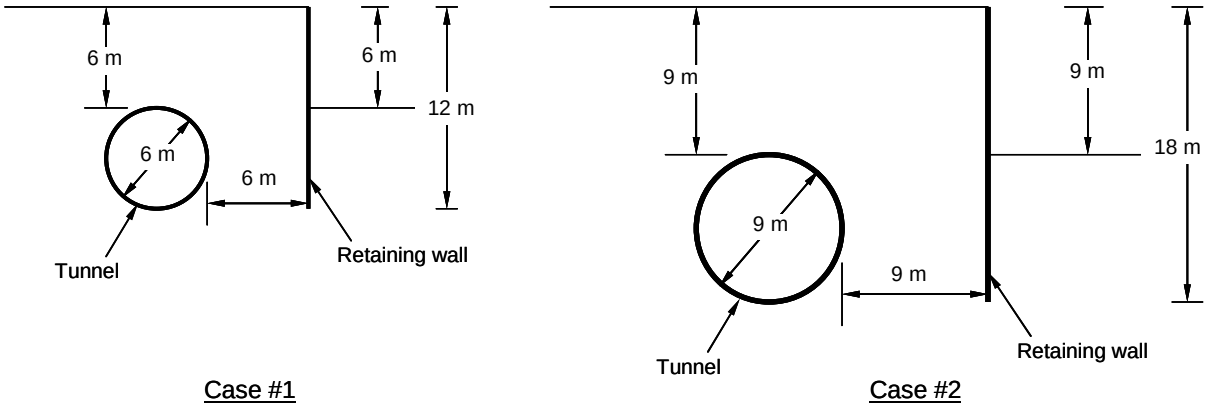

Figure 4.3 Dimensional analysis: Geometric configurations for the two cases

Table 4.1 Dimensional analysis: Input parameters for the structural components

Parameter	Symbol	Unit	Tunnel Lining	Retaining Wall
Modelled as	-	-	Plate	Plate
Type of behaviour	-	-	Elastic	Elastic
Normal stiffness	EA	kN/m	1.4E+07	2.4E+07
Flexural rigidity	EI	kNm^2/m	1.43E+05	2.4E+06
Equivalent thickness	d	m	0.35	0.8
Weight	w	kN/m	8.4	19.2
Poisson's ratio	μ	-	0.15	0.15

Table 4.2 Dimensional analysis: Input parameters for the soil layer

Parameter	Symbol	Unit	Case #1	Case #2
Model			Mohr-Coulomb	Mohr-Coulomb
Behaviour			Undrained	Undrained
Unit weight above water table	Γ_{unsat}	kN/m^3	16.0	16.0
Unit weight below water table	Γ_{sat}	kN/m^3	18.0	18.0
Horizontal permeability	K_x	cm/day	0.01	0.01
Vertical permeability	K_y	cm/day	0.01	0.01
Poisson's ratio	μ	-	0.3	0.3
Undrained Shear Strength at the top of the layer	S_{UO}	kPa	20	30
Young's Modulus at the top of the layer	E_O	kPa	10000	15000
Interface strength ratio	R_{int}	-	1.0	1.0
Rate of increase of undrained shear strength with depth	m_C	kPa/m	1	1
Rate of increase of Young's Modulus with depth	m_E	kPa/m	2500	2500

In addition to increasing all the linear dimensions, the Young's modulus and the undrained shear strength of the soil layer were also increased by a factor of 1.5 for Case #2 analyses (Table 4.2). The unit weight of the soil was kept the same for both Case #1 and Case #2.

4.3.2 Results

Table 4.3 shows a comparison of maximum horizontal displacement, maximum bending moment and maximum shear force induced in the retaining wall for Case #1 and Case #2 analyses.

Table 4.3 Dimensional analysis: Scaling factors for displacement, bending moment and shear force

Parameter	Unit	Without Tunnel			With Tunnel		
		Case #1	Case #2	Scaling Factor	Case #1	Case #2	Scaling Factor
Maximum horizontal displacement of the retaining wall	mm	20.4	30.3	1.49	21.1	31.3	1.49
Maximum bending moment in the retaining wall	kNm/m	56.6	102.7	1.82	62.3	106.7	1.71
Maximum shear force in the retaining wall	kN/m	73.1	95.8	1.31	77.6	119.1	1.53

The scaling factor for maximum horizontal displacement was 1.49, which matches closely with geometric scaling factor of 1.5. The scaling factors for the maximum bending moment and maximum shear force were in the range of 1.71-1.82 and 1.31-1.53, respectively, which can be considered reasonably close to the geometric scaling factor of 1.5 for most practical purposes. These results give some support to the applicability of design charts formulated using normalized parameters for different geometric configurations.

4.4 Formulation of Design Charts

4.4.1 Assumptions and Simplifications

The following assumptions and simplifications have been used while formulating design charts:

- The ground surface is assumed to be horizontal and free of any surcharge loading.
- The groundwater table is taken at the ground surface.
- Only one fully saturated soil layer of infinite depth is considered.
- Soil behaviour is considered undrained during deep excavation and is modelled using the Mohr-Coulomb model.
- The excavation pit is assumed to be dry, i.e. pore-water pressure acts only on the outside of the retaining wall supporting the excavation.
- Only one circular tunnel of 6 m diameter is assumed to exist adjacent to the deep excavation.
- The retaining wall is assumed to be 40 m deep and 1 m thick.
- Lateral support to the retaining wall is provided in the form of horizontal struts that are vertically spaced at 3 m centre to centre.

- Undrained shear strength at the top of the soil layer is taken equal to 40 kPa and the rate of increase of undrained shear strength with depth is taken equal to 4 kPa/m.
- The interfaces between the soil and the structural components (retaining wall and tunnel lining) are considered rigid, i.e. there is no possibility of slippage at these interfaces.

4.4.2 Key Parameters and Variables for the Design Charts

The main purpose of formulating the design charts is to be able to obtain quantitative estimates of deformation of the tunnel lining in response to adjacent deep excavation. In order to achieve this objective, it is important to identify factors that can influence the ground deformation behaviour. These factors, which were identified in Chapter 3 with the help of back analyses and parametric studies of two well-documented case histories, include:

- stiffness of the soil represented by its Young's modulus (E);
- stiffness of the tunnel lining represented by its thickness (t_L) ;
- depth of excavation (H);
- location of the tunnel with respect to the vertical face of the excavation (P); and
- location of the crown of the tunnel with respect to the ground surface (C).

It is, therefore, logical to consider these factors as variables whose influence on the deformation on the tunnel lining can be obtained using the design charts.

As discussed in the previous section, the deformation of the tunnel lining due to adjacent deep excavation can be characterized using:

- in-plane distortion of the tunnel lining (δD); and
- in-plane displacement of the tunnel lining (δC).

Additional stresses induced in the tunnel lining due to adjacent deep excavation can be characterized using:

- change in the maximum shear force in the tunnel lining ($\delta SF_{\max}$); and
- change in the maximum bending moment in the tunnel lining ($\delta BM_{\max}$).

These four quantities can be considered as parameters for the design charts. The values of these parameters for given values of soil stiffness, stiffness of the tunnel lining and the location of the tunnel can be obtained using the design charts.

4.4.3 Details of the Analyses

Figure 4.4 shows a general geometric outline and various components for the finite element analyses conducted using PLAXIS for the formulation of design charts. The input parameters for the soil layer and the structural components for all the analyses are given in Table 4.4 and Table 4.5, respectively.

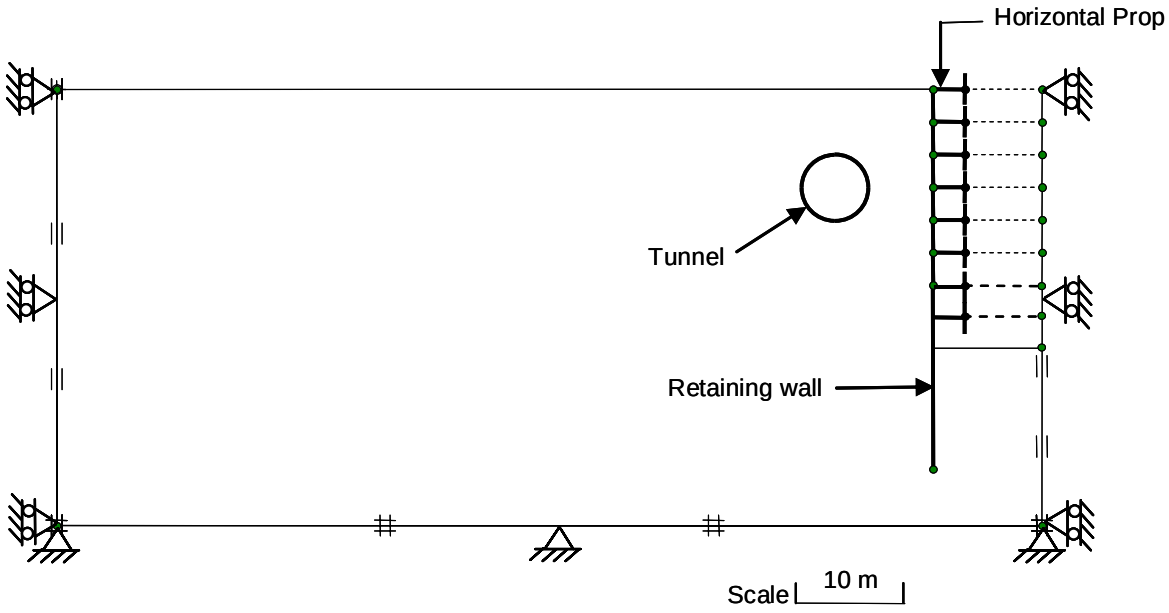

Figure 4.4 Formulation of design charts: General geometric outline for the finite element analyses

Table 4.4 Formulation of design charts: Input parameters for the soil layer

Parameter	Symbol	Unit	Value
Unit weight above water table	Γ_{unsat}	kN/m^3	18.0
Unit weight below water table	Γ_{sat}	kN/m^3	20.0
Horizontal permeability	K_x	cm/day	0.01
Vertical permeability	K_y	cm/day	0.01
Undrained Shear Strength at the top of the soil layer	S_{UO}	kPa	40
Rate of increase of undrained shear strength with depth	m_C	kPa/m	4
Interface strength ratio	R_{int}	-	1.0

Table 4.5 Formulation of design charts: Input parameters for structural components

Parameter	Symbol	Unit	Tunnel Lining	Retaining Wall	Horizontal Strut
Modelled as	-	-	Plate	Plate	Fixed anchor
Type of behaviour	-	-	Elastic	Elastic	Elastic
Normal stiffness	EA	kN/m	variable	4.0E+07	6.75E+06
Flexural rigidity	EI	kNm^2/m	variable	2.4E+06	-
Equivalent thickness	d	m	variable	1.00	-
Weight	w	kN/m	variable	24.00	-
Poisson's ratio	μ	-	0.15	0.15	-
Horizontal Spacing	L_s	m	-	-	6.0

Table 4.6 lists all the variables and their range of values that were used in these analyses. Figure 4.5 shows the 18 different positions of the tunnel with respect to both the vertical face of the excavation and the ground surface that were used in the analyses. In all, a total of 864 analyses were conducted.

Table 4.6 Formulation of design charts: Range of values for the variables

Variable	Number of values	Range of values
Young's Modulus (E_0) at the top of the soil layer	4	20000 kPa, 40000 kPa, 60000 kPa, 80000 kPa
Thickness of the tunnel lining (t_L)	3	0.3 m, 0.35 m, 0.4 m
H/D ratio	4	1, 2, 3, 4
C/D ratio	3	1, 2, 3
P/D ratio	6	1, 2, 3, 4, 5, 6
Total No. of Analyses [4 x 3 x 4 x 3 x 6] =	864	

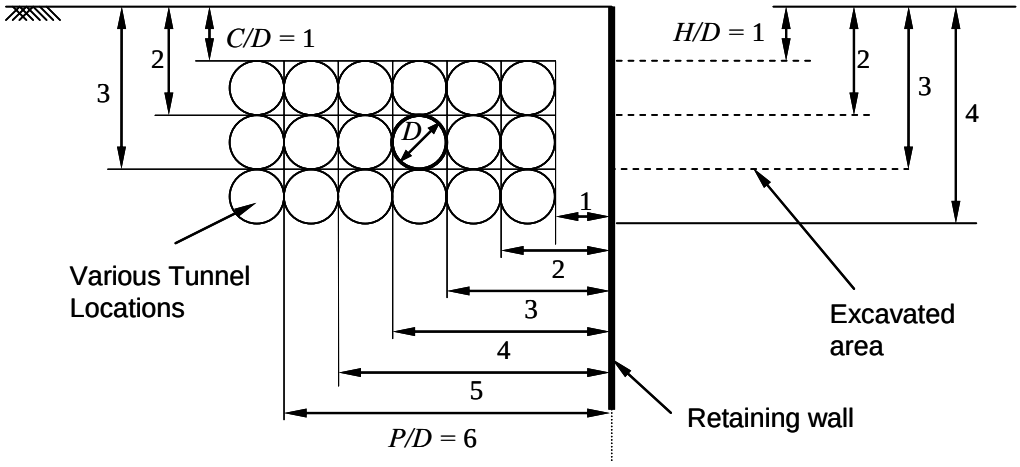

Figure 4.5 Formulation of design charts: Details of different geometric configurations used in the analyses

4.5 Presentation of Design Charts

In this Section, the design charts for the following four parameters are presented:

- In-plane distortion of the tunnel lining
- In-plane displacement of the tunnel lining
- Change in maximum shear force induced in the tunnel lining
- Change in maximum bending moment induced in the tunnel lining

Each of these design charts is presented in the form of contours plotted on a grid of *C/D* ratios on the y-axis and *P/D* ratios on the x-axis. Non-dimensional or normalized versions of the above parameters are used in these design charts.

4.5.1 In-plane Distortion of the Tunnel Lining

As described in Section 4.2, the in-plane distortion of the tunnel lining (δD) is given by $\delta D = D_{\max} - D_{\min}$. A non-dimensional or normalized form of in-plane distortion δD_N can be obtained as:

$$\delta D_N = \frac{\delta D}{D} \times \left(\frac{t_L}{H} \right) \qquad [4\text{-}1]$$

where t_L is the thickness of the tunnel lining, D is the diameter of the tunnel and H is the depth of the excavation. The inclusion of t_L in Eq.[4-1] is justified on the basis of the observation that a thicker tunnel lining undergoes less in-plane distortion. Similarly, the inclusion of H in Eq. [4-1] is based on the observation that the in-plane distortion of the tunnel lining increases with the increase in the depth of the excavation. Considerable amount of data reduction can be achieved by using Eq. [4-1] to normalize δD values. Only four design charts – one each for the four different Young's modulus values for the soil – are needed to estimate the magnitude of in-plane distortion of the tunnel lining. These four design charts are shown in Figure 4.6. Before plotting the contours for these design charts, all the values of δD_N were multiplied by 10^5 in order to avoid small contour levels. The reading obtained from these design charts, therefore, should be divided by 10^5 to obtain correct value of δD_N. For example, referring to the second design chart from the top in Figure 4.6, the reading for E = 40000 kPa, C/D = 2, and P/D = 4 is around 1.3; therefore, the value of δD_N is equal to $1.3/10^5 = 0.0000013$.

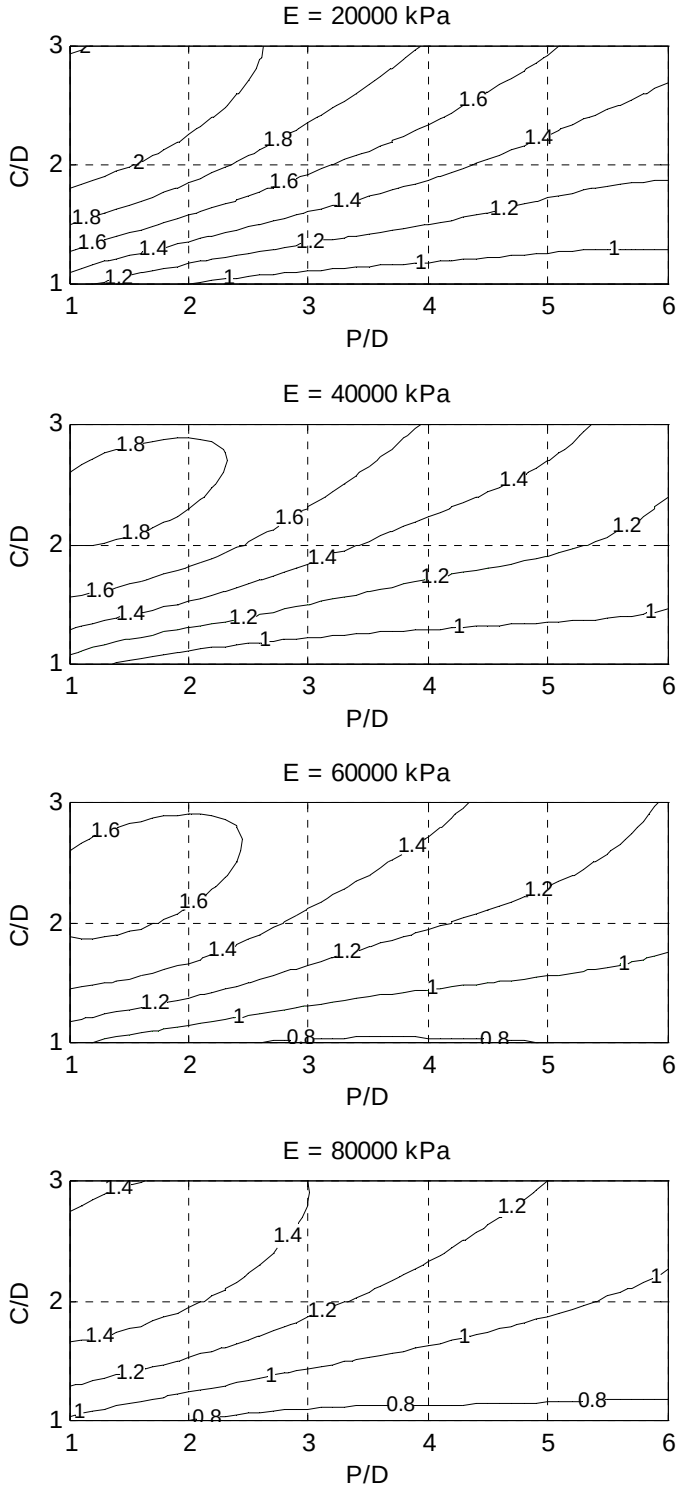

NOTE: Contour levels are shown in terms of δD_N x 10^5. Please divide the reading by 10^5 to obtain correct value of δD_N.

Figure 4.6 Design chart for the estimation of normalized in-plane distortion (δD_N) of the tunnel lining

4.5.2 In-plane Displacement of Tunnel Lining

As shown in Figure 4.1(b), the in-plane displacement of the tunnel lining is characterized by the shortest distance (δC) by which the centre of the tunnel cross-section moves towards the deep excavation. A non-dimensional or normalized form of δC can be obtained as:

$$\delta C_N = \frac{\delta C}{H} \qquad [4\text{-}2]$$

where H is the depth of the excavation. The normalization shown in Eq.[4-2] is based on the observation that the in-plane displacement of the tunnel lining increases with increase in the depth of the excavation. It is also noticed that the thickness of the tunnel lining (t_L) has virtually no effect on the in-plane displacement of the tunnel lining; therefore, the magnitude of in-plane displacement of the tunnel lining can be considered to be independent of the thickness of the tunnel lining. In reality, the in-plane displacement of the tunnel lining is likely to be influenced by the flexural stiffness of the tunnel section in the horizontal plane (see Figure 4.2), which, in turn, depends on the thickness of the tunnel lining and the type of tunnel cross-section (e.g. circular, box, etc). Such behaviour of tunnel cross-section is three-dimensional, and therefore, it cannot be captured using a 2-D plane strain finite element analysis. It should also be noted that a 2-D plane strain finite element analysis is also likely to overestimate the magnitude of in-plane displacement of the tunnel lining because of its inability to account for the three-dimensional behaviour. The estimates of in-plane displacement obtained from the design charts presented in this Section are, therefore, likely to be on the higher side.

Since in-plane displacement of the tunnel lining is considered independent of the thickness of the tunnel lining, only four design charts – one each for the four different Young's modulus values for the soil – are needed to estimate the magnitude of in-plane displacement of the tunnel lining due to adjacent deep excavation. These four design charts are shown in Figure 4.7. Before plotting the contours for these design charts, all the values of δC_N were multiplied by 1000 in order to avoid very small contour levels. A reading obtained from these design charts, therefore, should be divided by 1000 to obtain the correct value of δC_N. For example, referring to the third design chart from the top in Figure 4.7, the reading for E = 60000 kPa, C/D = 2, and P/D = 4 is around 0.75; therefore, the value of δC_N is equal to 0.75/1000 = 0.00075.

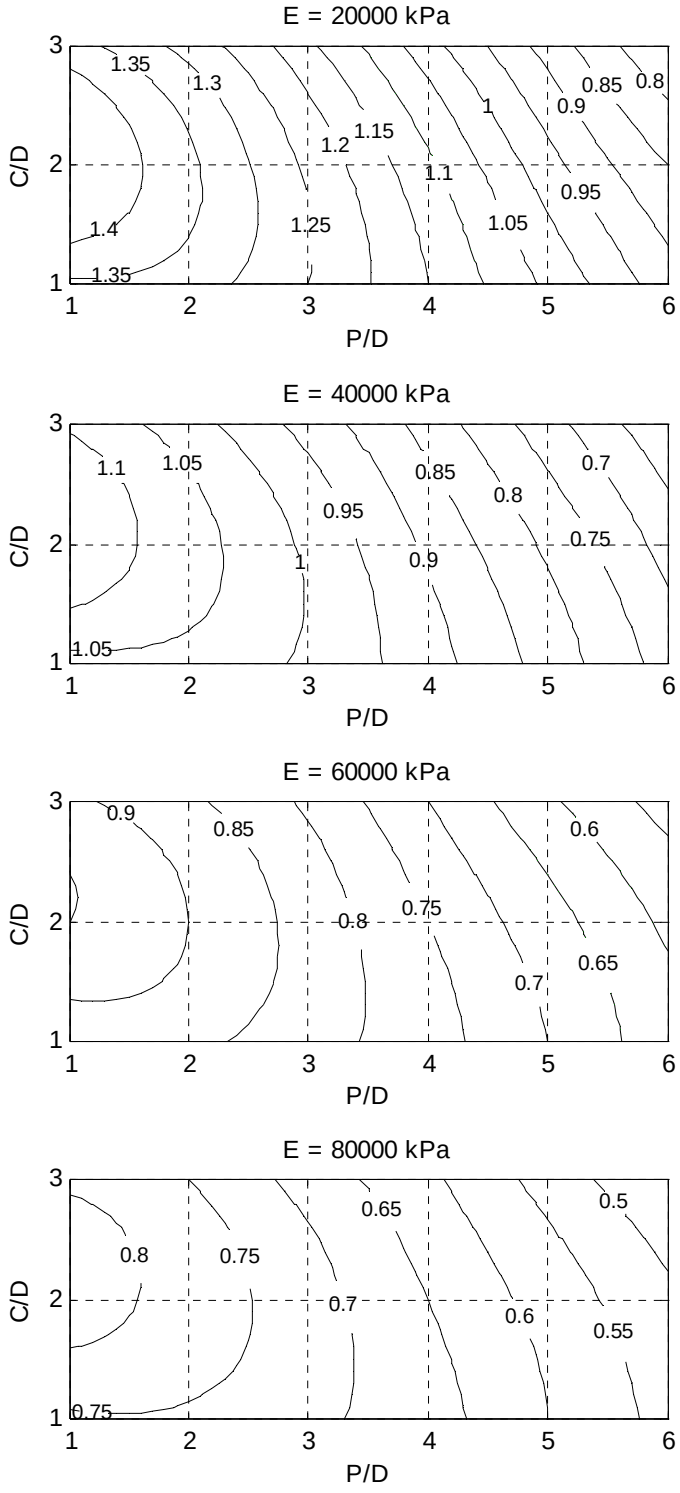

NOTE: Contour levels are shown in terms of δC_N x 1000. Please divide the reading by 1000 to obtain correct value of δC_N.

Figure 4.7 Design chart for the estimation of normalized in-plane displacement (δC_N) of the tunnel lining

4.5.3 Maximum Shear Force Induced in the Tunnel Lining

It is important to be able to estimate the change in maximum shear force (δSF_{max}) induced in the tunnel lining due to adjacent excavation for the purpose of assessing the structural health of the lining. High values of δSF_{max} may result in severe structural distress and even failure of the tunnel lining. A non-dimensional or normalized form of δSF_{max} can be obtained as:

$$\left[\delta SF_{max}\right]_N = \frac{\delta SF_{max}}{\Gamma_{sat} D H t_L} \qquad [4\text{-}3]$$

where Γ_{sat} is the saturated unit weight of the soil (in kN/m^3), H is the depth of the excavation (in m), D is the diameter of tunnel (in m), t_L is the thickness of the tunnel lining (in m), and δSF_{max} has units of kN. The justification for the normalization shown in Eq.[4-3] is that δSF_{max} is observed to increase with increase in H, t_L, and Γ_{sat}; D is simply used as a dummy variable to achieve the non-dimensional form.

Incorporation of H and t_L in Eq.[4-3] means that only four design charts – one each for the four different Young's modulus values for the soil – are needed to estimate the magnitude of change in maximum shear force in the tunnel lining due to adjacent deep excavation. These four design charts are shown in Figure 4.8. Before plotting the contours for these design charts, all the values of $[\delta SF_{max}]_N$ were multiplied by 100 in order to avoid very small contour levels. The reading obtained from these design charts, therefore, should be divided by 100 to obtain correct value of $[\delta SF_{max}]_N$. For example, referring to the first design chart from the top in Figure 4.8, the reading for E = 20000 kPa, C/D = 2, and P/D = 4 is around 4; therefore, the value of $[\delta SF_{max}]_N$ is equal to 4/100 = 0.04.

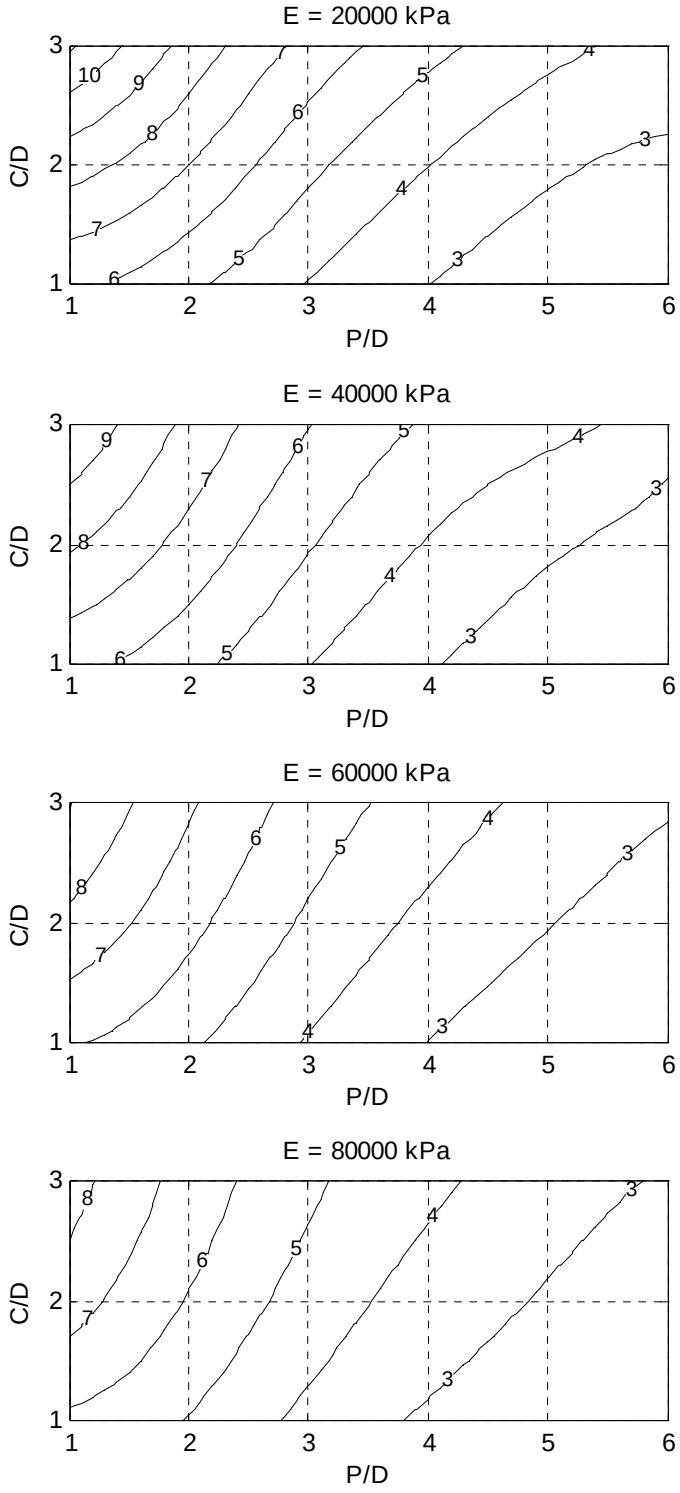

NOTE: Contour levels are shown in terms of $[\delta SF_{max}]_N$ x 100. Please divide the reading by 100 to obtain correct value of $[\delta SF_{max}]_N$.

Figure 4.8 Design chart for the estimation of normalized change in maximum shear force ($[\delta SF_{max}]_N$) in the tunnel lining

4.5.4 Maximum Bending Moment Induced in the Tunnel Lining

An increase in the maximum bending moment in the tunnel lining due to adjacent deep excavation is undesirable as it may lead to cracking of a concrete lining or opening of a gap at the seal between two segments in the case of a segmental tunnel lining. Consequently, corrosion of steel reinforcement and water leakage into the tunnel may occur, which, if left unchecked could render the tunnel unserviceable. Two types of bending moments – sagging and hogging – are induced in the tunnel lining depending on whether the tensile strains are occurring on the inside or the outside of the tunnel lining. It is in the case of a sagging bending moment that the inside of the tunnel lining experiences tensile strains, as shown in Figure 4.9.

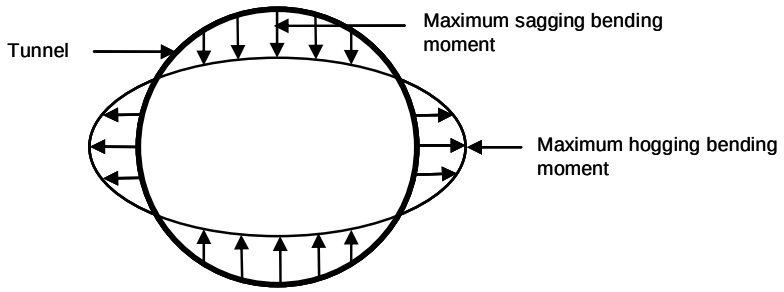

Figure 4.9 Typical bending moment distribution in a tunnel lining showing maximum sagging and maximum hogging bending moment

The change in maximum sagging bending moment ($\delta SBM_{\max}$) and the change in maximum hogging bending moment ($\delta HBM_{\max}$) can be made non-dimensional as:

$$\left[\delta SBM_{\max}\right]_N = \frac{\delta SBM_{\max}}{\Gamma_{sat} D^2 H t_L} \qquad [4\text{-}4a]$$

$$\left[\delta HBM_{\max}\right]_N = \frac{\delta HBM_{\max}}{\Gamma_{sat} D^2 H t_L} \qquad [4\text{-}4b]$$

where Γ_{sat} is the saturated unit weight of the soil (in kN/m^3), H is the depth of the excavation (in m), D is the diameter of tunnel (in m), t_L is the thickness of the tunnel lining (in m), and $\delta SBM_{\max}$ and $\delta HBM_{\max}$ have units of kNm. Both the maximum sagging and the maximum hogging bending moments are found to increase with increase in H, t_L, and Γ_{sat}; D is used as a dummy variable to achieve the non-dimensional form.

4.5.4.1 Design Charts for Change in Maximum Sagging Bending Moment

The normalization of change in maximum sagging bending moment shown in Eq.[4-4a] means that only four design charts – one each for the four different Young's modulus values for the soil – are needed to estimate the magnitude of change in maximum shear force in the tunnel lining due to adjacent deep excavation. These four design charts are shown in Figure 4.10. Before plotting the contours for these design charts, all the values of $[\delta SBM_{max}]_N$ were multiplied by 100 in order to avoid very small contour levels. The reading obtained from these design charts, therefore, should be divided by 100 to obtain correct value of $[\delta SBM_{max}]_N$. For example, referring to the bottom design chart in Figure 4.10, the reading for E = 80000 kPa, C/D = 2, and P/D = 3 is around 1.2; therefore, the value of $[\delta SBM_{max}]_N$ is equal to 1.2/100 = 0.012.

4.5.4.2 Design Charts for Change in Maximum Hogging Bending Moment

The normalization of change in maximum sagging bending moment shown in Eq.[4-4b] means that only four design charts – one each for the four different Young's modulus values for the soil – are needed to estimate the magnitude of change in maximum shear force in the tunnel lining due to adjacent deep excavation. These four design charts are shown in Figure 4.11. Before plotting the contours for these design charts, all the values of $[\delta HBM_{max}]_N$ were multiplied by 100 in order to avoid having to deal with very small contour levels. The reading obtained from these design charts, therefore, must be divided by 100 to obtain correct value of $[\delta HBM_{max}]_N$. For example, referring to the first design chart from top in Figure 4.11, the reading for E = 20000 kPa, C/D = 2, and P/D = 5 is around 0.6; therefore, the value of $[\delta HBM_{max}]_N$ is equal to 0.6/100 = 0.006.

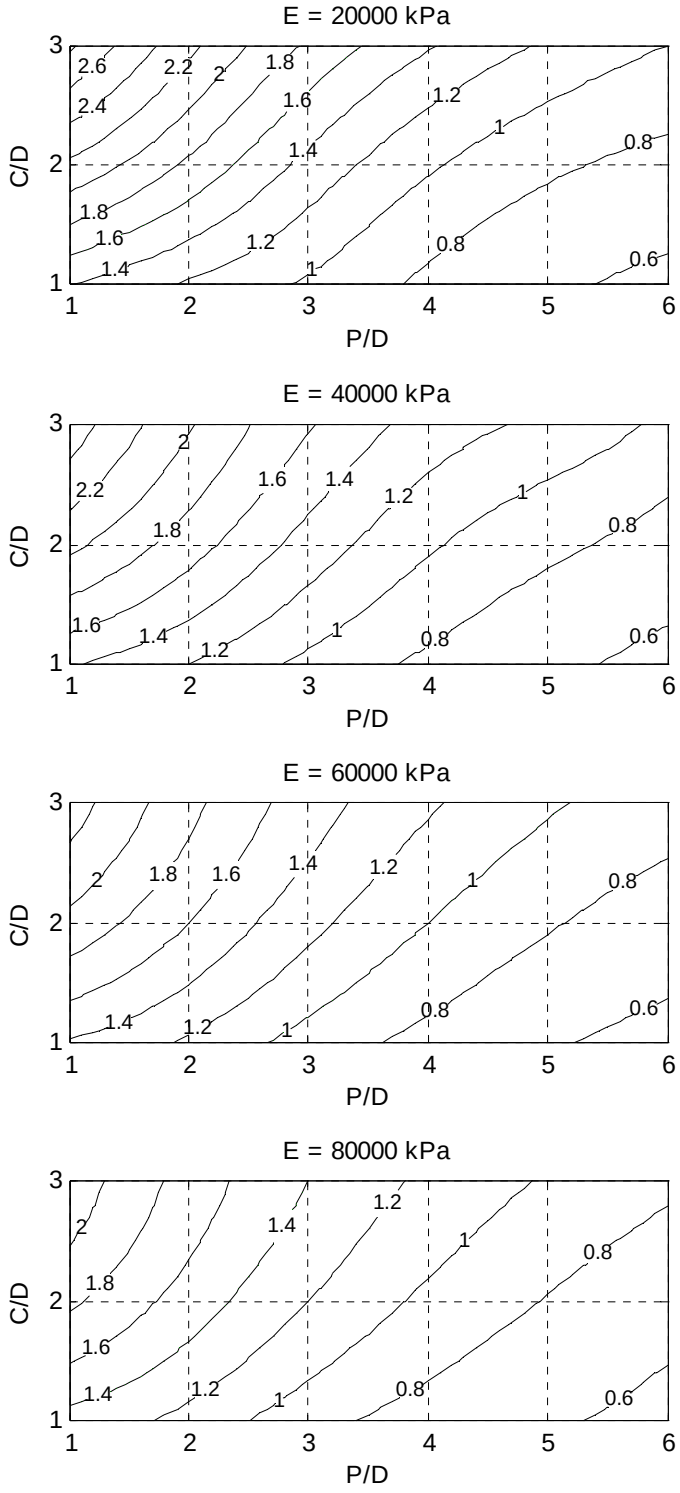

NOTE: Contour levels are shown in terms of $[\delta SBM_{max}]_N$ x 100. Please divide the reading by 100 to obtain correct value of $[\delta SBM_{max}]_N$.

Figure 4.10 Design chart for the estimation of normalized change in maximum sagging bending moment ($[\delta SBM_{max}]_N$) in the tunnel lining

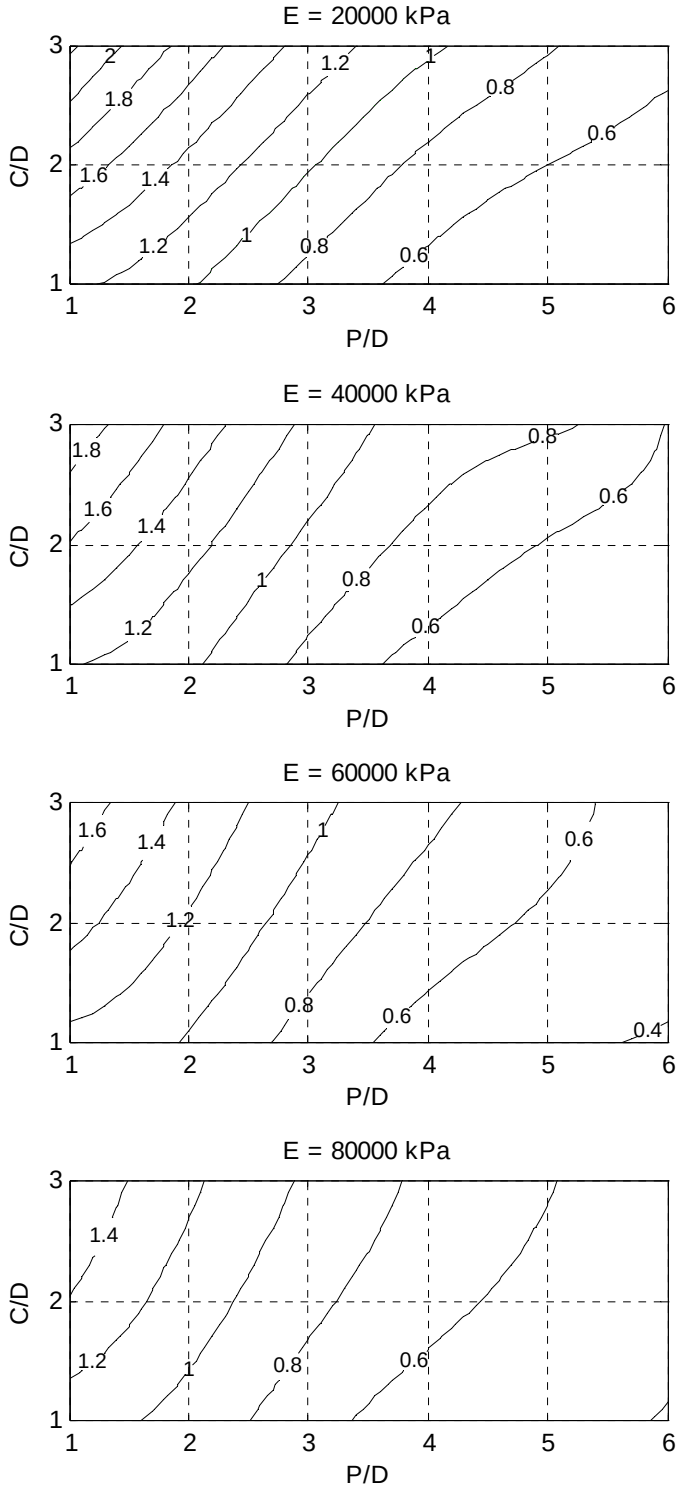

NOTE: Contour levels are shown in terms of $[\delta HBM_{max}]_N$ x 100. Please divide the reading by 100 to obtain correct value of $[\delta HBM_{max}]_N$.

Figure 4.11 Design chart for the estimation of normalized change in maximum hogging bending moment ($[\delta HBM_{max}]_N$) in the tunnel lining

4.5.5 An Example of the Use of Design Charts

The geometric configuration and the required dimensions for the example are shown in Figure 4.12. The groundwater table is located at the ground surface and the excavation pit is kept dry. The Young's modulus of the soil layer (E) and the saturated unit weight of the soil (Γ_{sat}) are 40000 kPa and 20 kN/m^3, respectively.

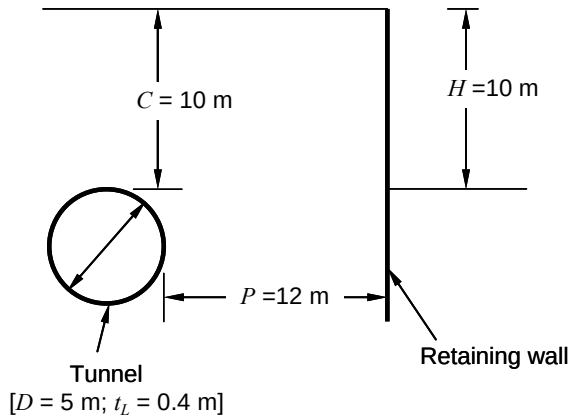

Figure 4.12 Geometric configuration and required dimensions of the example

Step 1: Calculate the C/D and P/D ratios.

$$\frac{C}{D} = \frac{10}{5} = 2.0 \text{ and } \frac{P}{D} = \frac{12}{5} = 2.4$$

Step 2: Get the normalized values of in-plane distortion, in-plane displacement, change in maximum shear force, change in maximum sagging and maximum hogging bending moments from the design charts for E = 40000 kPa, C/D = 2.0 and P/D = 2.4.

$\delta D_N = 1.6/10^5 = 1.6 \times 10^{-5}$ [Figure 4.6]

$\delta C_N = 1.04/1000 = 0.00104$ [Figure 4.7]

$[\delta SF_{max}]_N = 5.9/100 = 0.059$ [Figure 4.8]

$[\delta SBM_{max}]_N = 1.5/100 = 0.015$ [Figure 4.10]

$[\delta HBM_{max}]_N = 1.1/100 = 0.011$ [Figure 4.11]

Step 3: Convert the normalized values obtained in Step 2 into dimensional values using the given parameters.

$\delta D_N = \frac{\delta D}{D} \times \left(\frac{t_L}{H} \right)$, which gives δD = 0.002 m or 2 mm.

$\delta C_N = \frac{\delta C}{H}$, which gives δC = 0.0104 m or 10.4 mm.

$\left[\delta SF_{\max}\right]_N = \frac{\delta SF_{\max}}{\Gamma_{\text{sat}} D H t_L}$, which gives $\delta SF_{\max}$ = 23.6 kN.

$\left[\delta SBM_{\max}\right]_N = \frac{\delta SBM_{\max}}{\Gamma_{\text{sat}} D^2 H t_L}$, which gives $\delta SBM_{\max}$ = 30 kNm.

$\left[\delta HBM_{\max}\right]_N = \frac{\delta HBM_{\max}}{\Gamma_{\text{sat}} D^2 H t_L}$, which gives $\delta HBM_{\max}$ = 22 kNm.

4.6 Chapter Summary

In this Chapter, design charts for the estimation of in-plane distortion, in-plane displacement, change in maximum shear force, change in maximum sagging and maximum hogging bending moment in the tunnel lining due to an adjacent deep excavation are presented. These design charts are based on the results of finite element analyses using simplified ground conditions and idealized geometric configuration. The variables used in the preparation of these design charts were: Young's modulus of the soil layer, the thickness of the tunnel lining, the vertical distance of the crown of the tunnel from the ground surface, the horizontal distance of the tunnel from the vertical face of the excavation, and the depth of the excavation. These design charts are presented in terms of contours of normalized parameters.

These design charts are useful for obtaining approximate (ball park) estimates of tunnel lining deformation caused by adjacent deep excavation. The non-dimensional nature of these design charts makes it possible for these charts to be used for any depth of the deep excavation and for tunnels of varying sizes and varying depths of cover, located at varying distance from the vertical face of the excavation. It should, however, be kept in mind that the estimates obtained from these design charts are highly approximate and as such, should be taken as guidelines for decision making processes. These estimates do not replace site specific detailed analysis and monitoring.

5 Conclusions

5.1 Summary of Research

The main objective of the research project was to explore and quantify effects of deep excavation in soft ground conditions on adjacent existing circular tunnels. Study of deep excavation in itself is a broad topic as site conditions vary widely from one project to another and so do the configuration and the type of excavation support system. The scope of study expands further when deep excavations are undertaken close to existing underground structures such as circular tunnels. Given the wide scope of this soil-structure interaction problem, it is not surprising that important aspects of this problem have not been fully understood and there exists a need to do further research in this area. It is vital to limit the scope of the study from the point-of-view of identifying key mechanisms of soil-structure interaction. In the research presented in this thesis, this objective was achieved by identifying the most common site conditions encountered in deep excavation projects as well as the most common types and configurations for the deep excavation support system.

Extensive review of the literature published in the past four decades was carried out in order to understand the trends and developments in this area. The literature was broadly classified into four categories: (i) failures involving deep excavations in urban environment; (ii) the use of the Observational Method; (iii) the use of the finite element method for design as well as performance evaluation; and (iv) the development of design charts and guidelines. Important lessons in design, construction, monitoring and safety can be learnt from "post mortem" analyses of failed deep excavation projects, such as the 2004 Nicoll Highway Collapse in Singapore (Magnus et al. 2005). The concurrent use of the Observation Method along with the finite element method for monitoring and controlling the ground deformations around deep excavation has become an integral part of any deep excavation project. The literature review revealed that the development of design charts and guidelines have been initiated in some of the sectors of deep excavation such as the effects of deep excavation on adjacent raft foundations (Peck 1969b) or pile foundations (Broms and Pandey 1987, Poulos et

al. 1997); however, no such design guidelines were found for deep excavations adjacent to existing circular tunnels. Consequently, the need for further research in this area was identified and the development of simple-to-use preliminary design charts for estimating tunnel lining deformations caused by nearby deep excavations was established as one of the deliverables of this research project.

The research was initiated with detailed study and back analysis of two well-documented case studies – the Chicago Subway Renovation Project, USA (Finno et al. 2002), and the Tan Tock Seng Hospital (TTSH) Deep Excavation, Singapore (Sharma et al. 2001). The Chicago Subway Renovation Project involved monitoring and controlling the effect of deep excavation on a adjacent school's foundation using a sophisticated instrumented monitoring system, i.e. the Observational Method, coupled with inverse analyses based on the finite element method. In the TTSH Deep Excavation Project, the monitoring of the response of two existing circular tunnels of the Singapore Mass Rapid Transit (MRT) System to nearby deep excavation was achieved with the help of an automated instrumented monitoring system. The observed response of the tunnels was verified using numerical analyses.

The back analyses of these two case studies were carried out using the finite element software PLAXIS. Exact site conditions and input parameters for the soil and the structural components were incorporated as much as possible. Appropriate adjustment in the some of the input parameters was necessary to achieve a good match between the computed and the observed results. The back analyses were followed by parametric studies to identify important variables controlling the mechanisms of soil-structure interaction.

The variables identified from the parametric studies of the two case studies were: soil stiffness, tunnel lining thickness, the depth of the excavation, and the location of tunnel. These variables were used to conduct a series of finite element analyses using simplified geometry and ground conditions for the purpose of formulating preliminary design charts. A total of 864 numerical analyses were carried out using PLAXIS. Results from these analyses were recorded in terms of in-plane and out-of-plane distortion as well as additional shear force and bending moment induced in the tunnel lining due to adjacent deep excavation. These results were made non-dimensional before presenting them as contour plots. These contour plots constitute preliminary design charts, which can be used for the estimation of tunnel lining deformation caused by adjacent deep excavation.

5.2 Key Findings

Key findings of this research project can be summarized as follows:

- It is extremely important to incorporate details of construction processes accurately in the numerical model when using it to calibrate soil parameters on the basis of back analysis of an instrumented case history. The modeller must be aware of specific procedures prescribed by the modelling software to model these construction processes.
- It is possible to simulate both the mechanism and the magnitude of ground deformation around a deep excavation using a numerical model with simplified stratigraphy obtained by grouping several successive soil layers into one layer. There should, however, be some physical basis for such grouping of soil layers, such as common geological origin of these soil layers or common type of soil behaviour.
- Deep excavation is a relatively fast construction activity; therefore, the behaviour of ground surrounding the excavation can be modelled as undrained, provided the average permeability of the surrounding ground is sufficiently low.
- The ground deformations around a deep excavation are significantly influenced by the stiffness of the ground and the stiffness of the excavation support system. It is important, therefore, to obtain accurate estimates of soil stiffness in order to obtain accurate estimates of ground deformation.
- A stiff retaining wall is required for controlling horizontal ground movements resulting from deep excavation; however, when choosing a support system for the deep excavation, it should be kept in mind that even the stiffest of retaining wall will result in some horizontal displacement of the ground. Therefore, selecting a stiff retaining wall alone is not going to help eliminate all the horizontal ground movements.
- Although the use of a stiff retaining wall results in a reduction in horizontal movement of the ground, it is virtually ineffective in reducing the settlement of the ground behind the retaining wall. In fact, it appears to increase the settlements. If the major concern is to limit the ground settlement behind the retaining wall, it might be better to use a slightly flexible retaining wall system.
- The stiffness of the tunnel lining has significant effect on its deformation. A stiff tunnel lining can resist in-plane distortion (ovalization) better, but it mobilizes higher

maximum shear force and higher maximum bending moment compared to a flexible tunnel lining. The stiffness of the tunnel lining, however, has virtually no effect on the in-plane displacement of the tunnel lining, which is found to be influenced only by the stiffness of the surrounding soil, the location of the tunnel with respect to the vertical face of the deep excavation and the ground surface, and the depth of the excavation.

- At higher cover depth, the in-plane distortion of tunnel lining due to adjacent deep excavation increases because of large overburden depth of soil, but its in-plane displacement decreases because of the higher horizontal confinement provided by the soil. The in-plane displacement of the tunnel lining is found to be greater (by a factor of 4 to 5) than its in-plane distortion.

5.3 Conclusions

Based on the key findings of the research, the following conclusions can be drawn:

- A finite element program (such as PLAXIS) that is able to model construction processes associated with tunnelling and deep excavation in urban environment can be an invaluable tool in exploring the mechanism of ground deformation around the deep excavation and in quantifying the effects of ground deformation on existing adjacent structures. The modeller must, however, be aware of the fact that ways of modelling a particular construction process are different for different finite element programs. It is important to interpret the instructions given in the manual of the program correctly.
- Detailed back analyses of well-documented deep excavation case histories are vital from the point-of-view of building confidence in the selected finite element program. Such back analyses also have the potential to identify key variables influencing the soil-structure interaction.
- It is sometimes necessary to simplify the stratigraphy of the ground (e.g. by combining several soil layers into one layer or ignoring layers of fairly insignificant thickness) in order to reveal the mechanism of ground deformation around a deep excavation more clearly.
- Preliminary design charts proposed in this thesis are convenient for determining approximate values of tunnel lining deformation caused by adjacent deep excavation. The non-dimensional nature of these design charts makes it possible for these charts to

be used for any depth of the deep excavation and for tunnels of any size, depths of cover, and distance from the vertical face of the excavations.

- The proposed preliminary design charts can be used by engineers and contractors for initial estimation, selection and preliminary design of excavation support system, and are especially useful during the planning phase. Town planners and project managers, who need to decide on the feasibility, damage control and risk management aspects of a deep excavation project, may also find these design charts equally useful. It should, however, be kept in mind that the estimates obtained from these design charts are approximate and as such, should be taken as guidelines for decision making processes. These estimates do not replace site specific detailed analysis and monitoring.

5.4 Recommendations for Further Work

The research presented in this thesis has demonstrated the usefulness of preliminary design charts for planning of deep excavations and for estimation of their effects on adjacent structures. These design charts, however, were obtained after making several assumptions and simplifications. There is scope for improving the general applicability of these design charts by eliminating some of these assumptions and simplifications. For example, further analyses can be done to establish the effect of depth of embedment of the retaining wall with respect to the depth of the excavation. Similarly, the effect of changing the vertical spacing of the horizontal struts or changing the diameter of the tunnel could be investigated by conducting further analyses. Analyses could also be done to develop preliminary design charts for the estimation of the effect of deep excavation on other kinds of adjacent structures, such as raft foundations or piles and other types of deep foundations.

The preliminary design charts proposed in this thesis were developed using PLAXIS. From the point-of-view of confirming their validity further, another finite element program, such as SAGE-CRISP, SIGMA/W or ABAQUS, could be used to repeat some of the analyses needed to formulate these design charts.

References

Athanasiu, C.M., Simonsen, A.S. and Ronning, S. (1991). Back-calculation of case records to calibrate soil-structure interaction analysis by finite element method of deep excavation in soft soil. Proc. 10th European Conference on Soil Mechanics and Foundation Engineering, Vol. 1, pp. 297-300.

Atkinson, J.H. (2000). Non-linear soil stiffness in routine design. Géotechnique, Vol. 50, No. 5, pp. 487-508.

Boone, S.J., Nusink, R. and Westland, J. (1999). Comparative evaluation of building responses to an adjacent braced excavation. Canadian Geotechnical Journal, Vol. 36, pp. 210-223.

Bose, S.K. and Som, N.N. (1998). Parametric study of a braced cut by finite element method. Computers and Geotechnics, Vol. 22, pp. 91-107.

Brinkgreve, R.B.J., Broere, W. and Waterman, D. (2004). PLAXIS 2-D Professional Version 8.0 – User's Manual. PLAXIS b.v., The Netherlands.

Broms, B.B. and Pandey, P.C. (1987). Influence of ground movements from tunnelling on adjacent piles and remedial measures. Proc. the Japan Society of Civil Engineers, Tokyo, Japan, pp. 1-11.

Budhu, M. (2000). *Soil Mechanics and Foundations*. John Wiley and Sons, New York.

Burd, H.J., Houlsby, G.T., Augarde, C.E. and Liu, G. (2000). Modelling tunnelling-induced settlement of masonry buildings. Proceedings of the Institution of Civil Engineers: Geotechnical Engineering, Vol. 143, no. 1, pp. 17-29.

Burland, J.B. and Hancock, R.J.R. (1977). Underground car park at the House of Commons, London: Geotechnical aspects. Structural Engineer, Vol. 55, No. 2, pp. 81-100.

Calvello, M. (2002). Inverse analysis of supported excavations through Chicago glacial clays. PhD Thesis, Northwestern University, Evanston, Illinois, USA.

Calvello, M. and Finno, R.J. (2004). Selecting parameters to optimize in model calibration by inverse analysis. Computers and Geotechnics, Vol. 31, No. 5, pp. 411-425.

Chan, C.W. (1995). Displacement of MRT tunnels due to an adjacent excavation. Nanyang Technological University, M.Sc. Dissertation.

Chang, C.T., Sun C.W., Duann S.W. and Hwang R.N. (2001). Response of a Taipei Rapid Transit System (TRTS) tunnel to adjacent excavation. Tunnelling and Underground Space Technology, Vol. 16, No. 3, pp. 151-158.

Chen, L.T., Poulos, H.G. and Loganathan, N. (1999). Pile response caused by tunneling. ASCE Journal of Geotechnical and Geoenvironmental Engineering, Vol. 125, No. 3, pp. 207-215.

Clough, G.W. and O'Rourke, T.D. (1990). Construction induced movements of in-situ walls. Proc. ASCE Speciality Conference on Design and Performance of Earth Retaining Structures, Cornell University, New York, pp. 439-470.

Dell'Isola, A.J. (1982). *Value Engineering in the Construction Industry*. Third edition. Van Nostrand Reinhold, New York, USA.

De Moor, E.K. (1994). An analysis of bored pile/diaphragm wall installation effects. Géotechnique, Vol. 44, No. 2, pp. 341-347.

Duncan, J.M. and Chan, C.-Y. (1970). Nonlinear analysis of stress and strain in soil. ASCE Journal of Soil Mechanics and Foundation Engineering Division, Vol. 96, pp. 1629-1653.

Eisenstein, Z. and Medeiros, L.V. (1983). A deep retaining structure in till and sand – Part II: Performance and analysis. Canadian Geotechnical Journal, Vol. 20, pp. 131-140.

Finno, R.J., Bryson, L.S. and Calvello, M. (2002). Performance of a stiff support system in soft clay. Journal of Geotechnical and Geoenvironmental Engineering, ASCE, Vol. 128, No. 8, pp. 660-671.

Finno, R.J. and Harahap, I.S. (1991). Finite element analysis of HDR-4 excavation. ASCE Journal of Geotechnical Engineering, Vol. 117, No. 10, pp. 1590-1609.

Glass, P.R. and Powderham, A.J. (1994). Application of the Observational Method at the Limehouse Link. Géotechnique, Vol. 44, No. 4, pp. 665-679.

Gue, S.S. and Tan, Y.C. (2004). Prevention of failures related to geotechnical works on soft ground. Special Lecture, Proc. Malaysian Geotechnical Conference, 6-18 March, 2004, Sheraton Subang, Petaling Jaya, Malaysia.

Hashash, Y.M.A and Whittle, A.J. (1996). Ground movement prediction for deep excavations in soft clay. ASCE Journal of Geotechnical Engineering, Vol. 122, No. 6, pp. 474-486.

Hintze, S. (2002). Prediction and Impact on Nearby Structures during Deep Excavation for the Southern Link Road. Construction. Proc. 2nd International Conference on Soil Structure Interaction in Urban Civil Engineering, Vol. 1, pp.129-134.

Hu, Z.F., Tham, L.G., Yue, Z.Q. and Zhou, J. (2003). Design and construction of a deep excavation in soft soils adjacent to the Shanghai Metro tunnels. Canadian Geotechnical Journal, Vol. 40, No. 5, pp. 933-948.

Ikuta, Y., Maruoka, M., Aoki, M. and Sato, E. (1994). Application of the Observational Method to a deep basement excavated using the top-down method. Géotechnique, Vol. 44, No. 4, pp 655-664.

Janbu, N. (1963). Soil compressibility as determined by oedometer and triaxial tests. Proceeedings of European Conference on Soil Mechanics and Foundation Engineering, Wiesbaden, Germany, Vol. 1, pp. 19-25.

Koutsoftas, C.D., Kulesza, R., Meyersohn, D. and Wu, C.L. (2000). Deformations during cut-and-cover construction of Muni Metro Turnback Project. ASCE Journal of Geotechnical and Geoenvironmental Engineering, Vol. 126, No. 4, pp. 344-359.

Long, M. (2001). A case history of a deep basement in London Clay. Computers and Geotechnics, Vol. 28, pp. 397-423.

Magnus, R., Teh, C.I. and Ming, L.J. (2005). Report on the incident at the MRT circle worksite that led to the collapse of Nicoll Highway on 20 April 2004. Final report of the Committee of Inquiry appointed by the Minister for Manpower, The Ministry of Manpower, Singapore.

Meier, C.P. and Winsor, D. (2005). Delving beneath Delhi. Civil Engineering, August 2005, pp. 40-87.

Mana, A.I. and Clough, G.W. (1981). Prediction of Movements for Braced Cut in Clay. Journal of Geotechnical Engineering, ASCE, Vol. 107, No. 8, pp. 759-777.

Moormann, C. and Katzenbach, R. (2002). Three-dimensional effects of deep excavations with rectangular shape. Proc. 2nd International Conference on Soil Structure Interaction in Urban Civil Engineering, Vol. 1, pp. 135-142.

Muir-Wood, D. (1990). *Soil Behaviour and Critical State Soil Mechanics*. Cambridge University Press, Cambridge, UK.

Ng, C.W.W. and Lings, M.L. (2002). Effects of modelling soil non-linearity and wall installation on back analysis of deep excavation in stiff clay. Journal of Geotechnical and Geoenvironmental Engineering, Vol. 121, No. 10, pp. 687 - 695.

Ou, C.Y., Liao, J.T. and Cheng, W.L. (2000). Building response and ground movements induced by a deep excavation. Géotechnique, Vol. 50, No. 3, pp. 209-220.

Palmer, J.H.L. and Kenney, T.C. (1972). Analytical study of a braced excavation in weak clay. Canadian Geotechnical Journal, Vol. 9, pp. 145-164.

Peck, R.B. (1969a). Advantages and limitations of the Observational Method in applied soil mechanics. Géotechnique, Vol. 19, No. 2, pp. 171-187.

Peck, R.B. (1969b). Deep excavations and tunnelling in soft ground. Proc. 7th Int. Conf. on Soil Mech., Vol. 3, pp. 225-290.

Peck, R.B. (1985). The last sixty years. Proc. 11th International Conference on Soil Mechanics and Foundation Engineering, pp. 123-133.

Potts, D.M. and Fourie, A.M. (1984). The behaviour of a propped retaining wall: results of a numerical experiment. Géotechnique, Vol. 34, No. 3, pp. 383-404.

Poulos, H.G. (2002). Experience with soil-structure interaction in the Far East. Proc. 2nd International Conference on Soil Structure Interaction in Urban Civil Engineering, Vol. 1, pp. 39-65.

Poulos, H.G. and Chen, L.T. (1996). Pile response due to unsupported excavation-induced lateral soil movement. Canadian Geotechnical Journal, Vol. 33, pp. 670-677.

Poulos, H.G. and Chen, L.T. (1997). Pile response due to excavation-induced lateral soil movement. ASCE Journal of Geotechnical and Geoenvironmental Engineering, Vol. 123, No. 2, pp. 94-99.

Powderham, A. (1994). An overview of the Observational Method: Development in cut and cover and bored tunnelling projects. Géotechnique, Vol. 44, No. 4, pp. 619-636.

Powderham, A. (2002). The Observational Method – learning from projects. Proc. the Institution of Civil Engineers, Geotechnical Engineering, Vol. 115, No. 1.

Powrie, W. and Li, E.S.F. (1991). Finite element analyses of an in-situ wall propped at formation level. Géotechnique, Vol. 41, No. 4, pp. 499-514.

Roboski, J.F. (2001). Soil Parameters for Constitutive Models of Compressible Chicago Glacial Clays. M.Sc. Thesis, Northwestern University, Evanston, Illinois, USA.

Schanz, T. (1998). On the modelling of mechanical behaviour of frictional materials (Zur Modellierung des Mechanischen Verhaltens von Reibungsmaterialen). Habilitation dissertation, University of Stuttgart (in German).

Schanz, T., Vermeer, P.A. and Bonnier, P.G. (1999). Formulation and verification of the Hardening-Soil model. In *Beyond 2000 in Computational Geotechnics*. R.B.J. Brinkgreve (editor), AA Balkema, Rotterdam, pp. 281-290.

Seok, J.W., Kim, O.Y., Chung, C.K. and Kim, M.M. (2001). Evaluation of ground and building settlement near braced excavation sites by model testing. Canadian Geotechnical Journal, Vol. 38, pp. 1127-1133.

Sharma, J.S., Chu, J. and Zhao, J. (1999). Geological and Geotechnical Features of Singapore: An Overview. Tunnelling and Underground Space Technology, Vol. 14, No. 4, pp. 419 – 431.

Sharma, J.S., Hefny, A.M., Zhao, J. and Chan, C.W. (2001). Effect of large excavation on deformation of adjacent MRT tunnels. Tunnelling and Underground Space Technology, Vol. 16, pp. 93-98.

Shirlaw, J.N., Tham-Lee, S.K., Wong, F.K., Ang-Wong, L.P., Chen, D.C., Osborne, N. and Tan C.G. (2000). Planning the monitoring required to confirm the movement and rotation of tunnels and trackwork due to excavation and tunnelling. Proc. the international Conference on Tunnels and Underground Structures, Singapore, Tunnels and Underground Structures, pp. 489-494.

Simpson, B. (1992). Retaining structures: Displacement and design. Géotechnique, Vol. 42, No. 4, pp. 541-576.

Terzaghi, K. (1961). *From Theory to Practice in Soil Mechanics*. John Wiley and Sons, New York.

Viggiani, G. and Atkinson, J.H. (1995). Stiffness of fine-grained soil at very small strains. Géotechnique, Vol. 45, No. 2, pp. 249-265.

von Soos, P. (1980). Properties of Soil and Rock. In *Grundbautaschenbuch*, Part 4, Edition 4, Ernst and Sohn, Berlin. (in German).

Whittle, A.J., Hashash, Y.M.A. and Whitman, R.V. (1993). Analysis of deep excavation in Boston. ASCE Journal of Geotechnical Engineering, Vol. 119, No. 1, pp. 69-89.

Wong, K.S. and Broms, B.B. (1989). Lateral wall deflections of braced excavation in clays. ASCE Journal of Geotechnical Engineering, Vol. 115, No. 6, pp. 853-870.

Yoo, C. (2001). Behaviour of braced and anchored walls in soils overlying rock. Journal of Geotechnical and Geoenvironmental Engineering, Vol. 127, No. 3, pp. 225-233.

Young, D.K. and Ho, E.W.L. (1994). The observational approach to design of a sheet-piled retaining wall. Géotechnique, Vol. 44, No. 4, pp. 637-654.